Numerical loop calculations with contour deformation

Dissertation zur Erlangung des Grades eines
"Doktor rerum naturalium (Dr. rer. nat.)"
der Fachbereiche:

- 08 - Physik, Mathematik und Informatik,

- 09 - Chemie, Pharmazie und Geowissenschaften,

- 10 - Biologie,

- Universitätsmedizin

der Johannes Gutenberg-Universität,

JOHANNES GUTENBERG UNIVERSITÄT MAINZ

vorgelegt von
Sebastian Becker

August 13, 2012

Autor:

Sebastian Becker
Theoretische Hochenergiephysik
Institut für Physik
Johannes-Gutenberg-Universität Mainz
55128 Mainz

Max Planck Graduate Center:

Staudinger Weg 9 (Building 2413)
55128 Mainz

Datum der Doktorprüfung:

Dienstag, 02.10.2012
Johannes-Gutenberg-Universität Mainz
55099 Mainz

Abstract

This thesis is about the numerical calculation of loop integrals which appear at higher orders in perturbative theory. Analogous to the reel emission one can introduce subtraction terms which remove the collinear and soft divergencies of a loop integral. The phase space and the loop integration can then be performed numerical in single Monte Carlo integration. In this thesis we show how to perform such a numerical integration with the help of contour deformation. We also show how one can calculate the necessary integrands with recurrence relations.

Zusammenfassung

Gegenstand dieser Arbeit ist die nummerische Berechnung von Schleifenintegralen welche in höheren Ordnungen der Störungstheorie auftreten. Analog zur reellen Emission kann man auch in den virtuellen Beiträgen Subtraktionsterme einführen, welche die kollinearen und soften Divergenzen des Schleifenintegrals entfernen. Die Phasenraumintegration und die Schleifenintegration können dann in einer einzigen Monte Carlo Integration durchgeführt werden. In dieser Arbeit zeigen wir wie eine solche numerische Integration unter zu Hilfenahme einer Kontourdeformation durchgeführt werden kann. Ausserdem zeigen wir wie man die benötigten Integranden mit Rekursionsformeln berechnen kann.

Contents

Contents

1 Introduction

Understanding the final states of high energy particle collisions such as those at the Large Hadron Collider (LHC) is an extremely challenging theoretical problem. In a typically LHC event hundreds of particles are produced. In general these produced particles are not the partons from the theory but hadrons.

Parton Distribution Function (PDF) describe how the constituent partons are distributed in the hadron. At lowest order the PDF describes the probability to find a parton of a certain species with a certain momentum fraction of the hadron when a hadron is probed at a certain scale. In an event generator one factorises the calculation into different regimes, according to the scales of momentum transfer involved. At the highest scales we have the hard scattering process. The hard scattering process is a perturbative description of the interacting of two partons of the hadrons from the incoming beams. The hard process produces a relative small number of energetic outgoing partons. At the very lowest scale, of the order 1 GeV, we have hadronisation. The outgoing partons interact non-perturbatively to form the final state hadrons observed in the detector. These soft processes are modelled. The hard and soft regime are distinct but connected by a scale evolution which is described by a parton shower. This scale evolution produces a large number of additional partons which can participate in the hadronisation at the soft scale. In fig.(1.1) a schematic view of the factorisation is shown.

We now focus on the hard process. At the LHC multi-jet final states play an important role and therefore a calculation of the matrix element of the hard process with a large number of external particles is desirable. At leading order (LO) multi-jet events are easily modelled. To improve the accuracy of our theoretical predictions one needs to include higher order corrections in the calculations.

With an increasing number of external particles the next-to-leading order (NLO) calculations become considerable more difficult. The past decade has seen a tremendous progress in automated NLO calculations. The state of the art are $2 \to 5$ process like $V + 4$-jets [29; 30] or $e^+ e^- + 7$-jets [4]. Most groups using either methods based generalised unitary [26–37] or methods based on traditional Feynman graphs [38]. For both approaches a variety of packages are available [39–47]. A third approach uses numerical Monte Carlo integration for the computation of the one-loop amplitude. This approach uses local subtraction terms [1–3; 5] and contour deformation [2; 5–11] to be able to perform the integration purely nu-

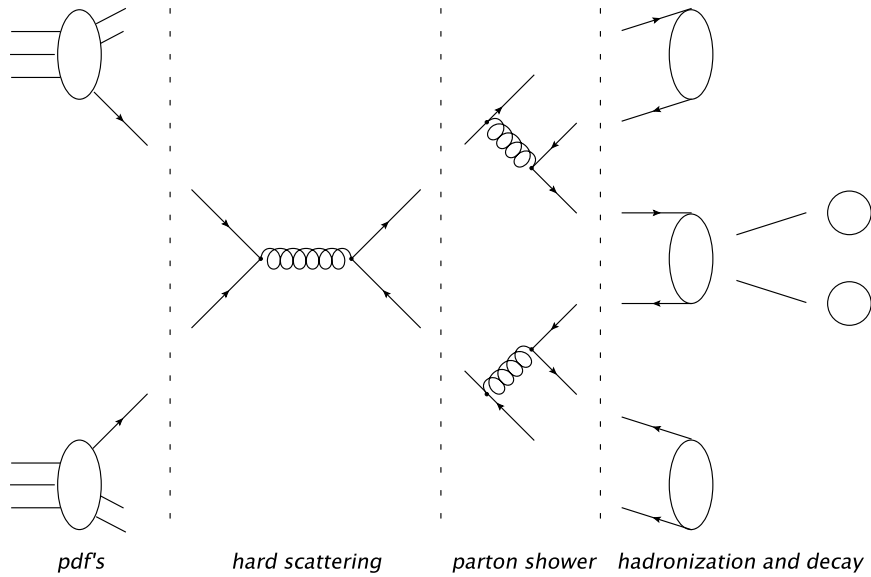pdf's   hard scattering   parton shower hadronization and decay

Figure 1.1: Schematic view of factorisation of hard collisions at hadron colliders.

merical. We note that most recently also a mix of the Feynman graphs approach and local subtraction was published [49]. In all approaches of NLO multi-parton calculations the virtual part is the most challenging.

Some subprocess are absent at tree-level such as the gluon fusion to diphoton subprocess $gg \rightarrow \gamma\gamma$ which is an important background process for the new heavy boson recently discovered at the LHC [48]. Because the basic process only appears at one-loop level, a NLO prediction of this subprocess requires a two-loop calculation.

Two-loop calculations are also required in any studies beyond NLO. Going to the next-to-next-to-leading order (NNLO) in perturbative theory is a promising way to high precision calculations. NNLO is available for all processes involving the production of a single vector or Higgs boson at the LHC. Processes with larger jet multiplicity are almost inexistent. There exits NNLO calculations for $e^+e^- \rightarrow 3$-jets [50] and most recently published $q\bar{q} \rightarrow t\bar{t}$ [51]. A NNLO matrix element generator is highly recommended. We expect that at NNLO the two-loop calculations are the most challenging ones.

To extend the subtraction method to NNLO calculations one needs the subtraction terms for the divergent amplitudes, a contour deformation for two-loop integrals and an efficient method to calculate the two-loop amplitudes. The latter two are provided by this thesis. At NNLO there existing subtraction schemes [18–25] for the double-real and the virtual-real contributions. These subtraction terms render the phase space integration finite in the regions where one or two external particles become soft or collinear. Local subtraction terms for the two-loop amplitude in the double-virtual contribution are not known yet.

In this thesis the numerical calculation of loop integrals which appears at higher orders in perturbative theory is discussed. The purely numerical calculation of loop integrals with contour deformation is motivated by the so called subtraction method. We give in chapter 2 a short review of this method which was developed by various physicist including the author. In chapter 3 we present an efficient way to construct the integrand of one- and two-loop primitive amplitudes. The largest space of the thesis is occupied by the numerical integration of loop integrals via contour deformation. Contour deformation is a method (like the name implies) to deform the integration variables into the complex plane such that poles in the integrand are avoided and a numerical integration is available. After we render the integral finite by subtraction and avoid the poles on the real axis of the integration variables by contour deformation, we are able to perform the integration numerically by Monte Carlo techniques. We distinguish two approaches to the contour deformation. The so called "Feynman deformation" and the so called "Direct deformation" approach. In the first, one makes use of the Feynman trick and simplifies the loop integrand by the price of introducing additional integration variables, the so called Feynman parameters. This approach has the advantage of a rather simple deformation of the integration variables, massive QCD is automatic included and the extension to higher loops is known. The drawbacks are numerical instabilities for large particle multiplicity due to the structure of the integrand after Feynman parametrisation. In chapter 4 we present a detailed construction rule for the Feynman deformation at one-loop level and methods to overcome the numerical instabilities of this approach. In the Direct deformation approach one deforms directly the loop momenta without the detour of Feynman parametrisation. Therefore one does not deal with numerical instabilities but with a much more involved deformation. So far a Direct deformation was only known at one-loop level and only for massless QCD. In chapter 5 we give a detailed construction rule for a Direct deformation suitable for massive QCD. In chapter 6 we discuss the extension of the Direct deformation to two- and three-loop integrals.

We summarise the outcome of this thesis. Recurrence relations for one- and two-loop primitive amplitudes are developed. We discuss in detail the Feynman deformation approach and develop improvements of this approach for processes with a large particle multiplicity. Furthermore we develop an extension of the Direct deformation to the massive QCD and we apply this deformation to multi-loop integrals.

The work in chapter 2 is based on the publications [1; 2; 4–6]. The work in chapter 3 mainly based on the publication [6], only the content of subsection 3.4 is new and first published here. The work in chapter 4 mainly based on the publication [5], only the content of subsection 4.3.2 is new and first published here. The work in chapter 5 and 6 is new and first published here.

1 Introduction

2 The subtraction method

In this chapter we present an efficient method for the numerical calculation of next-to-leading order (NLO) corrections.

2.1 Introduction

The subtraction method is based on local subtraction terms for the infrared and ultraviolet divergences of a one-loop amplitude, recursive relations for off-shell currents and contour deformation. The method is not new and has been discussed in the literature before. The contour deformation for one-loop amplitudes was discussed in [9; 11], the infrared subtraction terms were discussed in [3] and Berends Giele type recurrence relations for off-shell tree level currents were discussed in [63] and first attempts for recurrence relations at one-loop level were discussed in [64].

One milestone for an efficient implementation of the subtraction method was achieved when we recognised that the local infrared subtraction terms can be formulated at the amplitude level [1; 2]. In [5] we first combined the subtraction terms with the contour deformation in a suitable way. In the same publication we presented an efficient way of constructing the local ultraviolet subtraction terms via recurrence relations and subtraction terms for vertex and propagator corrections. As a proof of principles we present results for the cross sections in electron positron annihilation [4]. This was the first time a physical observable depending on a one-loop eight-point function was calculated. Most recently, we gave some technical insights into the method [6]. In this publication we discussed techniques to improve the efficiency of the subtraction method and presented in full detail the recurrence relations for the one-loop off-shell currents.

In the following we outline the subtraction method. For sake of simplification we neglect initial state radiation and parton distribution functions for the initial state partons in the discussion. This corresponds to an electron positron annihilation. But the subtraction method can also be used to calculate cross sections for hadron hadron collisions.

2.2 General framework

We want to calculate an observable at higher orders in perturbative theory. The master formula to calculate an observable at an electron-positron collider is given by

$$\langle \mathcal{O} \rangle = \frac{1}{K(s)} \frac{1}{n_{spin}(1) n_{spin}(2)} \sum_n \int d\phi_n \mathcal{O}_n (p_1, \ldots, p_n, q_1, q_2) |\mathcal{A}_n|^2, \quad (2.1)$$

where q_1 and q_2 are the momenta of the initial-state particles, $2K(s) = 2s$ is the flux factor and $s = (q_1 + q_2)^2$ is the center of mass energy squared. The factors $1/n_{spin}$ correspond to the averaging of the spins of the initial state particles. $d\phi_n$ is the invariant phase space measure for n final state particles and $\mathcal{O}_n (p_1, \ldots, p_n, q_1, q_2)$ is the observable, corresponding to n final state partons and two initial state particles. The integral is performed over the phase space of the n external particles.

We are interested in the perturbative expansion of the amplitudes $\mathcal{A}_n$ in the coupling constant. One can increase the order in the coupling constant by increasing the number of loops or the number of external (unresolved) partons in the amplitude. The leading-order contribution to a n-jet observable is given by

$$|\mathcal{A}_n|^2_{\text{LO}} = \left| \mathcal{A}_n^{(0)} \right|^2 \quad (2.2)$$

At the next-to-leading order (NLO) we have virtual and real contributions

$$|\mathcal{A}_n|^2_{\text{NLO}} = 2 \,\text{Re} \left(\mathcal{A}_n^{(0)*} \mathcal{A}_n^{(1)} \right) \quad (2.3)$$

$$|\mathcal{A}_{n+1}|^2_{\text{NLO}} = \left| \mathcal{A}_{n+1}^{(0)} \right|^2 \quad (2.4)$$

Here $A_n^{(l)}$ denotes an amplitude with n final-state partons and l loops. At NLO level we have to consider two contributions. The virtual contribution contains the interference term of a Born amplitude with an one-loop amplitude. The real contribution is given by the square of a Born amplitude with one additional unresolved final-state parton. The extra parton is unseen in the detector and corresponds therefore to a collinear or soft configuration. In a condensed notation we can write the leading and the next-to-leading order contributions to the observable $\mathcal{O}$ in the following form

$$\langle \mathcal{O} \rangle^{LO} = \int_n \mathcal{O}_n d\sigma^B, \quad (2.5)$$

$$\langle \mathcal{O} \rangle^{NLO} = \int_{n+1} \mathcal{O}_{n+1} d\sigma^R + \int_n \mathcal{O}_n d\sigma^V. \quad (2.6)$$

$d\sigma^B$ denotes the Born contribution whose matrix elements are given by eq.(2.2), $d\sigma^V$ denotes the virtual contribution whose matrix elements are given by eq.(2.3)

and $d\sigma^R$ denotes the real contribution whose matrix elements are given by eq.(2.4). The individual NLO contributions are divergent only their sum is finite. To be able to perform the phase-space integration numerically with Monte Carlo methods one subtracts and adds a suitably chosen piece [65–68].

$$\langle\mathcal{O}\rangle^{NLO} = \int\limits_{n+1} \left(\mathcal{O}_{n+1}d\sigma^R - \mathcal{O}_n d\sigma^A\right) + \int\limits_n \left(\mathcal{O}_n d\sigma^V + \mathcal{O}_n \int\limits_1 d\sigma^A\right). \quad (2.7)$$

The subtraction term $d\sigma^A$ must match the real contribution in the divergent regions and must be easily integrable over the unresolved phase space that the integral can be performed analytically. By construction, the first term on the right hand side is integrable over the $n+1$-particle phase space and can therefore be evaluate numerically. The analytic result of the integrated subtraction term can be written as

$$\int\limits_1 d\sigma^A = \mathbf{I} \otimes d\sigma^B. \quad (2.8)$$

The $\otimes$ notation implies colour correlations due to colour charge operators. The insertion operator $\mathbf{I}$ contains the infrared poles obtained from integrating the real contribution over the unresolved phase space. These poles are cancelled by the infrared poles obtained from integrating the virtual contribution over the loop momentum. So far this is a well established procedure.

In the subtraction method one extends the idea of subtraction to the virtual part such that a numerical evaluation of the loop integral is possible. For this purpose we split the renormalised one-loop amplitude into the bare amplitude and the counter term.

$$\mathcal{A}^{(1)} = \mathcal{A}^{(1)}_{\text{bare}} + \mathcal{A}^{(1)}_{\text{CT}} \quad (2.9)$$

The bare contribution involves the one-loop integral

$$\mathcal{A}^{(1)}_{\text{bare}} = \int \frac{d^D k}{(2\pi)^D} \mathcal{G}^{(1)}_{\text{bare}} \quad (2.10)$$

where $\mathcal{G}^{(1)}_{\text{bare}}$ denotes the integrand of the bare one-loop amplitude. We introduce local subtraction terms for the divergences of the bare amplitude. With the subtraction terms eq.(2.9) reads

$$\mathcal{A}^{(1)}_{\text{bare}} + \mathcal{A}^{(1)}_{\text{CT}} = \left(\mathcal{A}^{(1)}_{\text{bare}} - \mathcal{A}^{(1)}_{\text{soft}} - \mathcal{A}^{(1)}_{\text{coll}} - \mathcal{A}^{(1)}_{\text{UV}}\right)$$
$$+ \left(\mathcal{A}^{(1)}_{\text{CT}} + \mathcal{A}^{(1)}_{\text{soft}} + \mathcal{A}^{(1)}_{\text{coll}} + \mathcal{A}^{(1)}_{\text{UV}}\right) \quad (2.11)$$

where $\mathcal{A}^{(1)}_{\text{soft}}$ denotes the subtraction term for the soft divergences, $\mathcal{A}^{(1)}_{\text{coll}}$ denotes the subtraction term for the collinear divergences and $\mathcal{A}^{(1)}_{\text{UV}}$ denotes the subtraction term for the ultraviolet divergences of the bare one-loop amplitude. These

subtraction terms match the bare amplitude in the divergent regions in D dimensions. Therefore we can integrate the first bracket on the right hand side of eq.(2.11) in $D = 4$ dimensions. We introduce the integral representation of the subtraction terms.

$$\mathcal{A}_{\text{soft}}^{(1)} = \int \frac{d^4 k}{(2\pi)^4} \mathcal{G}_{\text{soft}}^{(1)}, \qquad \mathcal{A}_{\text{coll}}^{(1)} = \int \frac{d^4 k}{(2\pi)^4} \mathcal{G}_{\text{coll}}^{(1)}, \qquad \mathcal{A}_{\text{UV}}^{(1)} = \int \frac{d^4 k}{(2\pi)^4} \mathcal{G}_{\text{UV}}^{(1)} \tag{2.12}$$

The contribution of the first bracket on the right hand side of eq.(2.11) to the virtual NLO corrections can be written as

$$\int 2 \operatorname{Re} \left[\mathcal{A}^{(0)*} \left(\mathcal{A}_{\text{bare}}^{(1)} - \mathcal{A}_{\text{soft}}^{(1)} - \mathcal{A}_{\text{coll}}^{(1)} - \mathcal{A}_{\text{UV}}^{(1)} \right) \right] \mathcal{O}_n d\phi_n$$
$$= \int d\phi_n \int \frac{d^4 k}{(2\pi)^4} 2 \operatorname{Re} \left[\mathcal{A}^{(0)*} \left(\mathcal{G}_{\text{bare}}^{(1)} - \mathcal{G}_{\text{soft}}^{(1)} - \mathcal{G}_{\text{coll}}^{(1)} - \mathcal{G}_{\text{UV}}^{(1)} \right) \right] \mathcal{O}_n + \mathcal{O}(\epsilon). \tag{2.13}$$

The integral on the right hand side is finite and contains by construction only integrable singularities. The integration over the n-particle phase space and the loop momentum can be performed together with a single Monte Carlo integration. The subtraction terms have a form that can be integrated analytically over the loop momentum k. The result can be written as

$$2 \operatorname{Re} \left[\mathcal{A}^{(0)*} \left(\mathcal{A}_{\text{CT}}^{(1)} + \mathcal{A}_{\text{soft}}^{(1)} + \mathcal{A}_{\text{coll}}^{(1)} + \mathcal{A}_{\text{UV}}^{(1)} \right) \right] d\phi_n = \mathbf{L} \otimes d\sigma^B. \tag{2.14}$$

The ultraviolet poles of $\mathcal{A}_{\text{CT}}^{(1)}$ and $\mathcal{A}_{\text{UV}}^{(1)}$ cancel each other. The insertion operator $\mathbf{L}$ contains the poles in the dimensional regularisation parameter ϵ from the infrared divergences of a one-loop amplitude. These poles cancel with the infrared poles from the real emission and therefore we have

$$(\mathbf{I} + \mathbf{L}) \otimes d\sigma^B = \text{finite}. \tag{2.15}$$

The NLO contribution can be written as a sum of three finite pieces each suitable for Monte Carlo integration.

$$\langle \mathcal{O} \rangle^{NLO} = \langle \mathcal{O} \rangle_{\text{real}}^{NLO} + \langle \mathcal{O} \rangle_{\text{virtual}}^{NLO} + \langle \mathcal{O} \rangle_{\text{insertion}}^{NLO} \tag{2.16}$$

The real contribution is

$$\langle \mathcal{O} \rangle_{\text{real}}^{NLO} = \int_{n+1} \left(\mathcal{O}_{n+1} d\sigma^R - \mathcal{O}_n d\sigma^A \right). \tag{2.17}$$

The virtual contribution is

$$\langle \mathcal{O} \rangle_{\text{virtual}}^{NLO} = \int d\phi_n \int \frac{d^4 k}{(2\pi)^4} \mathcal{O}_n 2 \operatorname{Re} \left[\mathcal{A}^{(0)*} \left(\mathcal{G}_{\text{bare}}^{(1)} - \mathcal{G}_{\text{soft}}^{(1)} - \mathcal{G}_{\text{coll}}^{(1)} - \mathcal{G}_{\text{UV}}^{(1)} \right) \right]. \tag{2.18}$$

The contribution from the insertion term is

$$\langle \mathcal{O} \rangle^{NLO}_{\text{insertion}} \quad = \quad \int_n \mathcal{O}_n \left(\mathbf{I} + \mathbf{L} \right) d\sigma^B. \tag{2.19}$$

We note that the one-loop integration and the phase-space integration in eq.(2.18) are done in a single Monte Carlo integration. For the sake of completeness we give the result of the sum of the insertion operator $\mathbf{L}$ and the insertion operator $\mathbf{I}$. In the massless case we have

$$
\begin{aligned}
\mathbf{I} + \mathbf{L} \quad = \quad & \frac{\alpha_s}{2\pi} \text{Re} \Bigg[\sum_i \sum_{j \neq i} \mathbf{T}_i \mathbf{T}_j \left(\frac{\gamma_i}{\mathbf{T}_i^2} \ln \frac{|2p_i p_j|}{\mu_{UV}^2} - \frac{\pi^2}{2} \theta(2p_i p_j) \right) \\
& + \sum_i \left(\gamma_i + K_i - \frac{\pi^2}{3} \mathbf{T}_i^2 \right) - \frac{(n-2)}{2} \beta_0 \ln \frac{\mu_{UV}^2}{\mu^2} \Bigg] + \mathcal{O}(\epsilon). \tag{2.20}
\end{aligned}
$$

In this formula μ is the renormalisation scale and μ_{UV} a scale used in the ultraviolet subtraction terms. In our algorithm we choose μ_{UV}^2 purely imaginary with $\text{Im}\left(\mu_{UV}^2 \right) < 0$ and therefore $\mu \neq \mu_{UV}$. $\mathbf{T}_i$ denotes the colour charge operator of particle i. We further have

$$
\begin{aligned}
\mathbf{T}_q^2 = \mathbf{T}_{\bar{q}}^2 = C_F, \qquad & \mathbf{T}_g^2 = C_A, \\
\gamma_q = \gamma_{\bar{q}} = \frac{3}{2} C_F, \qquad & \gamma_g = \frac{1}{2} \beta_0, \\
K_q = K_{\bar{q}} = \left(\frac{7}{2} - \frac{\pi^2}{6} \right) C_F, \qquad & K_g = \left(\frac{67}{18} - \frac{\pi^2}{6} \right) C_A - \frac{10}{9} T_R N_f, \tag{2.21}
\end{aligned}
$$

β_0 is the first coefficient of the QCD $\beta-$function and given by

$$\beta_0 \quad = \quad \frac{11}{3} C_A - \frac{4}{3} T_R N_f \tag{2.22}$$

and for the colour factors we have

$$C_A \quad = \quad N_c, \qquad C_F \quad = \quad \frac{N_c^2 - 1}{2N_c}, \qquad T_R \quad = \quad \frac{1}{2}. \tag{2.23}$$

2.3 Colour decomposition and kinematics

The subtraction method makes use of the fact that an QCD amplitude can be decomposes into colour factors and kinematic factors called partial amplitudes [70–74]. In this section we also define the kinematic of a one-loop amplitude which we use through out this thesis.
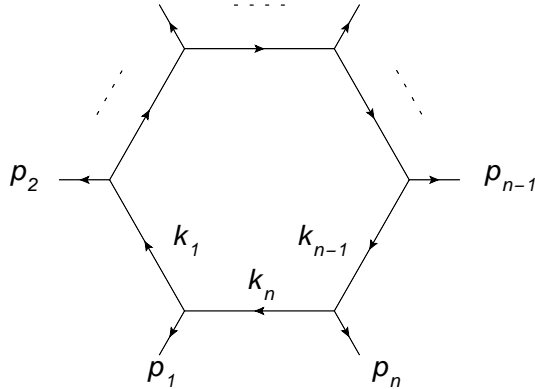
Figure 2.1: The labelling of the momenta of an one-loop primitive amplitude. The arrows denote the momenta flow.

At one-loop level one can decompose a partial amplitude further into primitive amplitudes. We write

$$\mathcal{A}^{(1)} = \sum_j C_j A_j^{(1)} \tag{2.24}$$

where the colour structures are denoted by C_j and the primitive amplitudes are denoted by $A_j^{(1)}$. A primitive amplitude is defined as a colour-stripped gauge-invariant set of Feynman diagrams with a fixed cyclic ordering of the external partons and a definite routing of the external fermion lines through the diagram [75].

The subtraction method exploits the properties of primitive amplitudes. The fixed cyclic ordering of the external partons ensures that only n different propagator occur in the loop, where n is the number of external particles. Therefore we have to take for the contour deformation only n propagators into account. In the construction of the infrared subtraction terms the method exploits explicitly the gauge invariance of primitive amplitudes and the fact that the type of each propagator in the loop is known, because of the definite routing of the external fermion lines thru the loop. In the following we focus on a single primitive amplitudes and keep in mind that we can reconstruct the full amplitude out of the the primitive amplitudes. Therefore we drop the index j in the primitive amplitude $A_j^{(1)}$.

Next we define the notation for a one-loop primitive amplitude $A^{(1)}$ which we use thru out this thesis. Because of the cyclic ordering only n propagators occur in the loop. We label the momenta clockwise by $p_1, p_2, \ldots, p_n$ and define

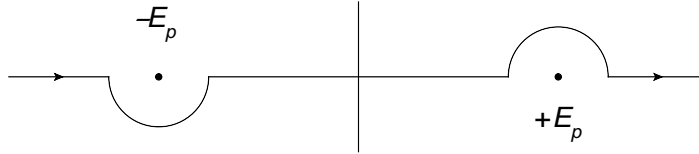$$q_i = \sum_{j=1}^{i} q_i \tag{2.25}$$

Figure 2.2: The Feynman boundary conditions predict the direction of the contour deformation.

The loop momenta are

$$k_i = k - q_i \tag{2.26}$$

For convenience we set

$$k_0 = k_n, \quad \text{and} \quad q_0 = q_n. \tag{2.27}$$

Due to momentum conversation we have

$$q_0 = q_n = 0. \tag{2.28}$$

For the bare contribution of an primitive one-loop amplitude we write

$$A_{\text{bare}}^{(1)} = \int \frac{d^D k}{(2\pi)^D} G_{\text{bare}}^{(1)}, \quad G_{\text{bare}}^{(1)} = P_{\text{bare}}(k) \prod_{i=1}^{n} \frac{1}{k_i^2 - m_i^2 + \imath\delta}. \tag{2.29}$$

$G_{\text{bare}}^{(1)}$ is the integrand of the primitive one-loop amplitude. $P_{\text{bare}}(k)$ is a polynomial in the loop momentum k. The $+\imath\delta$ is the so called Feynman prescription which follows from Feynman boundary conditions for Green functions. Feynman's boundary conditions are directly connected to the time ordering of field operators in the two-point correlation function. For the Klein Gordon theory we have

$$\langle 0|\mathbf{T}\phi(x)\phi(y)|0\rangle = D_F(x-y) = \int \frac{d^4 p}{(2\pi)^4} \frac{\imath}{p^2 - m^2 + \imath\delta} e^{-\imath p \cdot (x-y)} \tag{2.30}$$

The Feynman boundary conditions define how to close the integration contour or in other words in which direction we have to avoid the poles at $p^2 = m^2$. In the chapters 4 to 6 we present methods for a numerical implementation of a contour deformation predicted by Feynman's prescription for one- and multi-loop amplitudes.

2.4 Subtraction terms

In this section we give the results for the infrared subtraction terms and a construction rule for the ultraviolet subtraction terms. For massless QCD the sub-

traction terms for an primitive amplitude reads

$$G_{\text{soft}}^{(1)} = 4\imath \sum_{j \in I_g} \frac{p_j \cdot p_{j+1}}{k_{j-1}^2 k_j^2 k_{j+1}^2} A_j^{(0)} \tag{2.31}$$

$$G_{\text{coll}}^{(1)} = 4\imath \sum_{j \in I_g} \left[\frac{S_j g_{UV}(k_{j-1}^2, k_j^2)}{k_{j-1}^2 k_j^2} + \frac{S_{j+1} g_{UV}(k_j^2, k_{j+1}^2)}{k_j^2 k_{j+1}^2} \right] A_j^{(0)}. \tag{2.32}$$

The set I_g contains all the gluons circulating in the loop. $A_j^{(0)}$ is a partial tree level amplitude. If we take a subset of diagrams which contains gluon j in the loop and remove gluon j from all these diagrams we get a subset of tree diagrams. After removing copies of identical diagrams this subset forms the partial tree level amplitude $A_j^{(0)}$. The symmetry factor S_j is 1 if the external particle j is an fermion and 1/2 if the external particle is an gluon. The factor g_{UV} ensures the collinear subtraction term is ultraviolet finite. This implies the following properties for the function

$$\lim_{k_{j-1}||k_j} g_{UV}(k_{j-1}^2, k_j^2) = 1, \qquad \lim_{k \to \infty} g_{UV}(k_{j-1}^2, k_j^2) = \mathcal{O}\left(\frac{1}{|k|}\right) \tag{2.33}$$

One possible choice is

$$g_{UV}(k_{j-1}^2, k_j^2) = 1 - \frac{k_{j-1}^2 k_j^2}{[(k-Q)^2 - \mu_{UV}^2]}. \tag{2.34}$$

The fourvector Q is an arbitrary vector independent from the loop momenta and we can choose for its value whatever we want. The definition of Q depends on the method for the contour deformation that we use. In the Feynman deformation approach discussed in chapter 4 we have

$$Q = \frac{1}{x} \sum_{j=1}^{n} x_i q_i, \quad x = \sum_{j=1}^{n} x_i, \tag{2.35}$$

where the x_i are Feynman parameters. In the Direct deformation approach Q is not fixed but by applying advanced improvement techniques [6] we set

$$Q = \frac{1}{n} \sum_{j=1}^{n} q_j. \tag{2.36}$$

in the Direct deformation approach. The arbitrary scale μ_{UV}^2 we set purely imaginary and with $\text{Im}\left(\mu_{UV}^2\right) < 0$. This ensures that the UV-propagator

$$\frac{1}{(k-Q)^2 - \mu_{UV}^2} \tag{2.37}$$

introduce no additional singularities for the contour deformation. The infrared subtraction terms are also known for massive QCD [5]. They are formulated at amplitude level and are proportional to the corresponding Born amplitudes.

Analytic integration over the loop momentum yields for the infrared subtraction terms in massless QCD

$$
S_\epsilon^{-1} \mu^{2\epsilon} \int \frac{d^D k}{(2\pi)^D} G_{\text{soft}} = -\frac{1}{(4\pi)^2} \frac{e^{\epsilon\gamma_E}}{\Gamma(1-\epsilon)} \sum_{j \in I_g} \frac{2}{\epsilon} \left(\frac{-2p_j p_{j+1}}{\mu^2} \right)^{-\epsilon} A_j^{(0)} + \mathcal{O}(\epsilon),
$$

$$
S_\epsilon^{-1} \mu^{2\epsilon} \int \frac{d^D k}{(2\pi)^D} G_{\text{coll}} = -\frac{1}{(4\pi)^2} \frac{e^{\epsilon\gamma_E}}{\Gamma(1-\epsilon)} \sum_{j \in I_g} (S_j + S_{j+1}) \frac{2}{\epsilon} \left(\frac{\mu_{UV}^2}{\mu^2} \right)^{-\epsilon} A_j^{(0)} + \mathcal{O}(\epsilon),
$$

$$
\tag{2.38}
$$

with

$$
S_\epsilon = (4\pi)^\epsilon e^{-\epsilon\gamma_E} \tag{2.39}
$$

where γ_E denotes the Euler-Mascheroni constant, μ denotes the renormalisation scale in dimensional regularisation and ϵ is defined by $D = 4 - 2\epsilon$.

The subtraction term for the ultraviolet divergence can be constructed as followed. In QCD only vertex and propagator corrections are ultraviolet divergent. For each such divergent subgraph we construct a subtraction term. If these subtraction terms are known for once the full UV subtraction term can be constructed recursively. The UV subtraction term for a vertex or propagator correction are obtained by expanding the relevant propagators of the diagram around the ultraviolet propagator defined in eq.(2.37). For a single propagator we have

$$
\frac{1}{(k-p)^2 - m^2} = \frac{1}{\bar{k} - \mu_{UV}^2} + \frac{2\bar{k} \cdot (p-Q)}{\left(\bar{k}^2 - \mu_{UV}^2 \right)^2} - \frac{(p-Q)^2 - m^2 + \mu_{UV}^2}{\left(\bar{k}^2 - \mu_{UV}^2 \right)^2}
$$
$$
+ \frac{\left[2\bar{k} \cdot (p-Q) \right]^2}{\left(\bar{k}^2 - \mu_{UV}^2 \right)^3} + \mathcal{O}\left(\frac{1}{|k|^5} \right). \tag{2.40}
$$

If we replace the propagators in the vertex or propagators correction for which we like to construct the subtraction term by these expansion, the resulting expression matches the original expression in the ultraviolet limit. We can add finite terms to the subtraction term such that the finite piece of the integrated subtraction term is independent of Q and has the same prefactor as the $1/\epsilon$ pole. The integrated subtraction term have the form

$$
c \left(\frac{1}{\epsilon} - \ln \left(\frac{\mu_{UV}^2}{\mu^2} \right) \right) + \mathcal{O}(\epsilon) \tag{2.41}
$$

where c depends on for which vertex or propagator correction we construct the subtraction term. The form of the integrated subtraction ensures that the sum of all integrated UV subtraction terms is again proportional to a tree-level amplitude.

In this chapter we presented an efficient way for the calculation of observables at NLO level by extending the idea of subtraction known from the real emission

part to the virtual part. In the next chapter we discuss an efficient way of calculating the required amplitudes due method based on recurrence relations. In the following chapters we discuss the numerical calculation of loop integrals i.e. contour deformation in full detail.

3 Recursion relations

In this chapter we illustrate the construction of partial tree-level amplitudes, one- and two-loop primitive amplitudes and the ultraviolet subtraction term with Berends-Giele type recurrence relations.

3.1 Introduction

In the final formula eq.(2.17-2.19) of the subtraction method presented in the previous chapter only amplitudes occur. An efficient method to calculate the necessary amplitudes is based on recurrence relations. We review the recurrence method for the tree-level partial amplitudes [63] and for the primitive one-loop amplitudes [64]. These are the amplitudes needed for the subtraction method at NLO level. The recurrence relations for the primitive two-loop amplitude are new and are needed in a future extension of the subtraction method at NNLO level.

Berends-Giele type recurrence relations build partial tree-level amplitudes from colour ordered off-shell currents. An off-shell current is an object with n on-shell legs and one off-shell leg. The momentum of the off-leg is given by the sum of the momenta of the on-shell legs. Therefore momentum conservation is satisfied.

At tree-level recurrence relations relate off-shell currents with n on-shell legs to off-shell currents with fewer on-shell legs. At one-loop level the recurrence relations relate a one-loop off-shell current with n on-shell legs to a tree-level off-shell current and a one-loop off-shell current with fewer on-shell legs. It is also possible that the one-loop off-shell current couples directly to the loop. If the one-loop off-shell current couples directly to the loop we cut one of the propagators and introduce recurrence relations for off-shell currents with n on-shell legs and two off-shell legs, where the additional off-shell leg corresponds to the cut loop propagator. We note that the recurrence relations for the one-loop off-shell currents correctly avoid currents corresponding to diagrams which include an external self energy.

The generalisation to the two-loop level is almost straightforward. For the moment we restrict ourself to the calculation of an two-loop amplitude in the lead-

ing colour approximation. Therefore only configurations corresponding to planar diagrams are considered. The recurrence relations at two-loop level correctly calculate off-shell currents corresponding to the so called bow-tie diagrams. At two-loop level one needs recurrence relations for one-loop off-shell currents with n on-shell legs and two off-legs and recurrence relations for tree-level off-shell currents with n on-shell legs and three off-shell legs. The additional off-shell legs correspond to cut loop propagators. Again, external self energies are avoided correctly by the recurrence relations for the two-loop off-shell currents.

For the sake of simplification we use a toy model to discuss the recurrence relations. For the toy model we choose purely gluonic QCD without the four-gluon vertex. Therefore only the three-gluon vertex occurs in the calculation.

From an off-shell current one recovers the corresponding on-shell amplitude by removing the extra propagator, taking the off-shell leg on-shell and contracting the appropriate polarisation vector.

$$A_n^{(0)} = \epsilon_\mu^{\lambda_n}(p_n) \imath p_n^2 J^{\mu(0)}(1, n-1) \tag{3.1}$$

ϵ_μ^λ is the polarisation vector of the gluon corresponding to the polarisation λ. $A_n^{(0)}$ is the tree-level partial amplitude corresponding to n external particles. At loop level we are interested in the integrand of the primitive amplitude $A_n^{(l)}$, therefore we drag the loop integration out of the recurrence relation. We have

$$G_n^{(l)} = \epsilon_\mu^{\lambda_n}(p_n) \imath p_n^2 J^{\mu(l)}(1, n-1) \tag{3.2}$$

where $G_n^{(l)}$ is the integrand of an l-loop primitive amplitude with n external particles.

$$A_n^{(l)} = \int \prod_{i=1}^{l} \frac{d^D k^{(i)}}{(2\pi)^D} G_n^{(l)}. \tag{3.3}$$

In the following discussion we drop the dependence of the off-shell currents from the loop momenta in the notation.

3.2 Tree-level recursion

At tree-level the recurrence starts for $n = 1$ and the off-shell current is just the polarisation vector.

$$J_\mu^{(0)}(m, m) = \epsilon_\mu^{\lambda_m}(p_m). \tag{3.4}$$

The pictorial view of the tree-level recurrence relations is given by

(3.5)

The blob on the left hand side represents the sum of all possible tree-level diagrams. On the right hand side we sum over all vertices, in our toy model this is only the three-gluon vertex, involving the off-shell leg and off-shell currents with less external legs. In formula this reads

$$J_\mu^{(0)}(m,n) = -\frac{ig_{\mu\alpha}}{(P_{m,n})^2} \sum_{i=m}^{n-1} V^{\alpha\beta\gamma}(-P_{m,n}, P_{m,i}, P_{i+1,n}) J_\beta^{(0)}(m,i) J_\gamma^{(0)}(i+1,n)$$

(3.6)

where $V^{\mu\nu\rho}$ is the three-gluon vertex in colour ordered Feynman rules, see appendix A. The momenta $P_{i,j}$ are defined by

$$P_{i,j} = p_i + p_{i+1} + \ldots + p_j.$$

(3.7)

3.3 One-loop recursion

At pictorial view of the one-loop recurrence relation is given by

(3.8)

where the blob with the extra hole on the left hand side represents the sum over all possible one-loop diagrams. On the right hand side we sum over all possibilities

to connect the off-shell leg to a tree-level off-shell current and a one-loop off-shell current, plus the diagram where the off-shell leg connects directly to the loop. If the off-shell current couples directly to the loop we cut one line in the loop by introducing pseudo polarisation vectors.

$$\tag{3.9}$$

The pseudo polarisation vectors are defined by

$$g_{\mu\nu} \;=\; \sum_{i=1}^{4} s_{\mu}^{(i)} s_{\nu}^{(i)} \tag{3.10}$$

$$s^{(0)} \;=\; (1,0,0,0), \qquad s^{(1)} \;=\; (0,\imath,0,0),$$
$$s^{(2)} \;=\; (0,0,\imath,0), \qquad s^{(3)} \;=\; (0,0,0,\imath). \tag{3.11}$$

We replace the tensor structure of the line by a sum over pseudo polarisation vectors. In formula the recurrence relations for the one-loop off-shell current reads

$$\begin{aligned}
J_{\mu}^{(1)}(m,n) \;=\; & -\frac{\imath g_{\mu\alpha}}{\left(P_{m,n}\right)^2}\Bigg[\sum_{i=m}^{n-2} V^{\alpha\beta\gamma}(-P_{m,n}, P_{m,i}, P_{i+1,n}) J_{\beta}^{(0)}(m,i) J_{\gamma}^{(1)}(i+1,n) \\
& + \sum_{i=m+1}^{n-1} V^{\alpha\beta\gamma}(-P_{m,n}, P_{m,i}, P_{i+1,n}) J_{\beta}^{(1)}(m,i) J_{\gamma}^{(0)}(i+1,n) \\
& + \sum_{a=1}^{4} V^{\alpha\beta\gamma}(-P_{m,n}, -k_n, k_{m-1}) s_{\beta}^{(a)} J_{\gamma}^{(0,1)}(m,n;a) \Bigg]
\end{aligned} \tag{3.12}$$

where the loop momentum is denoted by k. In the last line we introduce the tree-level off-shell current with one extra off-shell leg $J^{(0,1)}$. The recurrence relations for $J^{(0,1)}$ are analogous to the tree-level recurrence relations but the recurrence starts with $n = 0$ on-shell legs. At the start of the recurrence for $J^{(0,1)}$ we close the loop which we previously cut and $J^{(0,1)}$ is just the pseudo polarisation vector times the loop propagator corresponding to the cut line.

$$J_{\mu}^{(0,1)}(m,m-1;a) \;=\; -\frac{\imath s_{\mu}^{(a)}}{\left(k_{m-1}\right)^2} \tag{3.13}$$

A pictorial view of the recurrence relation for the tree-level off-shell current with one extra off-shell leg is given by

$$(3.14)$$

and is pretty similar to the normal tree-level recursion relation shown in eq.(3.5). In formula this reads

$$J^{(0,1)}(m,n;a) \;=\; -\frac{\imath g_{\mu\alpha}}{k_n^2} \sum_{i=m-1}^{n-1} V^{\alpha\beta\gamma}(k_n, -k_i, P_{i+1,n}) J_\beta^{(0,1)}(m,i;a) J_\gamma^{(0)}(i+1,n).$$

$$(3.15)$$

We note that in the recurrence relations eq.(3.8) and eq.(3.12), only one-loop off-shell currents with at least two on-shell particles are connected to the off-shell leg and therefore diagrams with external self energies do not contribute. One would also produce an external self energy diagram if in eq.(3.14) and eq.(3.15) the tree-level off-shell current connected to the tree-level off-shell current with one extra off-shell leg contained $n-1$ on-shell legs where n is the number of the external particles of the considered amplitude. In this case we set the corresponding tree level off-shell current to zero.

3.4 Two-loop recursion

If we connect two lines circulating in an one-loop diagram by another line the result is obviously a planar two-loop diagram. We call this connecting line the internal loop line. To get all planar two-loop diagrams one takes all possible one-loop diagrams with all possible connections of internal loop lines. What is left are the diagrams where the two loops are separated by tree-level type diagrams. These are the so called bow-tie diagrams.

The pictorial view of the recurrence relations for the two-loop off-shell current

3 Recursion relations

is given by

$$ \tag{3.16} $$

where the blob on the left hand side represents the sum over all planar two-loop diagrams. On the right hand side we sum over all possibilities to connect the off-shell leg to a tree-level off-shell current and a two-loop off-shell current or to two one-loop off-shell currents, plus the diagram where the off-shell leg connects directly to the loop. The recurrence relations for the two-loop off-shell currents take the bow-tie diagrams where the two loops are separated by a tree-level diagram into account. Analogously to the one-loop recurrence relations we cut a loop line by introducing pseudo polarisation vectors.

$$ \tag{3.17} $$

In formula the two-loop off-shell recurrence relations reads

$$
\begin{aligned}
J_\mu^{(2)}(m,n) &= -\frac{\imath g_{\mu\alpha}}{(P_{m,n})^2}\Bigg[\sum_{i=m}^{n-2} V^{\alpha\beta\gamma}(-P_{m,n}, P_{m,i}, P_{i+1,n}) J_\beta^{(0)}(m,i) J_\gamma^{(2)}(i+1,n) \\
&\quad + \sum_{i=m+1}^{n-1} V^{\alpha\beta\gamma}(-P_{m,n}, P_{m,i}, P_{i+1,n}) J_\beta^{(2)}(m,i) J_\gamma^{(0)}(i+1,n) \\
&\quad + \sum_{i=m+1}^{n-2} V^{\alpha\beta\gamma}(-P_{m,n}, P_{m,i}, P_{i+1,n}) J_\beta^{(1)}(m,i) J_\gamma^{(1)}(i+1,n) \\
&\quad + \sum_{a=1}^{4} V^{\alpha\beta\gamma}(-P_{m,n}, -k_n^{(1)}, k_{m-1}^{(1)}) s_\beta^{(a)} J_\gamma^{(1,1)}(m,n;a)\Bigg]
\end{aligned}
$$

$$ \tag{3.18} $$

where the loop momenta are denoted by $k^{(1)}$ and $k^{(2)}$. In the last line we introduce the one-loop off-shell current with one extra off-shell leg $J^{(1,1)}$. The pictorial view of the recurrence relation for $J^{(1,1)}$ is given by

$$(3.19)$$

which is analogous to the recurrence relation for the one-loop off-shell current $J^{(1)}$. In the last diagram on the right hand side of eq.(3.19) we cut the second loop line by introducing pseudo polarisation vectors. This second cut corresponds to the cut of the internal loop line whose momentum is given by $k^{(1)} - k^{(2)}$.

$$(3.20)$$

In formula the recurrence relations for the one-loop off-shell current with one extra leg reads

$$
\begin{aligned}
J_\mu^{(1,1)}(m,n;a) &= -\frac{\imath g_{\mu\alpha}}{\left(k_n^{(1)}\right)^2}\Bigg[\sum_{i=m-1}^{n-1} V^{\alpha\beta\gamma}(k_n^{(1)}, -k_i^{(1)}, P_{i+1,n}) J_\beta^{(1,1)}(m,i;a) J_\gamma^{(0)}(i+1,n) \\
&\quad + \sum_{i=m-1}^{n-1} V^{\alpha\beta\gamma}(k_n^{(1)}, -k_i^{(1)}, P_{i+1,n}) J_\beta^{(0,1)}(m,i;a) J_\gamma^{(1)}(i+1,n) \\
&\quad + \sum_{b=1}^{4} V^{\alpha\beta\gamma}(k_n^{(1)}, -k_n^{(2)}, k^{(2)} - k^{(1)}) s_\beta^{(b)} J_\gamma^{(0,2)}(m,n;a,b) \Bigg]
\end{aligned}
$$

$$(3.21)$$

In the last line of eq.(3.21) we introduce the tree-level off-shell current with two extra off-shell legs $J^{(0,2)}$. A pictorial view of the recurrence relation for $J^{(0,2)}$ is

given by

which is the normal tree-level recurrence relation plus the diagram where we close one of the loops. In formula this reads

$$
\begin{aligned}
J_\mu^{(0,2)}(m,n;a,b) \;=\; & -\frac{i g_{\mu\alpha}}{\left(k_n^{(2)}\right)^2}\Bigg[\, \sum_{i=m-1}^{n-1} V^{\alpha\beta\gamma}(k_n^{(2)},-k_i^{(2)},P_{i+1,n})J_\beta^{(0,2)}(m,i;a)J_\gamma^{(0)}(i+1,n) \\
& -\frac{i}{(k^{(2)}-k^{(1)})^2}V^{\alpha\beta\gamma}(k_n^{(2)},k^{(1)}-k^{(2)},-k_n^{(1)})s_\beta^{(b)}J_\gamma^{(0,1)}(m,n;a)\Bigg]
\end{aligned}
$$

$$(3.23)$$

The recurrence relation for the remaining tree-level off-shell current with one extra off-shell leg $J^{(0,1)}$ was defined in the previous section. We note that for the new objects $J^{(0,2)}$ or $J^{(1,1)}$ no extra recurrence start conditions are needed.

To avoid diagrams corresponding to external self energies in eq.(3.16) and eq.(3.19) we connect the off-shell leg only with one- and two-loop off-shell currents with at least two on-shell legs. Furthermore we set the one-loop off-shell current in eq.(3.19) and the tree-level off-shell current in eq.(3.22) to zero if these currents contain $n-1$ on-shell legs where n is the number of external particles of the considered amplitude, to avoid external self energy diagrams.

3.5 UV-subtraction recursion

In this section we discuss the recursive calculation of the subtraction term for the ultraviolet divergences. The calculation is based on a tree-level recurrence relation where we insert the local subtraction terms for the divergent vertex and propagator corrections at the right spots. Therefore the calculation works along the lines of the calculation of counter terms in renormalisation theory with the difference that our subtraction terms are local in the loop momentum. The

pictorial view of the recurrence relations for the UV subtraction term is given by

$$(3.24)$$

where the cross represent ultraviolet divergent subgraphs. In formula this reads

$$
\begin{aligned}
J_\mu^{(UV)}(m,n) \;=\; & -\frac{\imath g_{\mu\alpha}}{(P_{m,n})^2}\Bigg[\sum_{i=m}^{n-2} V^{\alpha\beta\gamma}(-P_{m,n},P_{m,i},P_{i+1,n})J_\beta^{(0)}(m,i)J_\gamma^{(UV)}(i+1,n) \\
& + \sum_{i=m+1}^{n-1} V^{\alpha\beta\gamma}(-P_{m,n},P_{m,i},P_{i+1,n})J_\beta^{(UV)}(m,i)J_\gamma^{(0)}(i+1,n) \\
& + \sum_{i=m}^{n-1} S_V^{\alpha\beta\gamma}(-P_{m,n},P_{m,i},P_{i+1,n})J_\beta^{(0)}(m,i)J_\gamma^{(0)}(i+1,n) \\
& + S_P^{\alpha\beta}(P_{m,n})J_\beta^{(0)}(m,n)\Bigg]
\end{aligned}
$$

$$(3.25)$$

where we introduce the local subtraction terms for the vertex corrections $S_V^{\alpha\beta\gamma}$ and the propagator corrections $S_P^{\alpha\beta}$. We note that there are subtraction terms for the leading and the sub-leading colour contributions of the vertex and propagator corrections separately. Which subtraction term we insert in the recurrence relation depends on the considered primitive amplitude.
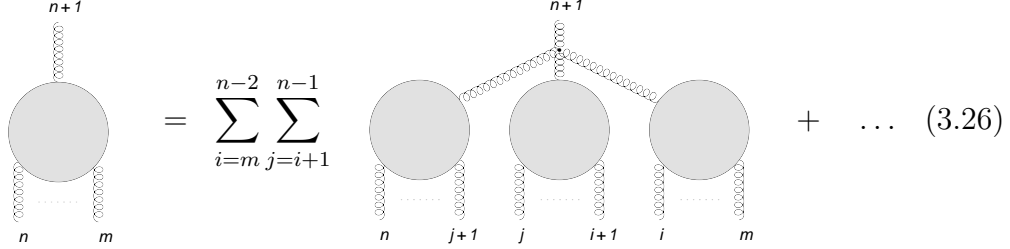
Because in our calculation no external self energies occur we set the tree-level current in last diagram on the right hand side in eq.(3.24) to zero if it contains $n-1$ on-shell legs where n the total number of on-shell legs of the primitive amplitude is.

3.6 Full QCD recursion

In this section we provide the reader with guiding principles to extend the recurrence relations of the previous sections to full QCD.
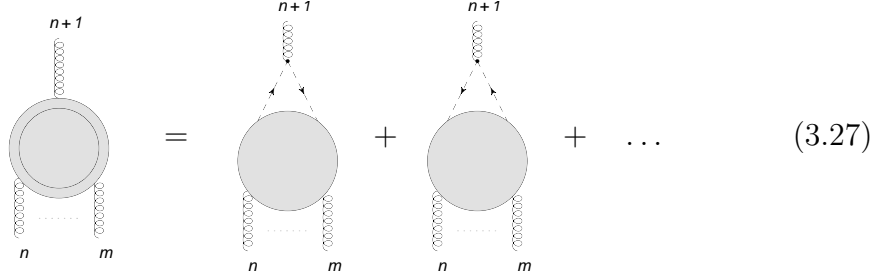
In full QCD we have to add diagrams to the gluon off-shell currents which corresponds to diagrams where the off-shell leg couples via a four-gluon vertex to the off-shell currents. For the gluon tree-level recurrence relations we get additional four-gluon contributions, for example
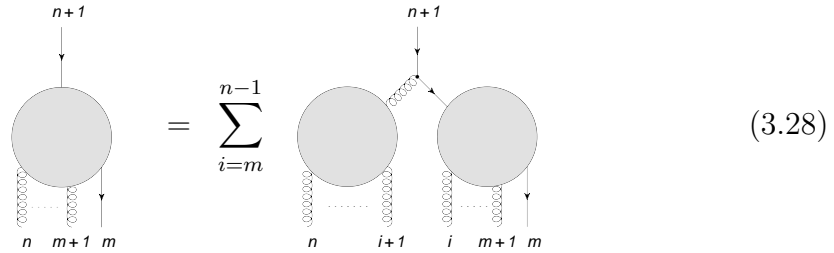
$$= \sum_{i=m}^{n-2} \sum_{j=i+1}^{n-1} \qquad\qquad\qquad + \quad \dots \quad (3.26)$$

If an gluon off-shell current couples directly to the loop we add a diagram where the gluon splits into two ghost lines. Because the ghost propagator contains no non-trivial tensor structure we need no pseudo polarisation vectors for the cut of a ghost line. We note that to reproduce the correct integrand of the primitive amplitude one has to sum over both contributions given by the direction of the fermion flow, right and left with respect to the ghost loop. For the gluon one-loop off-shell current we get the additional ghost contributions to the one-loop gluon off-shell current.
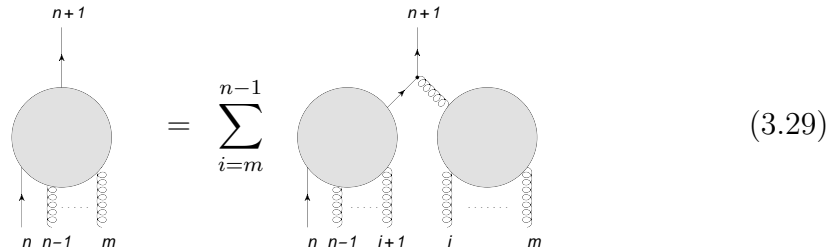
$$= \qquad + \qquad + \quad \dots \qquad (3.27)$$

In full QCD we have to consider fermion currents. Similar to the gluon currents one can write down recurrence relations for the quark and antiquark currents [6]. At tree-level with only a single fermion line we have for the quark current

$$= \sum_{i=m}^{n-1} \qquad\qquad\qquad\qquad (3.28)$$

and for the antiquark current we have

$$= \sum_{i=m}^{n-1} \qquad\qquad\qquad\qquad (3.29)$$

In formula the recurrence relation for the quark current reads

$$\bar{U}^{(0)}(m,n) \;\; = \;\; \imath \sum_{i=m}^{n-1} \bar{U}^{(0)}(m,i) V_{qg\bar{q}}^{\mu} J_{\mu}^{(0)}(i+1,n) \frac{\not{P}_{m,n}}{P_{m,n}^2} \tag{3.30}$$

and for the antiquark current

$$V^{(0)}(m,n) \;\; = \;\; -\imath \frac{\not{P}_{m,n}}{P_{m,n}^2} \imath \sum_{i=m}^{n-1} V_{qg\bar{q}}^{\mu} J_{\mu}^{(0)}(m,i) V^{(0)}(i+1,n) \tag{3.31}$$

where $V_{qg\bar{q}}$ denotes the colour ordered quark gluon vertex. We note that the objects $\bar{U}^{(0)}, V^{(0)}, V_{qg\bar{q}}$ and $\not{P}$ are matrices in Dirac space and their positions in the formula are relevant. The recurrence starts at

$$\bar{U}^{(0)}(m,m) \;\; = \;\; \bar{u}(p_m), \qquad V^{(0)}(m,m) \;\; = \;\; v(p_m). \tag{3.32}$$

The partial amplitude corresponding to a fermion off-shell current is recovered by removing the extra fermion propagator, taking the off-shell leg on-shell and contracting from the right with an antiquark spinor in the case of a quark current and otherwise contracting from the left with a quark spinor.

$$\begin{aligned}
A^{(0)}(1_q, 2, \dots, n-1, n_{\bar{q}}) \;\; &= \;\; \imath \bar{U}^{(0)}(1, n-1) \not{p}_n v(p_n) \\
&= \;\; -\imath u(p_1) \not{p}_1 V^{(0)}(2, n)
\end{aligned} \tag{3.33}$$

If we want to calculate the integrand of an primitive amplitude including fermions it can be necessary to cut a fermion line. To this end we rewrite the numerator of an off-shell fermion propagator as the sum of two on-shell contributions and express these on-shell contributions by corresponding Dirac spinors.

$$\not{k} \;\; = \;\; \not{k}^{\flat} + \frac{k^2}{2k \cdot q} \not{q}, \qquad k^{\flat} \;\; = \;\; k - \frac{k^2}{2k \cdot q} q \tag{3.34}$$

where q is an arbitrary light-like vector. $k^{\flat}$ is by construction light-like and we can replace the complicated tensor structure again in our calculation by a simple polarisation sum

$$\not{k}^{\flat} \;\; = \;\; \sum_{\lambda=\pm} u(k^{\flat}, \lambda) \bar{u}(k^{\flat}, \lambda), \qquad \not{q} \;\; = \;\; \sum_{\lambda=\pm} u(q, \lambda) \bar{u}(q, \lambda). \tag{3.35}$$

With the recurrence relations present in this chapter all tools for an efficient implementation of partial/primitive amplitudes up to two-loop level and the local subtraction terms for the one-loop primitive amplitude are provided. We expect that the local subtraction terms for an two-loop primitive amplitude can be constructed similarly but the local subtraction terms for the vertex and propagator corrections at two-loop level are not known yet.

4 Feynman deformation

In this chapter we discuss the numerical integration of an one-loop integral avoiding threshold singularities by deforming integration variables into the complex plane. In this chapter we dicuss an method based on Feynman parametrisation.

4.1 Introduction

If we calculate higher order corrections, different kinds of singularities occur, at different steps of the calculation. In chapter 2 we have seen that already in next-to-leading order (NLO) calculations singularities occur. A one-loop integral contain in general ultraviolet (UV) and infrared (IR) singularities. Integration over the unresolved phase space of a massless particle also leads to IR singularities. And there exist integrable singularities where one or more propagator in the loop go on-shell, these singularities we call threshold singularities. The IR and UV singularities can be regularised by dimensional regularisation, such that they appear as poles in $1/\epsilon$. If we combine all higher order calculations to a physical observable all the $1/\epsilon$ poles are cancelled order by order. By renormalisation of the parameters in the Lagrangian of our theory one can deal with the UV poles and the Kinoshita, Lee, Nauenberg (KLN) theorem [53; 54] tells us that the IR poles from the real emission cancel with the IR poles from the loop integrals.

However one has to extract the poles before these cancellations can be performed. In the method presented in this thesis we do this by subtraction, in the sense that we construct local subtraction terms which match our original complicated integrand in the IR and UV limit. The $1/\epsilon$ poles of these subtraction terms are easily calculable. In a loop calculation after subtraction one can introduce Feynman parameters to simplify the denominator structure and perform the loop and Feynman parameter integration numerically.

As a further motivation for the numerical calculation of Feynman parameter integrals we would like to mention a method called Sector decomposition [55–57]. In this method one factorises the $1/\epsilon$ poles from a complicated multi parameter integral such that one can easily extract the poles. For example in a multi loop integral one can introduce Feynman parameters such that one can perform the loop integration analytically, then use Sector decomposition to factorise the

poles and extract them. The remaining Feynman parameter integral can then be performed numerically [58].

In both methods, after one removed the IR and UV poles, one still has to deal with integrable threshold singularities. Even these singularities are integrable they lead to numerical instabilities. But one can avoid these singularities by deforming the integration contour into the complex plane. The direction of the deformation is defined by Feynman's $+i\delta$ prescription.

The method of contour deformation for a numerically loop integration was first introduced in [7] and later on it has been refined in different ways to be applied to one-loop [4; 5; 8–13] and to two-loop [14–17] calculations. In all these methods one deforms the integration contour by adding a purely imaginary functions to the real integration variables, $x_i \rightarrow \tilde{x}_i := x_i + if_i(x)$, where x_i can be a Feynman parameter or a component of a loop momenta. When deforming the integration contour in this way we make use of the multidimensional version of Cauchy's theorem which is widely used in one dimension. A simple proof of the multidimensional version of Cauchy's theorem is given in [7].

We combined the subtraction method presented in chapter 2 with contour deformation. Here we discuss the method where we parametrise our one-loop integral with Feynman parameters after subtraction of the IR and UV singularities. The introduction of Feynman parameters simplifies the denominator enormously and the contour deformation is rather simple. But there are also drawbacks. We investigate that for a high jet multiplicity, non-leading Landau singularities lead to numerical instabilities. An important part of this chapter is the discussion of improving the numerical stability of the Monte Carlo integration. It is likely that some of these improvements also work for the Feynman parameter integral which occur in the method based on Sector decomposition but this is not tested in this thesis.

4.2 General framework

In chapter 2.2 we discussed the subtraction method. After we subtracted out the UV and IR singularities from our one-loop integral we still cannot simply integrate the real loop momenta k^μ from minus infinity to plus infinity, because along the real axis one or more propagators can be on shell. As long as these singularities are not pinched we can avoid them by deforming the integration into the complex plane. Pinched singularities either correspond to IR singularities and are treated with the corresponding subtraction terms or integrable singularities. The contour deformation is not unique. There are many different choices which deform the contour correctly. The problem is to find a deformation which is suitable for Monte Carlo integration. Most deformations will lead to large

cancellations in different integration regions and therefore to large Monte Carlo errors. We construct a numerically stable deformation by the following steps.

First we introduce Feynman parameters as additional integration variables. This transforms the n singular region of the n propagators into a single region. For this single region a deformation of the loop momentum k can be easily done.

Secondly we have to deform the Feynman parameters into the complex plane because for vanishing loop momentum the deformation of the loop momentum vanishes too. The deformation of the Feynman parameters vanishes whenever Landau's equations [60] are satisfied.

Thirdly we have to introduce some techniques to improve numerical stability. The complete deformation vanishes when the loop momentum is zero and Landau's equations are satisfied for the Feynman parameters. For a large number of external particles this leads to numerical instabilities. The disadvantage of the Feynman parameter approach is that the power of the denominator rises linearly with the number of external particles. Therefore a singularity with $n_{sing} < n$ on-shell propagators is enhanced by Feynman parametrisation and leads to numerical instabilities for large n, where n is the number of external particles. To improve the numerical behaviour we expand our propagators around some small purely imaginary mass. To improve stability further we split the integration into different integration channels and choose for each channel a certain mapping of the Feynman parameters to "flatten" the integrand.

With the subtraction method one can write the integrand of the one-loop amplitude after we apply the local subtraction terms in the following way

$$
G_{bare}^{(1)} - G_{soft}^{(1)} - G_{coll}^{(1)} - G_{UV}^{(1)} \;\; = \;\; \frac{P(k)}{\prod\limits_{j=1}^{n} (k_j^2 - m_j^2 + \imath\delta)} + \frac{P_{UV}(k)}{(\bar{k}^2 - \mu_{UV}^2 + \imath\delta)^{n_{UV}}} \quad (4.1)
$$

with

$$
k_j \;\; = \;\; k - q_j, \qquad q_j \;\; = \;\; \sum_{a=1}^{j} p_a \qquad \text{and} \qquad \bar{k} \;\; = \;\; k - Q, \qquad (4.2)
$$

where $P(k)$ and $P_{UV}(k)$ are polynomials in the loop momenta k and the p_a's are the momenta of the external particles. Q and μ_{UV} are free parameters. $G_{bare}^{(1)}$ and $G_{soft}^{(1)}$ only contributes to the first term, $G_{UV}^{(1)}$ only contributes to the second term and $G_{coll}^{(1)}$ contributes to both terms in eq.(4.1). The real integer n_{UV} is defined by the UV behaviour of the *bare* one-loop amplitude and is chosen such that the subtracted integrand decrease at least like $1/|k|^5$ for large $|k|$. In the second term on the right hand side of eq.(4.1) singularities only occur on the single cone $\bar{k}^2 - \mu_{UV}^2 = 0$ and are therefore easy to handle. Further we choose μ_{UV}^2 purely

imaginary, by doing this we move the singular region of the UV propagator away from the integration contour.

In the construction of the contour deformation we only have to take into account the n physical propagators. We rewrite the above integrand into simpler form

$$\frac{P(k)}{\prod\limits_{j=1}^{n}(k_j^2 - m_j^2 + \imath\delta)} + \frac{P_{UV}(k)}{(\bar{k}^2 - \mu_{UV}^2 + \imath\delta)^{n_{UV}}} = \frac{R(k)}{\prod\limits_{j=1}^{n}(k_j^2 - m_j^2 + \imath\delta)} \quad (4.3)$$

where

$$R(k) = P(k) + P_{UV}(k)\frac{\prod\limits_{j=1}^{n}(k_j^2 - m_j^2 + \imath\delta)}{(\bar{k}^2 - \mu_{UV}^2 + \imath\delta)^{n_{UV}}}. \quad (4.4)$$

4.2.1 Feynman integrals

For the contour deformation we consider a Feynman integral of the following form

$$I = \int \frac{d^4k}{(2\pi)^4} \frac{R(k)}{\prod\limits_{i=1}^{n}(k_i^2 - m_i^2 + \imath\delta)}, \quad (4.5)$$

where the numerator function $R(k)$ is a polynomial in the loop momentum k. The integral above corresponds to a one-loop amplitude with n external particles. The $+\imath\delta$ prescription indicates the direction of the deformation. In the next step we introduce Schwinger parametrisation. Then we deform the loop momentum and the Schwinger parameters into the complex plane. One could start directly with Feynman parameters but the detour with Schwinger parameters has certain advantages. First we can close the contour at plus infinity and can therefore neglect boundary terms. Secondly, we do not have to deal with a delta distribution in the integrand and therefore the correct Jacobian is easier to calculate. After the deformation we integrate out one Schwinger parameter and get an equivalent formula to the Feynman parametrisation. With a certain mapping of the Feynman parameters we avoid the integration over the delta distribution such that the integral is suitable for numerical integration.

We now introduce Schwinger parametrisation. Assume that A and δ are real numbers, then we have

$$\frac{1}{A \pm \imath\delta} = \mp\imath \int\limits_{0}^{\infty} dt\, e^{\pm\imath t(A\pm\imath\delta)}. \quad (4.6)$$

We note that we do not perform any algebraic manipulation of the numerator function in eq.(4.5). To simplify the notation we set the numerator to 1 and

neglect the $+i\delta$ prescription for the moment. We rewrite the integrand of a scalar n point function with the help of the Schwinger parametrisation.

$$\frac{1}{\prod\limits_{i=1}^{n}\left(k_i^2-m_i^2\right)} \;=\; (-i)^n \int d^n t\, \exp\left\{i\sum_{i=1}^{n} t_i\left(k_i^2-m_i^2\right)\right\} \tag{4.7}$$

We introduce the matrix

$$S_{ij} \;=\; \left(q_i-q_j\right)^2 - m_i^2 - m_j^2 \tag{4.8}$$

which depends only on the kinematic variables of the external particles. With this matrix we can write the argument of the exponential function in eq.(4.7) in the following form.

$$\sum_{i=1}^{n} t_i\left(k_i^2-m_i^2\right) \;=\; t\left(k-\frac{1}{t}\sum_{i=1}^{n} t_i q_i\right)^2 + \mathcal{F}(t_1,\dots,t_n), \tag{4.9}$$

where

$$t \;=\; \sum_{i=1}^{n} t_i \qquad \text{and} \qquad \mathcal{F}(t_1,\dots,t_n) \;=\; \frac{1}{2t}\sum_{i,j=1}^{n} t_i S_{ij} t_j. \tag{4.10}$$

In the next step we deform the loop momentum k into the complex plane such that we always have a positive imaginary part in eq.(4.9). We set

$$k^\mu \;=\; \tilde{k}^\mu + i g_{\mu\nu}\tilde{k}^\nu + \frac{1}{t}\sum_{i=1}^{n} t_i q_i^\mu \tag{4.11}$$

where $g_{\mu\nu}$ is the well known metric tensor $g=diag(1,-1,-1,-1)$. The Jacobian is

$$\left|\frac{\partial k^\mu}{\partial \tilde{k}^\nu}\right| \;=\; -4i \tag{4.12}$$

Inserting eq.(4.11) into eq.(4.9) we have

$$\sum_{i=1}^{n} t_i\left(k_i^2-m_i^2\right) \;=\; 2it\tilde{k}\circ\tilde{k} + \mathcal{F}(t_1,\dots,t_n), \tag{4.13}$$

where $\tilde{k}\circ\tilde{k}$ denotes the Euclidean scalar product of the real loop momentum $\tilde{k}$. For $\tilde{k}$ equal zero the imaginary part in eq.(4.13) vanishes. The function $\mathcal{F}(t)$ can be zero, too. To avoid these singularities we deform the Schwinger parameters into the complex plane. The direction is indicated by Feynman's $+i\delta$ rule. A convenient ansatz is

$$t_a \;=\; \tilde{t}_a + i\lambda\tilde{t}_a\frac{\partial\mathcal{F}(\tilde{t}_1,\dots,\tilde{t}_n)}{\partial\tilde{t}_a}, \tag{4.14}$$
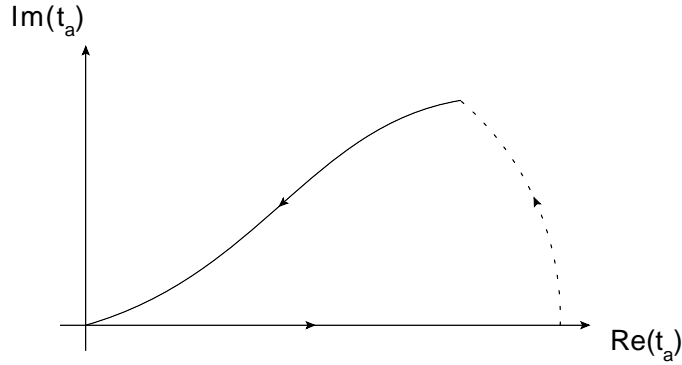
Figure 4.1: The integration contour of the Schwinger parameters is closed at zero and at infinity. The integration at infinity does not contribute to the integral.

where the $\tilde{t}_a$ are real and positive. The contour is closed at the points $\tilde{t}_a = 0$ and at infinity. Writing the function $\mathcal{F}$ in terms of the new variables and expanding it for infinitesimal small λ we get

$$\mathcal{F}(t_1, \ldots, t_n) = \mathcal{F}(\tilde{t}_1, \ldots, \tilde{t}_n) + \imath \lambda \sum_{j=1}^{n} \tilde{t}_j \left(\frac{\partial \mathcal{F}(\tilde{t}_1, \ldots, \tilde{t}_n)}{\partial \tilde{t}_j} \right)^2 + \mathcal{O}(\lambda^2). \quad (4.15)$$

The function $\mathcal{F}$ acquires a positive imaginary part of order λ. Therefore the deformation always points in the given direction. The only requirement is that the deformation starts in the right direction and never cross any poles by vary λ from zero to it's final value. The size of the scaling parameter λ will be determined later in this section.

In the next step we integrate out one variable and rewrite eq.(4.7) into the usual form known from introducing Feynman parameter. We note that with eq.(4.11) the loop momentum k^μ is homogeneous of degree 0 in the Feynman parameters t_i. Therefore the numerator function $R(k)$ is also homogeneous of degree 0 in the Feynman parameters t_i. The complex Feynman parameters t_i as functions of the real Feynman parameters $\tilde{t}_1, \ldots, \tilde{t}_n$ are homogeneous of degree 1. The Jacobian J of the Feynman parameter deformation

$$J(\tilde{t}) = \left| \frac{\partial t_i}{\partial \tilde{t}_j} \right| \quad (4.16)$$

is a homogeneous function of degree 0 in the variables $\tilde{t}_1, \ldots, \tilde{t}_n$ and is calculated numerical. Let $L(\tilde{k}; \tilde{t}_1, \ldots, \tilde{t}_n)$ be a homogeneous function of degree 1 in the

variables $\tilde{t}_1, \ldots, \tilde{t}_n$. Then we integrate out one variable

$$
\begin{aligned}
\int d^n \tilde{t} e^{\left(\imath L(\tilde{k};\tilde{t}_1,\ldots,\tilde{t}_n)\right)} &= \int d^n \tilde{t} \int d\hat{t} \, \delta \left(\hat{t} - \tilde{t}\right) e^{\left(\imath L(\tilde{k};\tilde{t}_1,\ldots,\tilde{t}_n)\right)} \\
&= \int d^n \tilde{x} \, \delta \left(1 - \tilde{x}\right) \int d\hat{t} \, \hat{t}^{n-1} e^{\left(\imath \hat{t} L(\tilde{k};\tilde{x}_1,\ldots,\tilde{x}_n)\right)} \\
&= \Gamma(n) \int d^n \tilde{x} \, \delta \left(1 - \tilde{x}\right) \left(-\imath L(\tilde{k};\tilde{x}_1,\ldots,\tilde{x}_n)\right)^{-n} \quad (4.17)
\end{aligned}
$$

with the substitution $\tilde{t}_i = \hat{t}\tilde{x}_i$. The deformation for the variables x_i reads analogously

$$
x_i = \tilde{x}_i + \imath \lambda \tilde{x}_i \frac{\partial \mathcal{F}(\tilde{x}_1,\ldots,\tilde{x}_n)}{\partial \tilde{x}_i} \tag{4.18}
$$

Putting everything together we arrive at

$$
I = 4\Gamma(n) \int \frac{d^4 \tilde{k}}{(2\pi)^4 \imath} \int d^n \tilde{x} \delta(1 - \tilde{x}) F(\tilde{k};\tilde{x}_1,\ldots,\tilde{x}_n) \tag{4.19}
$$

with

$$
F(\tilde{k};\tilde{x}_1,\ldots,\tilde{x}_n) = \frac{J(\tilde{x}_1,\ldots,\tilde{x}_n) R(\tilde{k})}{L(\tilde{k};\tilde{x}_1,\ldots,\tilde{x}_n)^n} \tag{4.20}
$$

and

$$
L(\tilde{k};\tilde{x}_1,\ldots,\tilde{x}_n) = 2\imath x \tilde{k} \circ \tilde{k} + \mathcal{F}(x_1,\ldots,x_n). \tag{4.21}
$$

Eq.(4.19) is the standard formula for Feynman parametrisation supplemented with the correct Jacobian corresponding to the deformation eq.(4.14) and eq.(4.18). But the integral in eq.(4.19) is still not suitable for a numerical integration. We have to replace the integration over the $(n-1)$-dimensional simplex by an integration over a n-dimensional hyper-cube $[0,1]^n$. This is discussed in the Appendix B. Furthermore we have to find a suitable mapping of the real loop momentum $\tilde{k}$ such that we can replace the integration over the $\mathbb{R}^4$ by a integration over the 4-dimensional hyper-cube $[0,1]^4$. This is also discussed in the Appendix B.

4.2.2 Scaling of the deformation

In this subsection we discuss the definition of the scaling parameter λ. In the previous subsection we already saw that our deformation always points into the right direction. Because we want deform as far as possible away from the singularities we have to choose λ as large as possible by not crossing any poles. Therefore we have to consider also higher orders in λ in the calculation.

First we write down the sum of all Feynman parameters explicitly.

$$x \;=\; \tilde{x} + \imath\lambda \sum_{i=1}^{n} \tilde{x}_i \frac{\partial \mathcal{F}}{\partial \tilde{x}_i} \tag{4.22}$$

$$=\; \tilde{x} + \imath\lambda \frac{1}{2\tilde{x}} \sum_{i,j=1}^{n} \tilde{x}_i S_{ij} \tilde{x}_j \tag{4.23}$$

were we use

$$\frac{\partial \mathcal{F}}{\partial \tilde{x}_i} \;=\; \frac{1}{\tilde{x}} \sum_{j=1}^{n} S_{ij} \tilde{x}_j - \frac{1}{2\tilde{x}^2} \sum_{j,k=1}^{n} \tilde{x}_j S_{jk} \tilde{x}_k. \tag{4.24}$$

We are interested in the imaginary part of the denominator in eq.(4.19). We observe that x is never zero. Therefore it is unproblematic to multiply the denominator function L with x. In following discussion the definition

$$\tilde{v}_i \;=\; \sum_{j=1}^{n} S_{ij} \tilde{x}_j \tag{4.25}$$

is helpful. The imaginary part of xL reads

$$\mathrm{Im}(xL) \;=\; \mathrm{Im}\left(2\imath x^2 \tilde{k} \circ \tilde{k} + \frac{1}{2} \sum_{i,j=1}^{n} x_i S_{ij} x_j \right)$$

$$=\; 2\tilde{k} \circ \tilde{k} \left(\tilde{x}^2 - \left(\frac{\lambda}{2\tilde{x}} \sum_{i=1}^{n} \tilde{x}_i \tilde{v}_i \right)^2 \right)$$

$$+\; \frac{\lambda}{2\tilde{x}^2} \sum_{i,j=0}^{n} \tilde{x}_i \left((\tilde{v}_i - \tilde{v}_j)^2 + \tilde{v}_i \tilde{v}_j \right) \tilde{x}_j \tag{4.26}$$

We observe that the second term on the right hand side of eq.(4.26) is always positive. Considering the first term on the right hand side of eq.(4.26) a reasonable choice for λ is

$$\lambda \;=\; \frac{1.8\tilde{x}}{\sqrt{\displaystyle\sum_{i=1}^{n} \tilde{v}_i^2}} \tag{4.27}$$

With this choice of λ we ensure that eq.(4.26) is always positive and we observe a good numerical behaviour of the integral. We note that λ is a homogeneous function of degree 0 in the Feynman parameters.

4.2.3 Deformation for the UV propagator

We now discuss the impact of the contour deformation developed so far on the UV subtraction term in eq.(4.3). We have

$$I_{UV} = \frac{P_{UV}}{(\bar{k}^2 - \mu_{UV}^2)^{n_{UV}}} \tag{4.28}$$

with

$$\bar{k}^\mu = k^\mu - Q^\mu. \tag{4.29}$$

We have to ensure that the imaginary part of the UV propagator is always positive. For the arbitrary fourvector Q^μ we can make the choice

$$Q^\mu = \frac{1}{x} \sum_{i=1}^{n} x_i q_i^\mu. \tag{4.30}$$

Since the Feynman parameters x_i are complex the fourvector Q^μ is also complex. Consider the deformation of the loop momentum in eq.(4.11) we have for the UV propagator

$$\bar{k}^2 - \mu_{UV}^2 = 2\imath \tilde{k} \circ \tilde{k} - \mu_{UV}^2. \tag{4.31}$$

The Euclidean norm $\tilde{k} \circ \tilde{k}$ is always positive. By setting μ_{UV}^2 purely imaginary with $\mathrm{Im}(\mu_{UV}^2) < 0$ we ensure that the UV propagator is never zero.

4.3 Improving the numerical stability

In the next section we discuss problems connected to the numeric stability of the integrand which arise at a high multiplicity of external particles. The origins of these instabilities are integrable singularities which are enhanced due to Feynman parametrisation. To improve numerical stability we present two approaches. First we introduce an artificial small mass into the denominator to avoid the integrable singularities and expand the denominator around this small parameter. Secondly we decompose the integration into different regions and choose for each region a certain coordinate system such that the integrand gets flattened.

Let us discuss under which conditions the denominator in eq.(4.19) vanishes. We write the denominator in first order of λ.

$$L(\tilde{k}; \tilde{x}_1, \ldots, \tilde{x}_n) = 2\imath \tilde{x} \tilde{k} \circ \tilde{k} + \mathcal{F}(\tilde{x}_1, \ldots, \tilde{x}_n) + \mathcal{O}(\lambda) \tag{4.32}$$

Then the necessary (but not sufficient) conditions for a vanishing denominator are given by the Landau equations [60]. We have

$$\frac{\partial L}{\partial \tilde{k}} = 0 \tag{4.33}$$

and

$$\tilde{x}_i \quad = \quad 0 \tag{4.34}$$

or

$$\frac{\partial \mathcal{F}}{\partial \tilde{x}_i} \quad = \quad 0 \tag{4.35}$$

for all $i \in \{1, \ldots, n\}$. Since $\partial L / \partial \tilde{k} = 0$, the condition $\partial \mathcal{F} / \partial \tilde{x}_i = 0$ is equivalent to the condition $\partial L / \partial \tilde{x}_i = 0$ i.e. according to the definition eq.(4.21) and eq.(4.13)

$$k_i^2 - m_i^2 \quad = \quad 0. \tag{4.36}$$

We note that with eq.(4.15) the imaginary part up to order λ of the denominator vanishes if the Landau equations are fulfilled.

We come back to the discussion of the numerical instabilities. Consider now that eq.(4.33) is fulfilled. Furthermore we have a subset $M \subset \{1, \ldots, n\}$ of n_{sing} elements. If eq.(4.35) is fulfilled for all $i \in M$ and eq.(4.34) is fulfilled for all $i \in \{1, \ldots, n\} \backslash M$, Landau's equations are fulfilled. For $n_{sing} < n$ this is called a non-leading Landau singularity. In the final formula the denominator appear to the power n. But we have shown that only if eq.(4.35) is fulfilled the corresponding singularity corresponds to the underlying physical configuration i.e. a physical propagator goes on-shell. Therefore only n_{sing} powers are physical and the other $n - n_{sing}$ powers are artificially introduced by the Feynman parameters. These extra unphysical powers are compensated in an analytic integration over the Feynman parameters in the directions corresponding to $\{1, \ldots, n\} \backslash M$. However, the integration is done numerically with Monte Carlo methods. Therefore we observe numerical instabilities for large n in regions were the function L is close to zero.

One can think about reducing the power n to which the function L is raised. We have discussed this approach in [5] but it turnes out that this approach is not sufficient for a numerical implementation, because in this approach we add up terms of equal order with alternating signs which lead to a large Monte Carlo error. Therefore we discuss in the following two other approaches to improve the numerical stability.

4.3.1 Infrared mass approach

To avoid that the denominator function L gets close to zero we introduce a small mass parameter μ_{IR}^2, with μ_{IR}^2 purely imaginary and $\text{Im}(\mu_{IR}^2) < 0$. A Taylor expansion leads to the identity

$$L^{-n} \quad = \quad (L - x\mu_{IR}^2)^{-n} \frac{1}{\Gamma(n)} \sum_{n_{IR}=0}^{\infty} \frac{\Gamma(n_{IR} + n)}{\Gamma(n_{IR} + 1)} \left(\frac{-x\mu_{IR}^2}{L - x\mu_{IR}^2} \right)^{n_{IR}}. \tag{4.37}$$

The definition above of the parameter μ_{IR}^2 ensures that

$$\text{Im}(L - x\mu_{IR}^2) \;>\; 0 \tag{4.38}$$

It follows that the expression $L - x\mu_{IR}^2$ is never zero.

Because L has positive imaginary part at leading order in λ we have

$$\left| \frac{-x\mu_{IR}^2}{L - x\mu_{IR}^2} \right| \;\leq\; 1. \tag{4.39}$$

Therefore, the sum on the right hand side of eq.(4.37) converges until $L = 0$ but then the expression on the left side is ill defined anyway. So we can truncate the series at order N_{IR} and calculate each single summand with a single Monte Carlo integration. We have

$$L^{-n} \;\approx\; (L - x\mu_{IR}^2)^{-n} \frac{1}{\Gamma(n)} \sum_{n_{IR}=0}^{N_{IR}} \frac{\Gamma(n_{IR} + n)}{\Gamma(n_{IR} + 1)} \left(\frac{-x\mu_{IR}^2}{L - x\mu_{IR}^2} \right)^{n_{IR}}. \tag{4.40}$$

We replace the critical expression L^{-n} by the expression $(L - x\mu_{IR}^2)^{-n-n_{IR}}$ which is never zero. This improves numerical stability significantly.

We can improve numerics by performing the following replacement

$$L^{-n} \;=\; L^{-n} \left[\left(\frac{L}{L - x\mu_{IR}^2} \right)^n \sum_{i=0}^{\infty} c_i^{(n)} \left(\frac{-x\mu_{IR}^2}{L - x\mu_{IR}^2} \right) \right]^{M_{IR}} \tag{4.41}$$

with

$$c_i^{(n)} \;=\; \frac{\Gamma(i + n)}{\Gamma(n)\Gamma(i + 1)}. \tag{4.42}$$

For $M_{IR} = 1$ this is again the identity eq.(4.37). We then make use of the well known identity

$$\sum_{i=0}^{\infty} a_i \sum_{j=0}^{\infty} b_i \;=\; \sum_{i=0}^{\infty} \sum_{j=0}^{i} a_j b_{i-j} \tag{4.43}$$

to obtain

$$L^{-n} \;=\; L^{-n} \left(\frac{L}{L - x\mu_{IR}^2} \right)^{nM_{IR}} \sum_{i_{M_{IR}}}^{\infty} \tilde{c}_{i_{M_{IR}}}^{(n)} \left(\frac{-x\mu_{IR}^2}{L - x\mu_{IR}^2} \right)^{i_{M_{IR}}} \tag{4.44}$$

where the coefficients $\tilde{c}_i$ are recursively defined by

$$\tilde{c}_{i_j}^{(n)} \;=\; \sum_{i_{j-1}=0}^{i_j} \tilde{c}_{i_{j-1}}^{(n)} c_{i_j - i_{j-1}}^{(n)} \tag{4.45}$$

and the recursion starts with $j = 1$

$$\tilde{c}_{i_1}^{(n)} = c_{i_1}^{(n)}. \tag{4.46}$$

We truncate the series again at N_{IR} and get the final result

$$L^{-n} = \frac{L^{n(M_{IR}-1)}}{(L - x\mu_{IR}^2)^{nM_{IR}}} \sum_{i_{M_{IR}}}^{N_{IR}} \tilde{c}_{i_{M_{IR}}}^{(n)} \left(\frac{-x\mu_{IR}^2}{L - x\mu_{IR}^2}\right)^{i_{M_{IR}}} \tag{4.47}$$

The replacement of the original expression L^{-n} depends on three parameters, N_{IR}, M_{IR} and μ_{IR} which we can use to control the quality of our approximation.

4.3.2 Splitting of the integration regions

In this section we discuss a method which is based on the decomposition of the integration region into different sectors. This approach is inspired by the algorithm called "Sector Decomposition" which is a constructive method to isolate divergences from parameter integrals. But the method discussed in this section should not be confused with the usual "Sector Decomposition".

We define a splitting of the integration region by choosing $k < n$ ordered according to size Feynman parameters out of the n Feynman parameters from the Feynman integral.

$$\tilde{x}_{i_1} > \ldots > \tilde{x}_{i_k} > \{\tilde{x}_{i_{k+1}}, \ldots, \tilde{x}_{i_n}\} \tag{4.48}$$

We have n over k possibilities to choose k out of n parameters and $k!$ possibilities to order these k parameters. Therefore we split the original integration region into $n!/(n-k)!$ regions.

The Monte Carlo generator provides us with n random numbers.

$$v_1, \ldots, v_n \in [0, 1) \tag{4.49}$$

In the following we discuss how to map these random numbers to the Feynman parameter of a certain integration region eq.(4.48). We choose the mapping such that the corresponding Jacobian almost has the form of the imaginary part of the denominator function $(L - x\mu_{IR}^2)$. If $(L - x\mu_{IR}^2)$ is close to zero the integrand becomes flat because of the Jacobian. To ease up notation we discuss only the mapping for a certain region. The Feynman parameters of this region are defined by

$$u_1 > \ldots > u_k > \{u_{k+1}, \ldots, u_n\}. \tag{4.50}$$

We construct the Feynman parameters u_i iteratively starting by $i = 1$. The mapping of the random numbers v_i to the Feynman parameters u_i is defined by

$$u_1 \;=\; v_1 \tag{4.51}$$

$$u_i \;=\; f_{\lambda_i}(v_i; u_1, \ldots, u_{i-1}) \qquad \text{for} \qquad i > 1, \tag{4.52}$$

where $f_\lambda(x; \ldots)$ is a strict monotonically increasing function in x. We have

$$f_\lambda(x; \ldots): \qquad [0, 1) \rightarrow [0, \lambda) \tag{4.53}$$

with

$$f_\lambda(0; \ldots) \;=\; 0 \tag{4.54}$$

and

$$\lim_{x \rightarrow 1} f_\lambda(x; \ldots) \;=\; \lambda. \tag{4.55}$$

By defining

$$\lambda_i \;:=\; \begin{cases} u_{i-1} & : \quad i \in \{2, \ldots, k\} \\ u_k & : \quad i \in \{k+1, \ldots, n\} \end{cases} \tag{4.56}$$

the conditions for the Feynman parameters defined in eq.(4.50) are automatically fulfilled. What is left is the definition of the function $f_\lambda(x; \ldots)$.

$$f_{\lambda_i}(v_i; u_1, \ldots, u_{i-1}) \;=\; \lambda_i v_i \Lambda_i^{1-v_i} \tag{4.57}$$

with

$$\Lambda_i \;=\; \frac{a_i(u_1, \ldots, u_{i-1})}{s/2 + a_i(u_1, \ldots, u_{i-1})} \tag{4.58}$$

and s the center of mass energy squared of the considered process. The function $a(u_1, \ldots, u_{i-1})$ is given by

$$a_i(u_1, \ldots, u_{i-1}) \;=\; \sum_{j=1}^{i-1} u_j \left(2\tilde{k} \circ \tilde{k} - \text{Im}(\mu_{IR}^2) + b_j(u_1, \ldots, u_{i-1}) \right) \tag{4.59}$$

with

$$b_j(u_1, \ldots, u_{i-1}) \;=\; \frac{0.9 \sum\limits_{k=1}^{i-1} u_k \left(\left(\sum\limits_{a=1}^{i-1} u_a (S_{ja} - S_{ka}) \right)^2 + \sum\limits_{a,b=1}^{i-1} S_{ja} u_a S_{kb} u_b \right)}{\left(\sum\limits_{k=1}^{i-1} u_k \right)^2 \sqrt{\sum\limits_{a=1}^{i-1} \left(\sum\limits_{b=1}^{i-1} S_{ab} u_b \right)^2}}. \tag{4.60}$$

With these definitions $0 < \Lambda_i < 1$ and therefore $f_\lambda(v_i; u_1, \ldots, u_{i-1})$ fulfills the conditions defined earlier. Equation(4.60) looks rather complicated but if we calculate

$$\sum_{i=1}^{n} u_i b_i(u_1, \ldots, u_n) \tag{4.61}$$

we see this is exactly the imaginary part we know from eq.(4.26) multiplied by a factor $1/\tilde{x}$. Therefore the function $a_i(u_1, \ldots, u_{i-1})$ almost matches the imaginary part of $(L - x\mu_{IR}^2)$. Next we show that the Jacobian is proportional to $a_i(u_1, \ldots, u_{i-1})$ and matches therefore the imaginary part of $(L - x\mu_{IR}^2)$ as predicted.

The Jacobian matrix of the mapping is obviously a triangle matrix and therefore the Jacobian determinate is just the product of the diagonal elements.

$$\left| \frac{\partial f_{\lambda_i}(v_i; u_1, \ldots, u_{i-1})}{\partial u_j} \right| = \prod_{i=2}^{n} \frac{\partial f_{\lambda_i}(v_i; u_1, \ldots, u_{i-1})}{\partial u_i} \tag{4.62}$$

So we can write for the phase space weights

$$du_1 = dv_1 \tag{4.63}$$
$$du_i = \lambda_i \Lambda_i^{1-v_i} \left(1 + v_i \ln(\Lambda_i)\right) dv_i \qquad \text{for} \qquad i > 1. \tag{4.64}$$

Because the random numbers v_i are smaller than 1 the Jacobian in eq.(4.64) converges to zero for $\Lambda_i \to 0$. This improves the numerical stability of the Feynman integral.

4.4 Checks and examples

In this section we present results calculated with the contour deformation presented in the previous section. We show how the improvements of the contour deformation influences the results in regions were the integral is instable. In the top level diagram of a one-loop amplitude with n external particles, in general n internal propagators occur. The difficulty of the integration rises with the number of the internal propagators.

We are testing our method by using a configuration with n external particles. By pinching $(n - 3)$ of the internal particles we obtain a one-loop three-point function, see fig.(4.4). In the test program we have $n = 6$ and the external momenta of the three-point function are:

$$P_1 = p_1 + p_2, \quad P_2 = p_3 + p_4, \quad P_3 = p_5 + p_6. \tag{4.65}$$
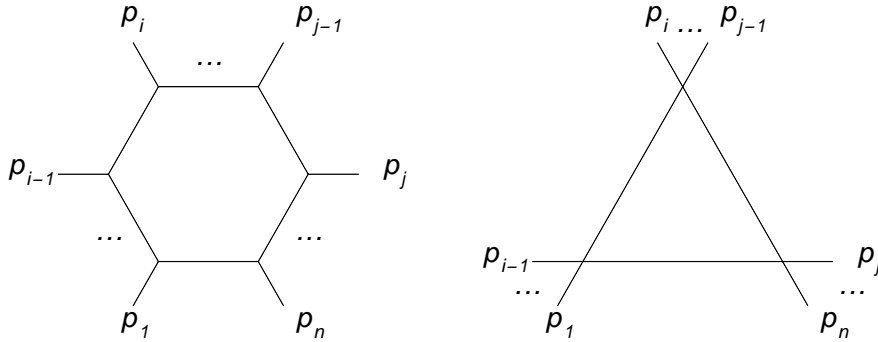
Figure 4.2: The diagram on the left shows the top level diagram for a process with n external legs. Pinching $(n-3)$ loop propagators results in a three point function shown on the right.

where the p_i are massless and on-shell. We have to calculate the massless one-loop scalar three-point function

$$I = -\imath 16\pi^2 \int \frac{d^4 k}{(2\pi)^4} \frac{1}{k^2 (k-P_1)^2 (k-P_1-P_2)^2} \qquad (4.66)$$

which is finite for $P_1^2 \neq 0$, $P_2^2 \neq 0$ and $P_3^2 \neq 0$. The analytical result is well known [76–78]. In the test program we use the program LoopTools [59] for the analytic calculation of the three-point function. The numerical integration of the three-point function is almost trivial. To consider more internal propagators in the integration we multiply and divide the integrand with the propagators we have pinched and introduce Feynman parameters for the extra factors in the denominator. We have

$$I_n = -\imath 16\pi^2 \int \frac{d^4 k}{(2\pi)^4} \int d^n x \, \frac{\delta \left(1 - \sum\limits_{i=1}^{n} x_i\right) \prod\limits_{i=1}^{n-3} D_{2i}}{\left[\sum\limits_{i=1}^{3} x_{2i-1} D_{2i-1} + \sum\limits_{i=1}^{n-3} x_{2i} D_{2i}\right]^n} \qquad (4.67)$$

with

$$D_i = (k - q_i)^2 - m_i^2 \qquad \text{and} \qquad q_i = \sum\limits_{j=1}^{i} p_j. \qquad (4.68)$$

In the test program we use the VEGAS [79; 80] algorithm from the CUBA library [81]. We use a warm up phase of five runs to adjust the integration grid and then perform 20 runs with this grid. Each VEGAS run is performed with the same statistic. For the results presented here we use 10^6 iterations per run. The VEGAS algorithm provides us with a reasonable error for each run therefore we do not use the arithmetic average but the weighted arithmetic average of the results of the 20 runs. x_i is the result of a single VEGAS run and σ_i the

corresponding error provided by the VEGAS algorithm. The final result of the numerical calculation is then

$$\bar{x} \;\; = \;\; \frac{\sum_i \frac{x_i}{\sigma_i^2}}{\sum_i \frac{1}{\sigma_i^2}} \tag{4.69}$$

and the error is

$$\sigma_{\bar{x}} \;\; = \;\; \frac{1}{\sqrt{\sum_i \frac{1}{\sigma_i^2}}}. \tag{4.70}$$

The integration of I_3 up to I_5 is unproblematic and we can generate numerical results in the per mille accuracy with just the methods described in section (4.2.1) but we observe numeric instabilities i.e. large statistical errors by calculating I_6. In fig.(4.3) we plotted the numerical results normalised to the analytic result for I_n with $n \in \{3, 4, 5, 6\}$.

The stability can be improved by methods discussed in section(4.3.1) and section (4.3.2). We start with the infrared mass approach. This method introduces three parameters N_{IR}, M_{IR} and the mass μ_{IR}. It is convenient to parametrise μ_{IR} by a dimensionless number η_{IR} through

$$\mu_{IR}^2 \;\; = \;\; -\imath \eta_{IR}^2 s^2 \tag{4.71}$$

where s is the center of mass energy of the considered process.

First we keep $M_{IR} = 1$ fixed and plot the numerical results normalised to the analytic results for I_6 against the parameter N_{IR} for different mass parameters η_{IR}. This plot is shown in fig.(4.4). We observe that the correct value is approached by increasing N_{IR}. The series converges faster for small η_{IR} but smaller η_{IR} imply larger statistical errors. However by a suitable choice of η_{IR} and N_{IR} one obtains a precision in the per mille level.

In fig.(4.5) we plotted the results of the three-point function for a fixed value of $N_{IR} = 6$ against various mass parameter η_{IR}. Because we performs a single Monte Carlo integration for each summand in the series we need for $N_{IR} = 6$ almost seven times more computer time compared with the results from fig.(4.3). To compensate for this fact we use seven times more statistics to calculate the $\eta_{IR} = 0$ point in fig.(4.5). Even with increased statistics the integral I_6 is still instable in a basic Monte Carlo without the improvements presented in the previous section. For larger η_{IR} it seems that the numerical result underestimate the analytic result if we stop the series at $N_{IR} = 6$. But increasing N_{IR} just adds noise to the result and is more time consuming. To be save we choose a small mass parameter in the following discussion.

Next we vary the parameter M_{IR} and keep $\eta_{IR} = 0.02$ fixed. In the plot in fig.(4.6) we compare the convergence behaviour of the numerical results for
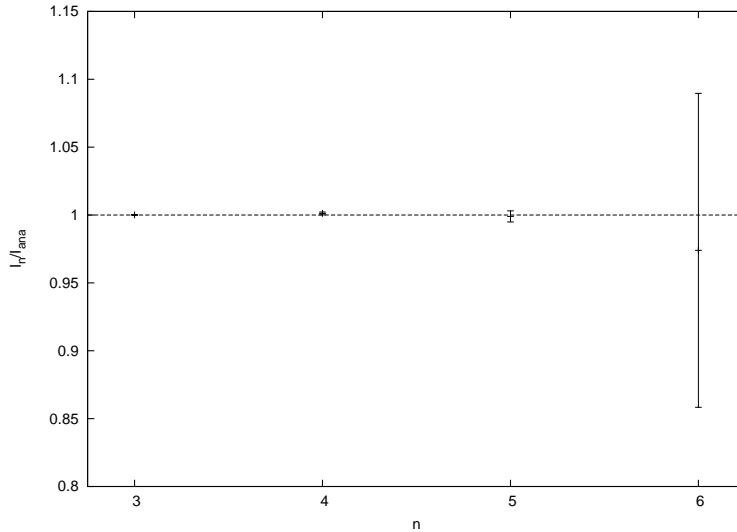
Figure 4.3: Results for the numerical integration of the three-point function normalised to the analytical result for a contour based on n external particles. The errorbars indicate the statistical error of the Monte Carlo integration.

various values of M_{IR}. By increasing the parameter M_{IR} we observe a similar convergence behaviour like the one obtained by increasing the mass parameter η_{IR}.

In fig.(4.7) we plotted the results of the three-point function for a fixed value of $N_{IR} = 6$ and fixed mass parameter $\eta_{IR} = 0.02$ against various M_{IR}. We observe that the statistical error does not depend strongly on M_{IR} for $M_{IR} \geq 1$. For $N_{IR} = 6$, $M_{IR} = 3$ and $\eta_{IR} = 0.02$ we have a good compromise between precision and convergence.

Next we investigate the impact of the sector decomposition discussed in section (4.3.2) on the numerical behaviour of the integral of the three-point function I_6. We set $M_{IR} = 0$ and $\eta_{IR} = 0$ and decompose the integration region into $n!/(n-k)!$ subregions with $n = 6$ and $k \in \{0, 1, 2, 3\}$. In fig.(4.8) we plot the numeric result of I_6 normalised to the analytic result against the parameter k. Naively, it seems that the statistical error is strictly decreasing with increasing k. But we calculate each single integration region with an individual Monte Carlo run. Therefore we have for $k = 3$ overall 120 times more statistic compared to the case $k = 0$ where we have only a single integration region. In fig.(4.9) we compensate this by increasing the statistic for an individual Monte Carlo depending on k such that we get for all k's the same overall statistic. We observe the best efficiently wise choice is $k = 1$.

Figure 4.4: Results for the numerical integration of the three-point function normalised to the analytical result for a contour based on six external particles for various values of η_{IR} and N_{IR}. The errorbars indicate the statistical error of the Monte Carlo integration.

Figure 4.5: Results for the numerical integration of the three-point function normalised to the analytical result for a contour based on six external particles for $N_{IR} = 6$ and various values of η_{IR}. The errorbars indicate the statistical error of the Monte Carlo integration.

Figure 4.6: Results for the numerical integration of the three-point function normalised to the analytical result for a contour based on six external particles for $\eta_{IR} = 0.02$ and for various values of N_{IR} and M_{IR}. The errorbars indicate the statistical error of the Monte Carlo integration.
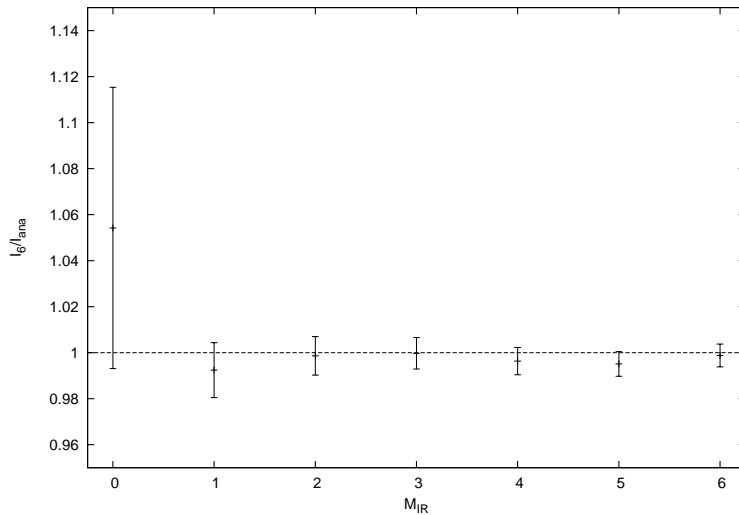
Figure 4.7: Results for the numerical integration of the three-point function normalised to the analytical result for a contour based on six external particles for $\eta_{IR} = 0.02$, $N_{IR} = 6$ and various values of M_{IR}. The errorbars indicate the statistical error of the Monte Carlo integration.
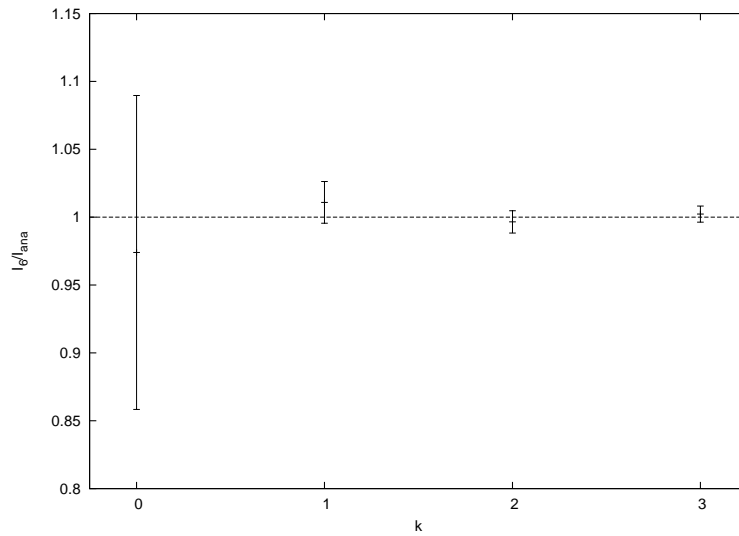
Figure 4.8: Results for the numerical integration of the three-point function normalised to the analytical result for a contour based on six external particles for various values of k and fixed statistics for each integration region. The errorbars indicate the statistical error of the Monte Carlo integration.
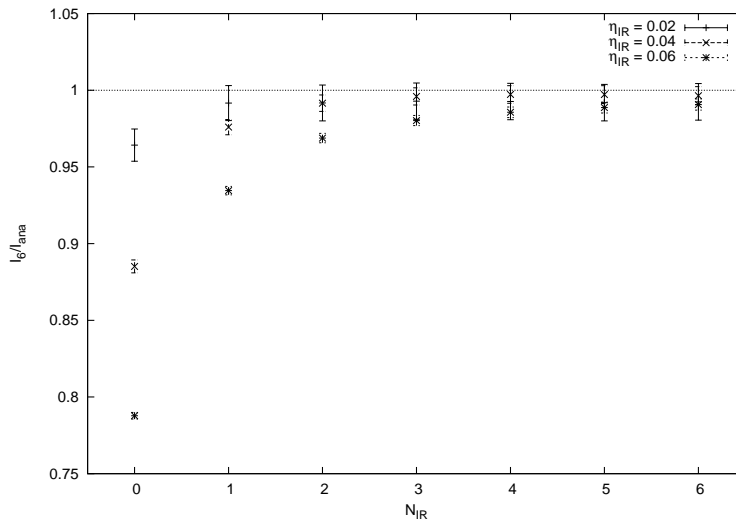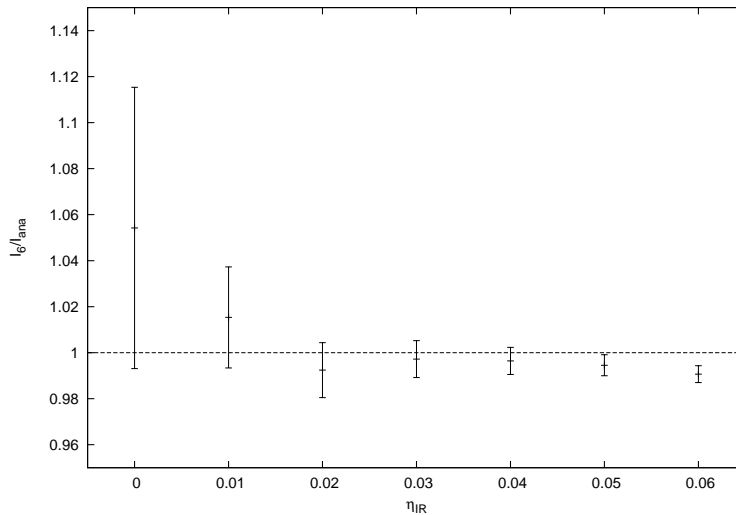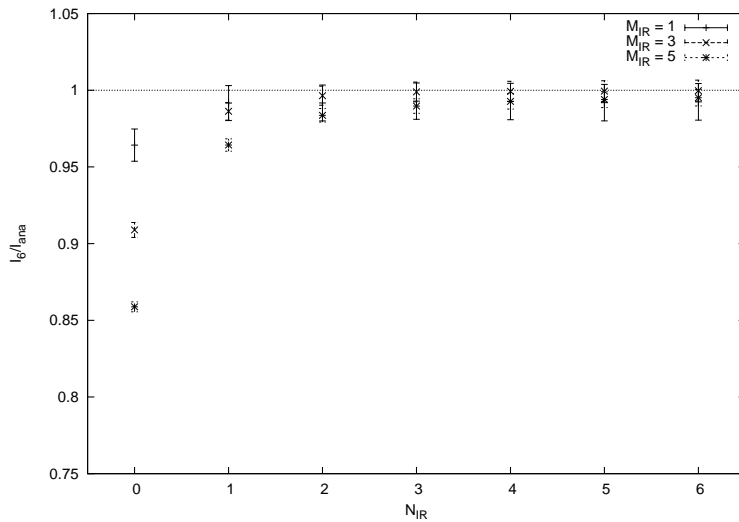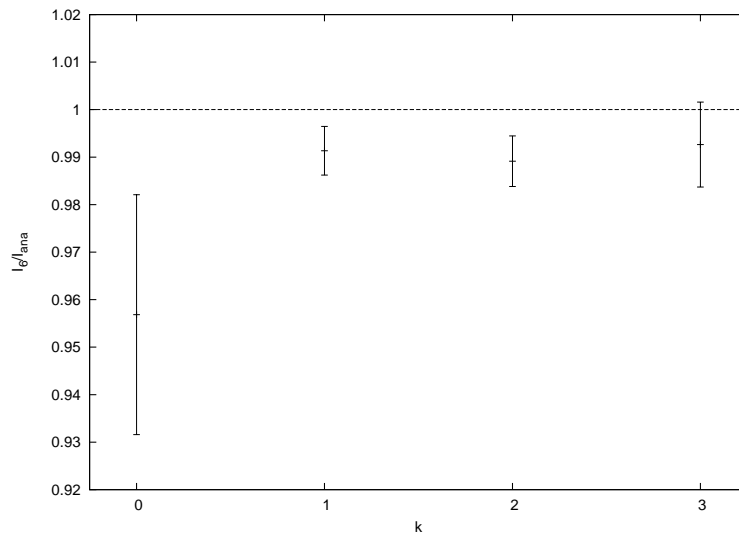

Figure 4.9: Results for the numerical integration of the three-point function normalised to the analytical result for a contour based on six external particles for various values of k and fixed overall statistics for each k. The errorbars indicate the statistical error of the Monte Carlo integration.

So far we have only considered the massless case with no masses in the loop. In chapter 5 we compare the performance of the Feynman deformation with the Direct deformation presented in chapter 5 in the massive case.

In this chapter we motivated the numerical integration over an Feynman parameter integral and for the deformation of the integration contour into the complex plane. We provided a step by step instruction for the deformation of the loop momentum and the Feynman parameters. We discussed in detail the issues of these method at high particle multiplicity and how to overcome them by introducing advanced methods. These advanced methods were tested extensively for a simple example.

5 Direct deformation

In this chapter we discuss the numerical integration of a one-loop integral avoiding threshold singularities by deforming the loop momentum into the complex plane.

5.1 Introduction

We are interested in calculating numerically a one-loop integral. In the method discussed in this thesis we deal with the ultraviolet (UV) and infrared (IR) divergencies by subtraction as discussed in chapter 2. After subtraction we are still faced with threshold singularities of the one-loop integral. In chapter 4 we discussed in detail how one can avoid threshold singularities of a one-loop integral by introducing first Feynman parameters and then deform these parameters together with the loop momentum into the complex plane. But the results based on the subtraction method for $e^+e^- \to n$-jets concerning five massless quark flavours [4] were produced with a contour deformation which does not introduce Feynman parameters but deforms the loop momenta directly. This deformation is discussed in detail together with some efficiency improvements for numerical computations of next-to-leading order (NLO) corrections in [6] and is based on the work of [11]. For up to $n = 5$-jets the deformations based on the Feynman approach and direct integration lead to the same results for $e^+e^- \to n$-jets. But for larger n the Feynman approach is too inefficient and not practical any longer. One advantage of the Feynman approach is that regarding the contour deformation there is no difference between a massive or massless theory. For the direct integration approach this is not the case. So far, only a deformation for massless theories is known in the direct integration approach. If we now want to apply the subtraction method to processes which include massive degrees of freedom like $e^+e^- \to t\bar{t} + n$-jets for the planed international linear collider (ILC) or $t\bar{t}$ production for the large hadron collider (LHC) a new deformation is needed. In this chapter we present a contour deformation based on direct integration of the loop momentum which is suitable for theories containing massive particles. The generalisation from the massless to the massive case is not a trivial task because of the more complicated structure of the threshold singularities. In the massless case the surface of a threshold singularity is a simple light cone whereas in the massive case, we have a mass hyperboloid. Especially the intersection of these surfaces become much more complicated.
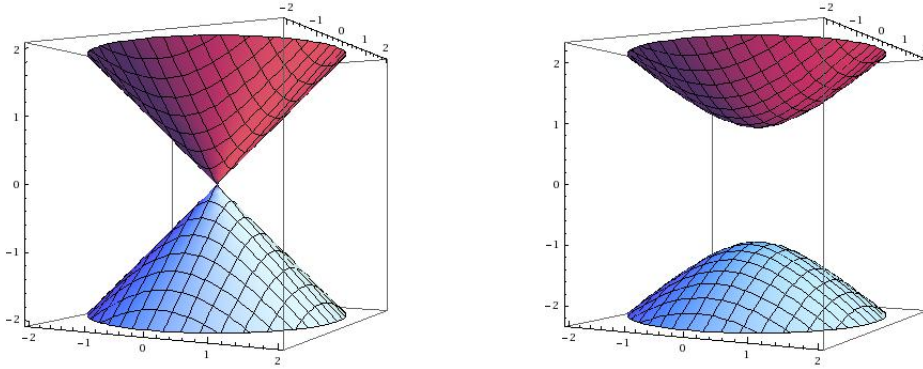
Figure 5.1: Examples for the surfaces of threshold singularities in three dimensions. The diagram on the left corresponds to a cone with its origin at (0,0,0). The diagram on the right corresponds to a two sheet circular hyperboloid with its origin at (0,0,0). If the time component of a surface is positive we call it a forward cone/hyperboloid and otherwise a backward cone/hyperboloid.

5.2 General framework

We recommence with eq.(4.1) and eq.(4.3) from chapter 4. So after we apply the subtraction terms for the UV and IR singularities we can write the loop integral

$$I \quad = \quad \int \frac{d^4 k}{(2\pi)^4} \frac{R(k)}{\prod\limits_{j=1}^{n} (k_j^2 - m_j^2 + \imath\delta)} \tag{5.1}$$

with

$$R(k) \quad = \quad P(k) + P_{UV}(k) \frac{\prod\limits_{j=1}^{n} (k_j^2 - m_j^2 + \imath\delta)}{(\bar{k}^2 - \mu_{UV}^2 + \imath\delta)^{n_{UV}}}. \tag{5.2}$$

We have to avoid the remaining threshold singularity where one or more propagators are on-shell by deforming the integration contour into the complex plane. In the massless case the threshold singularities lie on light cones and in the massive case on two sheet circular hyperboloids with origins at $q_0, q_1, \ldots, q_{n-1}$. Since

$$p_i \quad = \quad q_i - q_{i-1}, \tag{5.3}$$

the external momenta p_i connect the origins of the surfaces of the singularities. We plot now the origins of the singularities together with their connecting lines in the loop momentum space where we only show the k^0 and k^3 components of the loop momentum fig.(5.2). For a generic primitive one-loop amplitude the kinematics can be displayed as in diagram (a) where we have two initial state
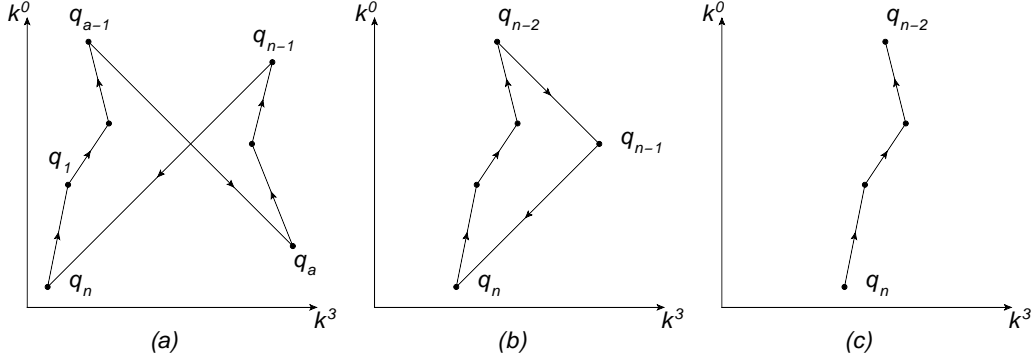
Figure 5.2: The sketch show the k^0 and k^3 component of the loop momenta k. The two transverse components come out of the plane and are not seen. Diagram (a) corresponds to a generic primitive amplitude, diagram (b) corresponds to a primitive amplitude, where the two incoming particles are adjacent, diagram (c) corresponds to the situation in electron-positron annihilation, where the poles due to q_{n-1} are absent.

particles (the momenta with negative time component) and two strands. For a primitive one-loop amplitude where the two initial state particles are adjacent the diagram degenerates to diagram (b) with only a single strand. If the two internal state particles couples only through an intermediate particle to the loop like a γ/Z-boson in e^+e^- collision the kinematics are shown in diagram (c).

A threshold singularity occurs when

$$0 \quad = \quad k_i^2 - m_i^2. \tag{5.4}$$

To avoid these singularities we deform the loop momentum into the complex plane by introducing the deformation vector κ.

$$k \to k \quad = \quad \tilde{k} + \imath \kappa(\tilde{k}) \tag{5.5}$$

Applying this deformation to a single propagator

$$k_i^2 - m_i^2 \quad \to \quad \tilde{k}_i^2 - m_i^2 - \kappa^2 + 2\imath \kappa \cdot \tilde{k}_i \tag{5.6}$$

introduces an imaginary part $2\imath \kappa \cdot \tilde{k}_i$. Feynman's $+\imath \delta$ description tells us in which direction we have to deform. If the propagator is on-shell the corresponding imaginary part has to be positive.

$$\tilde{k}_i^2 - m_i^2 \quad = \quad 0 \qquad \Rightarrow \qquad \kappa \cdot \tilde{k}_i \quad \geq \quad 0, \tag{5.7}$$

where the equal sign on the right hand side of eq.(5.7) only occurs if the singularity is pinched. The one-loop integral now reads

$$I \quad = \quad \int \frac{d^4\tilde{k}}{(2\pi)^4} \left| \frac{\partial k}{\partial \tilde{k}} \right| \frac{R(k(\tilde{k}))}{\prod\limits_{j=1}^{n} (\tilde{k}_j^2 - m_j^2 - \kappa^2 + 2\imath \kappa \cdot \tilde{k})} \tag{5.8}$$

where the integration is over $\mathbb{R}^4$. In appendix B we discuss how to map the four dimensional hypercube $[0,1]^4$ to $\mathbb{R}^4$ such that the integration is suitable for a Monte Carlo integration. In the following we discuss in detail the construction of the deformation vector κ. We note that it is crucial for the method that the deformation vector not only deforms correctly but is also suitable for a numerical integration i.e. leads to small statistical errors.

5.3 Definition of the deformation vector κ

We construct the deformation for the most generic primitive one-loop amplitude fig.(5.2) (a). The points $q_1, \ldots, q_n$ in fig.(5.2) (a) are contained in a finite region. We split the loop momentum space into two regions, the "internal" and the "external" region. The internal region is defined by the intersection of the interior of the forward light cone of q_n with the interior of the backward light cone of q_{a-1} together with the intersection of the interior of the forward light cone of q_a with the interior of the backward light cone of q_{n-1}. The external region is defined by the complement of the internal region. We note that only in the internal region intersections of forward hyperboloids with backward hyperboloids occur. Therefore, the deformation for the internal region is much more involved compared to the deformation for the external region. We split the deformation vector into two contributions.

$$\kappa \;=\; \lambda\left(\kappa_{int} + \kappa_{ext}\right) \tag{5.9}$$

We discuss the construction of the two contributions $\kappa_{ext}, \kappa_{int}$ and the scaling parameter λ separately.

5.3.1 Definition of some help functions

We define some functions which are important in the following discussion:

$$h_{\delta\pm}(k, m^2) \;=\; \frac{\left(\pm k^0 - \sqrt{\vec{k}^2 + m^2}\right)^2}{\left(\pm k^0 - \sqrt{\vec{k}^2 + m^2}\right)^2 + M_1^2} \tag{5.10}$$

If k lies on the forward mass hyperboloid defined by

$$k^2 - m^2 \;=\; 0 \qquad \text{and} \qquad k^0 \;\geq\; 0 \tag{5.11}$$

the function $h_{\delta+}$ is zero. If k lies on the backward mass hyperboloid defined by

$$k^2 - m^2 \;=\; 0 \qquad \text{and} \qquad k^0 \;\leq\; 0 \tag{5.12}$$

the function $h_{\delta-}$ is zero. Depending on the parameter M_1 the function $h_{\delta\pm}$ is a smooth function near the hyperboloid. If k is far away from the hyperboloid the function converges to $h_{\delta\pm} = 1$.

$$
h_\delta(k, m^2) \;=\; \begin{cases} \dfrac{\left(|k^0| - \sqrt{\vec{k}^2 + m^2}\right)^2}{\left(|k^0| - \sqrt{\vec{k}^2 + m^2}\right)^2 + M_1^2} & : \quad m^2 > 0 \\[4ex] \dfrac{\left(\sqrt{(k^0)^2 - m^2} - |\vec{k}|\right)^2}{\left(\sqrt{(k^0)^2 - m^2} - |\vec{k}|\right)^2 + M_1^2} & : \quad m^2 < 0 \end{cases}
\tag{5.13}
$$

If k lies on the mass hyperboloid defined by

$$
k^2 - m^2 \;=\; 0,
\tag{5.14}
$$

the function h_δ is zero. Depending on the parameter M_1 the function h_δ is a smooth function near the hyperboloid. If k is far away from the hyperboloid the function converges to $h_\delta = 1$. So, h_δ has a similar behaviour as $h_{\delta\pm}$ with the difference that h_δ vanishes regardless of whether k lies on the forward or backward hyperboloid and h_δ is also defined for negative masses squared $m^2 < 0$. A good choice for the parameter M_1 is $M_1^2 = s/800$, where s is the center of mass energy squared of the considered process.

Concerning eq.(5.6) the imaginary part of a propagator is given by the Minkowski scalar product of two fourvectors. By rewriting the scalar product to

$$
u \cdot v \;=\; \left(\frac{u+v}{2}\right)^2 - \left(\frac{u-v}{2}\right)^2.
\tag{5.15}
$$

we interpret the region where $u \cdot v = 0$ as a mass hyperboloid at the origin $k = (u+v)/2$ and mass $m^2 = (u-v)^2/4$. We define the function

$$
h_\theta(u, v) \;=\; h_\delta\left(\frac{u+v}{2}, \frac{(u-v)^2}{4}\right) \theta\left(-u \cdot v\right)
\tag{5.16}
$$

where $\theta(x)$ is the well known Heaviside function. The function $h_\theta(u,v)$ vanishes whenever the scalar product $-u \cdot v$ is smaller than zero because of the Heaviside function. The function h_δ provides a smooth behaviour near the hyperboloid defined by $u \cdot v = 0$ and $h_\theta(u,v)$ converges to $h_\theta(u,v) = 1$ for $-u \cdot v \gg 0$.

5.3.2 Definition of the deformation vector κ_{ext}

If a threshold singularity occurs in the external region the loop momentum lie either on a forward hyperboloid or on a backward hyperboloid. In the external region we have by definition no intersections between forward and backward mass hyperboloids. Therefore we split the deformation vector into two pieces, one piece
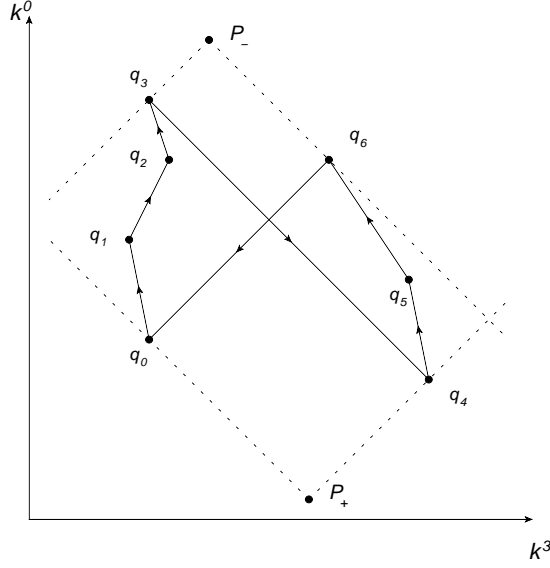
Figure 5.3: Example for the vectors P_+ and P_- in the loop momenta space for a generic primitive amplitude with $n = 7$ and $a = 4$.

which deforms correctly if the loop momentum lies on a forward hyperboloid and one piece which deforms correctly if the loop momentum lies on a backward hyperboloid. The deformation vector for the external region is given by

$$\kappa_{ext}^{\mu}(k) \;\; = \;\; g_{\mu\nu}\left(c_+ k_+^{\nu} + c_- k_-^{\nu}\right) \tag{5.17}$$

with

$$k_{\pm} \;\; = \;\; k - P_{\pm}. \tag{5.18}$$

and $g_{\mu\nu}$ the metric tensor. The Lorentz indices are such that an Minkowski scalar product with κ_{ext} is equal to an Euclidean scalar product with $k_{\pm}$. For an arbitrary fourvector v we have

$$v \cdot \kappa_{ext} \;\; = \;\; c_+ v \circ k_+ + c_- v \circ k_- \tag{5.19}$$

where $\circ$ demand the Euclidean scalar product.

First we discuss the coefficients $c_{\pm}$ and then the fourvectors $P_{\pm}$. With the help function $h_{\delta\pm}$ defined in eq.(5.10), the coefficients are simply defined by

$$c_{\pm} \;\; = \;\; \prod_{i=1}^{n} h_{\delta\mp}\left(k_i, m_i^2\right). \tag{5.20}$$

If the loop momentum k lies on any backward hyperboloid defined by

$$k_i^2 - m_i^2 \;\; = \;\; 0 \quad\quad \text{and} \quad\quad k^0 \;\; \leq \;\; 0, \quad i \in \{1, \dots, n\} \tag{5.21}$$

$h_{\delta-} = 0$ and therefore $c_+ = 0$. Analogously if the loop momentum k lies on any forward hyperboloid defined by

$$k_i^2 - m_i^2 \;=\; 0 \qquad \text{and} \qquad k^0 \;\geq\; 0, \quad i \in \{1, \dots, n\} \tag{5.22}$$

$h_{\delta+} = 0$ and therefore $c_- = 0$. The coefficients $c_\pm$ filter the threshold singularities corresponding to the forward/backward hyperboloids out of the integration region.

The vector P_+ is chosen such that $g_{\mu\nu}k_+^\nu$ always deforms correctly if k lies on a forward hyperboloid and P_- is chosen such that $g_{\mu\nu}k_-^\nu$ always deforms correctly if k lies on a backward hyperboloid. Consider a generic primitive amplitude fig.(5.2) (a), the vectors $(q_a - q_n)$ and $(q_{a-1} - q_{n-1})$ are spacelike. We define P_+ such that q_a and q_n lie on the forward light cone at the origin P_+ with a maximised zero component of P_+ and we define P_- such that q_{a-1} and q_{n-1} lie on the backward light cone at the origin P_- with a minimised zero component of P_-. In formulas, these conditions read

$$
\begin{aligned}
0 &= (q_a - P_+)^2 = (q_n - P_+)^2 = (q_a - P_+) \circ (q_n - P_+) \\
0 &\leq q_a^0 - P_+^0, \qquad 0 \leq q_n^0 - P_+^0 \\
0 &= (q_{a-1} - P_-)^2 = (q_{n-1} - P_-)^2 = (q_{a-1} - P_-) \circ (q_{n-1} - P_-) \\
0 &\geq q_{a-1}^0 - P_-^0, \qquad 0 \geq q_{n-1}^0 - P_-^0
\end{aligned} \tag{5.23}
$$

and are shown in fig.(5.3). The following equation fulfils all the conditions above.

$$
\begin{aligned}
P_+ &= Z_+(q_a + q_n, q_a - q_n) \\
P_- &= Z_-(q_{a-1} + q_{n-1}, q_{a-1} - q_{n-1})
\end{aligned} \tag{5.24}
$$

with

$$Z_\pm^\mu(x,y) \;=\; \frac{1}{2}\left(x^\mu \pm \frac{y_\nu}{|\vec{y}|}\left(g^{0\mu}y^\nu - g^{0\nu}y^\mu \right) \right). \tag{5.25}$$

For the degenerate diagrams in fig.(5.2) (b) and (c) we simple have

$$
\begin{aligned}
P_+ &= q_n \\
P_- &= q_{n-2}.
\end{aligned} \tag{5.26}
$$

In appendix C we proof that κ_{ext} always deforms correctly in the external region.

Next we discuss the UV behaviour of a propagator. We note that k_i^2 can be small even if the loop momentum k is in the UV region. We demand that after contour deformation the propagator falls of like $k \circ k$ in the UV region. In the external region at least one of the coefficients $c_\pm$ is non-zero. One can expect that the scaling parameter λ is of order 1 in the UV region were the loop momentum

k is very large. The imaginary part of a propagator in the UV region can be estimated by

$$k_i \cdot \kappa \quad \approx \quad k \cdot \kappa_{ext} \quad \approx \quad k \circ k \tag{5.27}$$

therefore the UV behaviour of all propagators after contour deformation is well defined.

5.3.3 Definition of the deformation vector $\kappa_{\textbf{int}}$

In the internal region we have to take regions into account where a forward hyperboloid intersects with a backward hyperboloid. In the massless case we can also have cones which are tangential to each other. Therefore we split the deformation vector for the internal region into two pieces, one piece which is suitable for the massless case and one piece which provides a correct deformation when two mass hyperboloids intersect. In the massless case it suffices to define

$$\kappa_{int}^{\mu} \quad = \quad -\sum_{i=1}^{n} c_i k_i^{\mu} \tag{5.28}$$

but in the massive case we need complicated extra terms

$$\kappa_{int}^{\mu} \quad = \quad -\sum_{i=1}^{n} c_i k_i^{\mu} - \sum_{\substack{i,j=1 \\ i<j}}^{n} c_{ij} k_{ij}^{\mu} \tag{5.29}$$

with

$$k_i \quad = \quad k - q_i \qquad \text{and} \qquad k_{ij} \quad = \quad k - v_{ij}. \tag{5.30}$$

First we discuss the coefficients c_i and c_{ij} and then discuss the vectors v_{ij}. The coefficients are defined such that they are zero if the corresponding vector deforms into the wrong direction. In terms of formulas, we have

$$k_a^2 - m_a^2 \quad = \quad 0 \quad \text{and} \quad \begin{cases} -c_i k_i \cdot k_a & < & 0 & \Rightarrow & c_i & = & 0 \\ -c_{ij} k_{ij} \cdot k_a & < & 0 & \Rightarrow & c_{ij} & = & 0 \end{cases}$$
$$\forall a \in \{1, \ldots, n\}. \tag{5.31}$$

This ensures that the deformation vector κ_{int} never deforms into the wrong direction. We have

$$c_i \quad = \quad g(k) \prod_{x=1}^{n} d_{i,x} \qquad \text{and} \qquad c_{ij} \quad = \quad \alpha_{ij}^2 \, g(k) \prod_{x=1}^{n} d_{ij,x} \tag{5.32}$$

with the function

$$g(k) \quad = \quad \frac{s}{(k_+ + k_-) \circ (k_+ + k_-) + s} \tag{5.33}$$

which ensures that the deformation vector κ_{int} falls off like $1/(k \circ k)$ in the UV region and s is the center of mass energy squared of the considered process. The factor α_{ij} is an empirically determined factor which ensures that in certain massive cases the second term on the right hand side of eq.(5.29) dominates. We have

$$\alpha_{ij} = \max \left\{ 1, \frac{m_i m_j}{M_2(m_i + m_j)} \right\} \qquad M_2 = \frac{\sqrt{s}}{90}, \tag{5.34}$$

with s the center of mass energy squared.

The factors $d_{i,x}$ are defined by

$$d_{i,x} = \begin{cases} 1 & : \ i = x, m_x = 0 \\ h_{\delta\pm}(k_x, m_x^2) & : \ (q_i - q_x)^2 = 0, \ q_i^0 \lessgtr q_x^0, \ m_x = 0 \\ \max\left[h_\delta(k_x, m_x^2), h_\theta(k_x, k_i)\right] & : \ \text{otherwise} \end{cases} \tag{5.35}$$

The idea is that the $d_{i,x}$ check all propagators for the conditions $k_x^2 = m_x^2$ and $-k_i \cdot k_x < 0$. If both conditions are fulfilled $d_{i,x}$ is zero. This ensures the behaviour of the coefficients c_i predicted by eq.(5.31). To proof that fact, we set

$$k_a^2 - m_a^2 = 0. \tag{5.36}$$

It follows that $h_\delta(k_a, m_a^2) = 0$ and for $x \neq a$ the functions $h_\delta(k_x, m_x^2)$ and $h_{\delta\pm}(k_x, m_x^2)$ are of order one. Therefore, if only one propagator is one-shell we can estimate $c_i \approx d_{i,a}$. We have to check that $d_{i,a} k_i \cdot k_a \geq 0$ for all $i \in \{1, \ldots, n\}$.

- $i = a$ and $m_a = 0$:

$$-k_i \cdot k_a = -k_a^2 = 0 \tag{5.37}$$

  therefore we can set $d_{a,a} = 1$.

- $(q_i - q_a)^2 = 0$, $q_i^0 < q_a^0$ and $m_a = 0$:

$$-k_i \cdot k_a = (q_i - q_a) \cdot k_a = k_a^0 \left(q_i^0 - q_a^0\right)(1 - \cos(\phi)) \tag{5.38}$$

  by setting $d_{i,a} = h_{\delta+}(k_a, m_a^2)$ we ensure that either $k_a^0 < 0$ or $d_{i,a} = 0$.

- $(q_i - q_a)^2 = 0$, $q_i^0 > q_a^0$ and $m_a = 0$:

$$-k_i \cdot k_a = (q_i - q_a) \cdot k_a = k_a^0 \left(q_i^0 - q_a^0\right)(1 - \cos(\phi)) \tag{5.39}$$

  by setting $d_{i,a} = h_{\delta-}(k_a, m_a^2)$ we ensure that either $k_a^0 > 0$ or $d_{i,a} = 0$.

- otherwise: By construction $h_\theta(k_i, k_a) = 0$ if $-k_i \cdot k_a < 0$, therefore either $d_{i,a} = 0$ or $-k_i \cdot k_a > 0$.

In eq.(5.38) and eq.(5.39) we make use of the definition

$$\cos(\phi) \;=\; \frac{\vec{k}_a}{k_a^0} \cdot \frac{\vec{q}_i - \vec{q}_a}{q_i^0 - q_a^0} \;\in (-1, 1). \tag{5.40}$$

One can ask why we do not simply define

$$d_{i,x} \;=\; \max\left[h_\delta(k_x, m_x^2), h_\theta(k_x, k_i)\right] \tag{5.41}$$

because with this construction eq.(5.31) is automatically for the coefficients c_i fulfilled. The exceptions in eq.(5.35) are taking the massless nature of the process into account. The deformation would vanish in the collinear limit without these exceptions but even if the contour is pinched we are allowed to deform along the tangential direction of the two intersection cones. By implementing these exceptions we observe an improvement of the numerical stability whenever we have massless propagators in the loop. For the massive case we have no need of such exceptions and we define

$$d_{ij,x} \;=\; \max\left[h_\delta(k_x, m_x^2), h_\theta(k_x, k_{ij})\right]. \tag{5.42}$$

So far, we have ensured that the deformation vector κ_{int} never deforms into the wrong direction and is suitable for the massless case. With κ_{ext} we already have a deformation vector which always deforms correctly if the loop momentum k lies either on a forward hyperboloid or a backward hyperboloid. Next, we define the vectors v_{ij} such that κ_{int} deforms correctly whenever k lies on the intersection of a forward and a backward hyperboloid.

First we define the two variables

$$\begin{aligned} x_{ij} &= |q_i^0 - q_j^0| - m_i - \sqrt{(\vec{q}_i - \vec{q}_j)^2 + m_j^2} \\ z_{ij} &= (q_i - q_j)^2 - (m_i + m_j)^2 \end{aligned} \tag{5.43}$$

If $z_{ij} > 0$ there exists an intersection region of a forward and a backward hyperboloid. If $x_{ij} > 0$ and $x_{ji} > 0$ the minimum of the forward hyperboloid lies in the interior of the backward hyperboloid and the maximum of the backward hyperboloid lies in the interior of the forward hyperboloid, otherwise at least one of the extremes of a hyperboloid lies outside the other hyperboloid. These two statements are proven in the appendix C. We note that $x_{ij} > 0$ is a stronger condition than $z_{ij} > 0$

$$x_{ij} \;>\; 0 \quad \Rightarrow \quad z_{ij} \;>\; 0. \tag{5.44}$$

We observe a better numerical performance by defining the vector v_{ij} differently in the region $x_{ij} > 0, x_{ji} > 0$ and the region where only $z_{ij} > 0$.

$$v_{ij} \;=\; \begin{cases} \frac{q_i k_j^0 - q_j k_i^0}{q_i^0 - q_j^0} &: \;\; x_{ij} > 0 \quad \text{and} \quad x_{ji} > 0 \\[2mm] \frac{V_{ij} + V_{ji}}{2} &: \;\; (x_{ij} < 0 \;\text{or}\; x_{ji} < 0) \;\text{and}\; z_{ij} > 0 \end{cases} \tag{5.45}$$
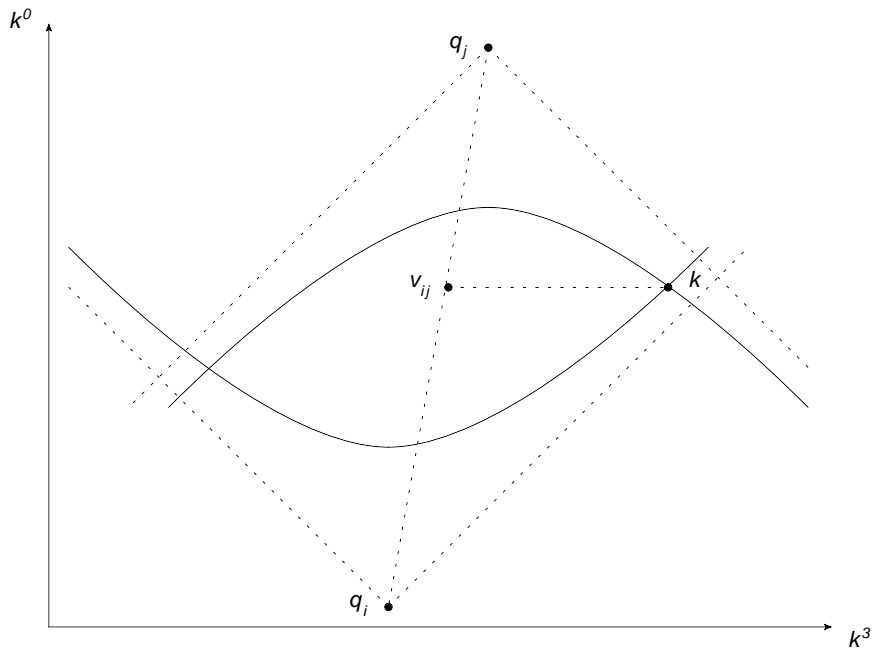
Figure 5.4: Definition of the vector v_{ij} for $x_{ij} > 0, x_{ji} > 0$; the loop momentum k lies on the forward mass hyperboloid with origin q_i and on the backward mass hyperboloid with origin q_j. The vector v_{ij} lies on the line connecting the points q_i and q_j with the time component $v_{ij}^0 = k^0$.
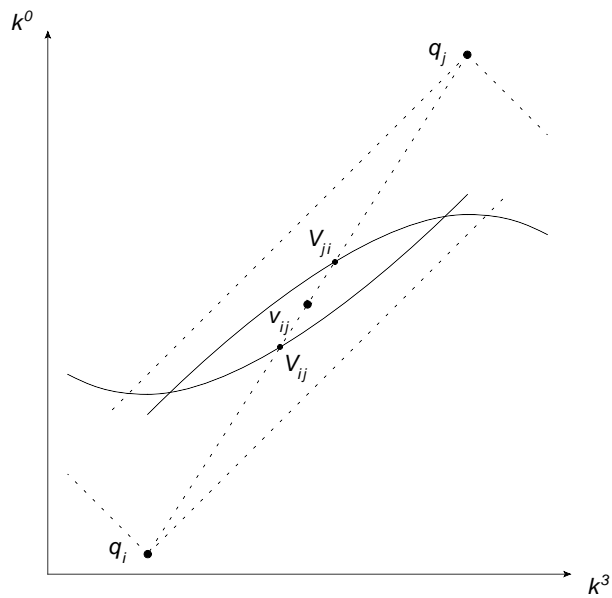
Figure 5.5: Definition of the vector v_{ij} for $x_{ij} < 0, x_{ji} < 0$ and $z_{ij} > 0$. The line connecting the points q_i and q_j cuts the mass hyperboloids at the two points V_{ij} and V_{ji}. The vector v_{ij} is at half of the distance of these two cutting points.

with

$$V_{ab} \quad = \quad q_a - m_a \frac{q_a - q_b}{\sqrt{(q_a - q_b)^2}} \tag{5.46}$$

For $x_{ij} > 0, x_{ji} > 0$ the vector v_{ij} lies on the line defined by $(q_i - q_j)$ with the time component $v_{ij}^0 = k^0$, see fig.(5.4). Otherwise with $z_{ij} > 0$ the vector v_{ij} is given by one half of the distance of the points where the line $(q_i - q_j)$ cuts the mass hyperboloids, see fig.(5.5). We note that for $z_{ij} \leq 0$ no v_{ij} is necessary and we simply set in eq.(5.29) $c_{ij} = 0$ in this case. The definition in eq.(5.45) ensures that whenever the loop momentum lies on the intersection of a forward hyperboloid with a backward hyperboloid there exists a vector which lies in the interior of both hyperboloids. Therefore the deformation vector κ_{int} deform correctly even in these critical regions. In the appendix C we give a detailed proof of the deformation.

5.3.4 Definition of the scaling parameter λ

The definition of the scaling parameter works along the lines of [11] with some minor changes because of the masses which can appear in the loop propagators. The deformation is given by $k \to k + \imath\kappa$ where

$$\kappa \quad = \quad \lambda\kappa_0. \tag{5.47}$$

In the previous sections we discussed the construction of $\kappa_0 = \kappa_{int} + \kappa_{ext}$ in detail. In appendix C we give a detailed proof that this deformation points always in the right direction for all loop momenta k. If λ is infinitesimal we have a correct deformation. But for the sake of numerical stability we want to deform as far away as possible from the singularities and therefore we need to make λ as large as possible. We now have to ensure that we do not cross any poles by varying the size of λ from zero to its final value. We define for each propagator in the loop a scaling parameter λ_i such that we do not cross any poles of the given propagator by varying λ_i from zero to its final value. By taking λ as the minimum of these λ_i we ensure that we do not cross any poles. We write for the ith propagator

$$D_i \quad = \quad (k_i + \imath\lambda\kappa_0)^2 - m_i^2 \quad = \quad k_i^2 + 2\imath\lambda\kappa_0 \cdot k_i - \lambda^2\kappa_0^2 - m_i^2 \tag{5.48}$$

The function D_i vanishes for values of λ given by

$$\lambda \quad = \quad \imath\sqrt{X_i} \pm \sqrt{Y_i - X_i} \tag{5.49}$$

where we introduce the functions

$$X_i \quad = \quad \left(\frac{\kappa_0 \cdot k_i}{\kappa_0^2}\right)^2 \quad \text{and} \quad Y_i = \frac{k_i^2 - m_i^2}{\kappa_0^2}. \tag{5.50}$$

If $Y_i > X_i$ and $X_i \to 0$ we have a pole at the real axis with value

$$\lambda \;=\; \sqrt{Y_i}. \tag{5.51}$$

To avoid these poles we limit the value of λ to one half of the value of this pole. If instead $Y_i < X_i$ the poles of the propagator D_i are on the imaginary λ axis and we can choose the real value of λ as big as we like. We define

$$\lambda_i^2 \;=\; \begin{cases} Y_i/4 & : & 2X_i \;<\; Y_i \\ X_i - Y_i/4 & : & 0 \;<\; Y_i \;<\; 2X_i \\ X_i - Y_i/2 & : & Y_i \;<\; 0 \end{cases}$$

Next we discuss the case that the loop momentum is near a collinear singularity. The collinear singularities emerging from q_i are given by

$$k \;\to\; q_i + x(q_{i+1} - q_i) \qquad x \in (0,1) \tag{5.52}$$
$$k \;\to\; q_i + x(q_{i-1} - q_i) \qquad x \in (0,1) \tag{5.53}$$

These two lines meet at q_i for $x = 0$. At a collinear singularity one can not deform away from the singularity but only deform along the line defined by eq.(5.52) or eq.(5.53). In this case we have $\kappa_0 \cdot k_i = \kappa_0^2 = 0$ and in the definitions of X_i and Y_i the numerator and the denominator vanishes. So the scaling parameter need some special treatment in the collinear limit. Near the collinear limit we approximate the deformation vector by a vector alongside the collinear line plus a small vector perpendicular to it. We write

$$\kappa_0 \;=\; -Ck_i + \epsilon_\perp \tag{5.54}$$

where C is the sum over all coefficients from the internal region which can contribute to the collinear limit

$$C \;=\; \sum_{i=1}^{n} c_i + \sum_{\substack{i,j=1 \\ i<j}}^{n} c_{ij}. \tag{5.55}$$

We note

$$\kappa_0^2 \;=\; C^2 k_i^2 - 2Ck_i \cdot \epsilon_\perp + \mathcal{O}(\epsilon_\perp^2)$$
$$2C\kappa_0 \cdot k_i \;=\; -2C^2 k_i^2 + 2Ck_i \cdot \epsilon_\perp \tag{5.56}$$

by adding these two equations we get

$$2\kappa_0 \cdot k_i \;=\; -Ck_i^2 - \frac{\kappa_0^2}{C} \tag{5.57}$$

and squaring the last equation and introducing the definitions from eq.(5.50) yields

$$2X_i \;=\; Y_i + \frac{C^2}{2} Y_i^2 + \frac{1}{2C^2} \;>\; Y_i. \tag{5.58}$$

Near the collinear limit we are never in the region $2X_i < Y_i$. For $Y_i > 0$ we estimate

$$
\begin{aligned}
\lambda_i^2 &= X_i - \frac{1}{4}Y_i \\
&= \frac{1}{4}Y_i + \frac{C^2}{4}Y_i^2 + \frac{1}{4C^2} \quad > \quad \frac{1}{4C^2}
\end{aligned}
\tag{5.59}
$$

and for $Y_i < 0$ we estimate

$$
\begin{aligned}
\lambda_i^2 &= X_i - \frac{1}{2}Y_i \\
&= \frac{C^2}{4}Y_i^2 + \frac{1}{4C^2} \quad > \quad \frac{1}{4C^2}.
\end{aligned}
\tag{5.60}
$$

Thus near the collinear limit we have

$$
\lambda_i \quad > \quad \frac{1}{2C}.
\tag{5.61}
$$

To ensure that λ is a smooth function near the collinear limit we define

$$
\lambda_{coll} \quad = \quad \frac{1}{4C}.
\tag{5.62}
$$

and define λ as the minimum of all the λ_i's and λ_{coll}

$$
\lambda \quad = \quad \min\left[1, \lambda_i, \lambda_{coll}\right] \qquad i \in \{1, \ldots, n\}.
\tag{5.63}
$$

So far, we have considered all the propagators in the loop and the collinear limit but we also have to ensure that we do not run into poles of the UV propagator

$$
D_{UV} \quad = \quad \left(\bar{k} + \imath\lambda\kappa_0\right)^2 - \mu_{UV}^2 \quad = \quad \bar{k}^2 + 2\imath\lambda\kappa_0 \cdot \bar{k} - \lambda^2\kappa_0^2 - \mu_{UV}^2.
\tag{5.64}
$$

The mass μ_{UV}^2 is purely imaginary with $\mathrm{Im}(\mu_{UV}^2) < 0$. We have to ensure by scaling that the imaginary part introduced through the deformation is larger than $\mathrm{Im}(\mu_{UV}^2)$.

$$
2\lambda_{UV}\kappa_0 \cdot \bar{k} \quad > \quad \mathrm{Im}(\mu_{UV}^2)
\tag{5.65}
$$

We define

$$
\lambda_{UV} \quad = \quad
\begin{cases}
1 & : \quad 4\kappa_0 \cdot \bar{k} > \mathrm{Im}(\mu_{UV}^2) \\
\frac{\mathrm{Im}(\mu_{UV}^2)}{4\kappa_0 \cdot \bar{k}} & : \quad 4\kappa_0 \cdot \bar{k} \leq \mathrm{Im}(\mu_{UV}^2)
\end{cases}
\tag{5.66}
$$

and

$$
\lambda \quad = \quad \min\left[1, \lambda_i, \lambda_{coll}, \lambda_{UV}\right] \qquad i \in \{1, \ldots, n\}.
\tag{5.67}
$$

This ensures that the deformation is suitable for the UV propagator.
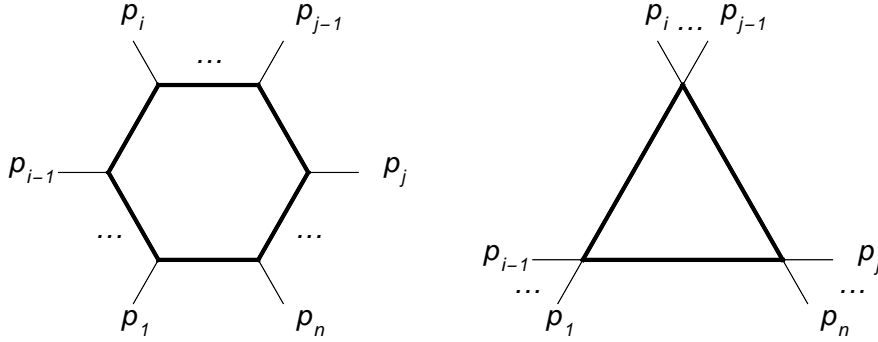
Figure 5.6: The diagram on the left shows the top level diagram for a process with n massless external legs with a closed massive line. Pinching $(n-3)$ loop propagators results in a three point function shown on the right.

Figure 5.7: The diagram on the left shows the top level diagram for a process with $n-2$ massless and 2 massive external legs. The massive line goes left around in the loop. Pinching $(n-3)$ loop propagators results in a three point function shown on the right.
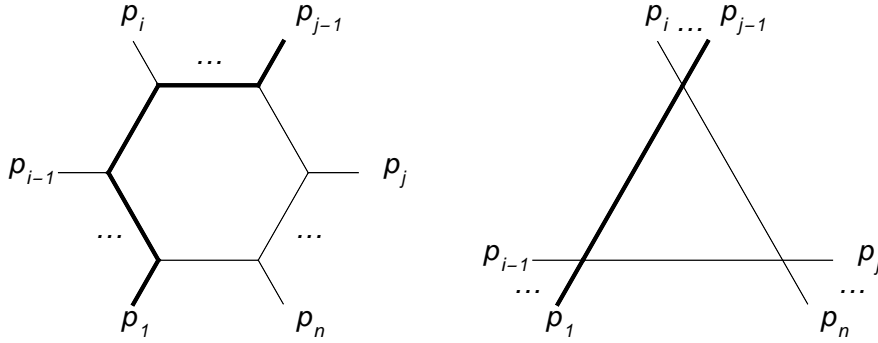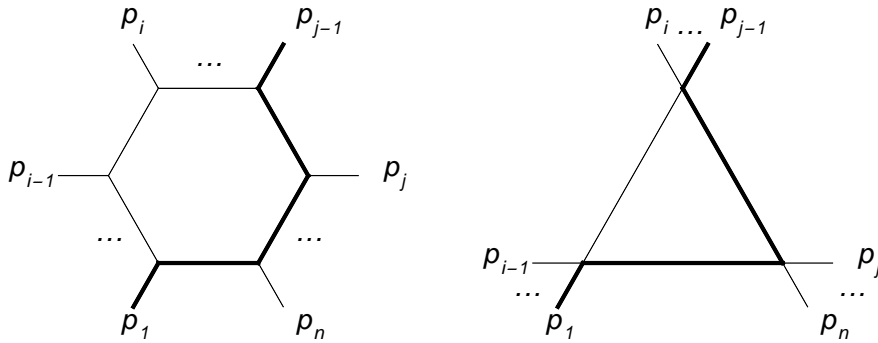

Figure 5.8: The diagram on the left shows the top level diagram for a process with $n-2$ massless and 2 massive external legs. The massive line goes right around in the loop. Pinching $(n-3)$ loop propagators results in a three point function shown on the right.
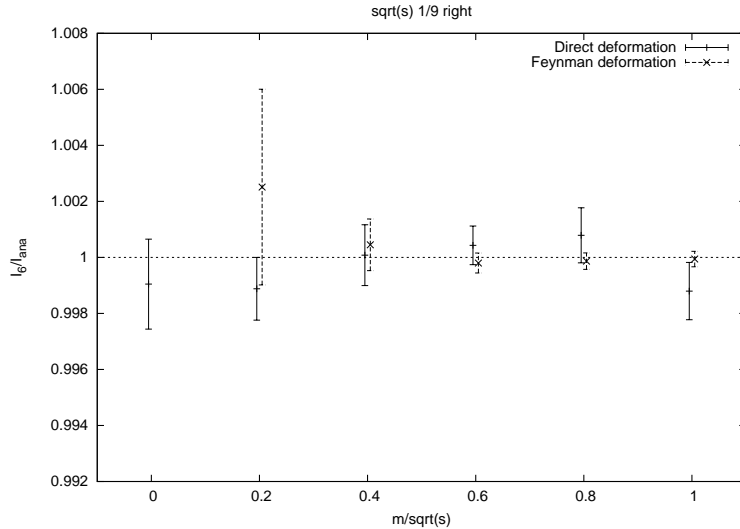
Figure 5.9: Results for the numerical integration of the three-point function normalised to the analytical result for a contour based on six external particles for various masses in the loop. For $m = 0$ we do not show the result for the Feynman deformation due its large statistical error.

5.4 Checks and examples

In this section we present results calculated with the contour deformation presented in the previous sections. We are testing by using a configuration with n massless external particles with a closed massive line, see fig.(5.6), and a configuration with $n - 2$ massless and two massive external particles, see fig.(5.7). By pinching $(n - 3)$ of the internal particles we obtain a one-loop three-point function as shown in fig.(5.6) and fig.(5.7). By permuting the position of one of the massive external particles we can vary the number of massive lines in the loop from 1 to $n - 1$. Like in chapter 4 we use LoopTools to compare our numerical results with the analytical results of the three point function.

In the plots we show the numerical results for the three-point function considering six external particles normalised to the analytic results. We show results calculated with the "Feynman deformation" discussed in chapter 4 and with the "Direct deformation" discussed in this chapter to compare each other. For the integration we use the VEGAS algorithm in the same way as discussed in section 4.4. The final result is given by the weighted arithmetic average of 20 independent VEGAS runs with 10^6 iterations per run and a warm up phase with five runs.

First we discuss the set up shown in fig.(5.6), a closed massive line in the loop.

The plot in fig.(5.9) show the impact of a closed massive line in the loop to the numerical stability of the integrand. It is shown the normalised results against the ratio of the mass in the loop to the center of mass energy. In this framework we use none of the improvement techniques for the Feynman deformation. We observe that the statistical error of the results calculated with the Feynman deformation are strongly dependent on the mass circulating in the loop. The larger the mass the more stable the integration. But because of the very large energy of the LHC compared to the heaviest known particle, the top quark, a large mass to center of mass energy ratio is very unlikely.

Next we discuss the framework shown in fig.(5.7) and fig.(5.8). We keep the position in the loop of one of the massive external particles fixed and permute the other massive external particle around the loop. By doing this we can vary the number of massive lines in the loop from 1 to $(n-1)$, here $n = 6$. To improve the stability of the Feynman deformation we use the following choice of parameters: $k = 1$, $\eta = 0.02$, $N_{IR} = 6$ and $M_{IR} = 3$. For $k = 1$ and $N_{IR} = 6$ we split the original integration into 36 integrations, each region is performed with 10^5 iterations per VEGAS run. To give comparable results we perform the integration with the Direct deformation with an 36 times larger statistic. The plots in fig.(5.10-5.13) shows the normalised results for the one-loop three-point function for different masses moving left or right around the loop against the number of massive lines in the loop.

We observe that the Feynman deformation and the Direct deformation provide both reasonable results. Overall, the Direct deformation seems to lead to smaller statistical errors expect the case that a massive line circulate in the loop. The integrand of the three-point Feynman integral concerning six external particles is of course more complicate than the integrand of a simple three-point function. But still the tests shown that the Direct deformation is very suitable for an numerical integration of one-loop integrals with massive propagators involved. Also is the Direct deformation absolutely process independent and therefore we can use it to integrate multi-loop integrals numerically. How this is done, is content of the next chapter.

Figure 5.10: Results for the numerical integration of the three-point function normalised to the analytical result for a contour based on six external particles for various numbers of massive propagators in the loop. The massive line is left moving with mass $m = \sqrt{s}/9$.

Figure 5.11: Results for the numerical integration of the three-point function normalised to the analytical result for a contour based on six external particles for various numbers of massive propagators in the loop. The massive line is right moving with mass $m = \sqrt{s}/9$
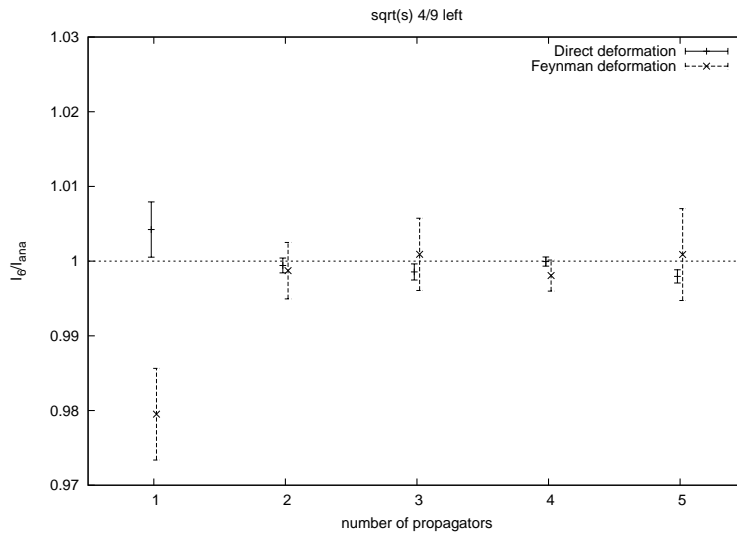
Figure 5.12: Results for the numerical integration of the three-point function normalised to the analytical result for a contour based on six external particles for various numbers of massive propagators in the loop. The massive line is left moving with mass $m = 4\sqrt{s}/9$.
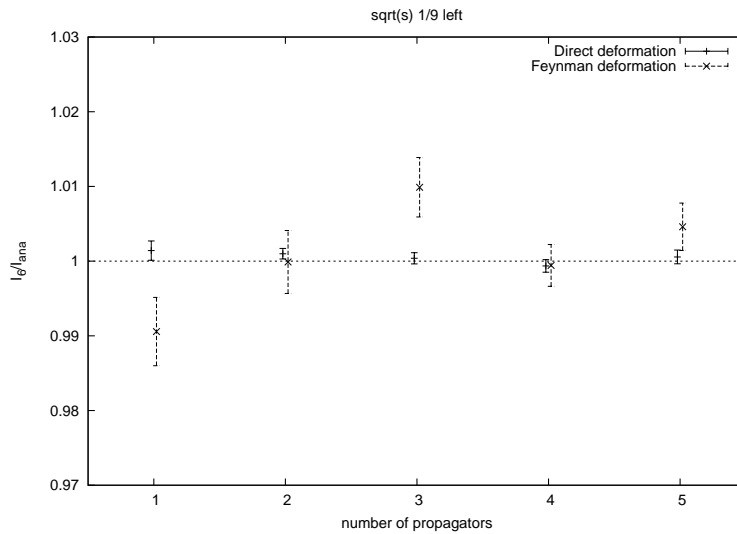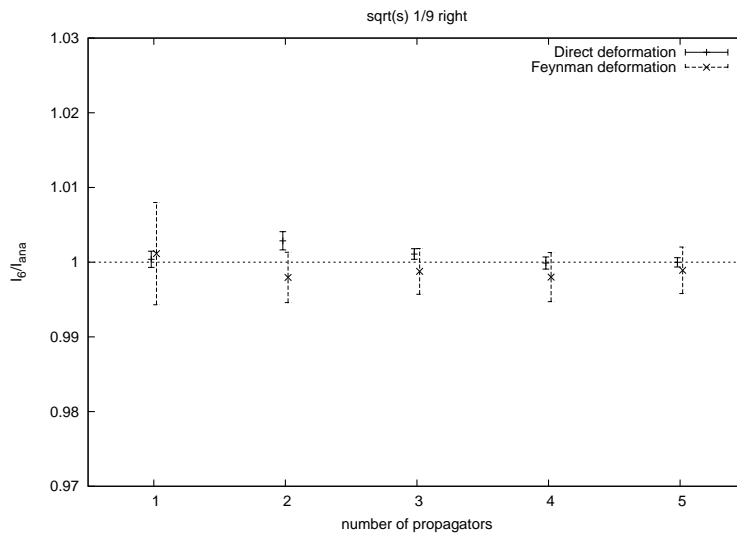

Figure 5.13: Results for the numerical integration of the three-point function normalised to the analytical result for a contour based on six external particles for various numbers of massive propagators in the loop. The massive line is right moving with mass $m = 4\sqrt{s}/9$.
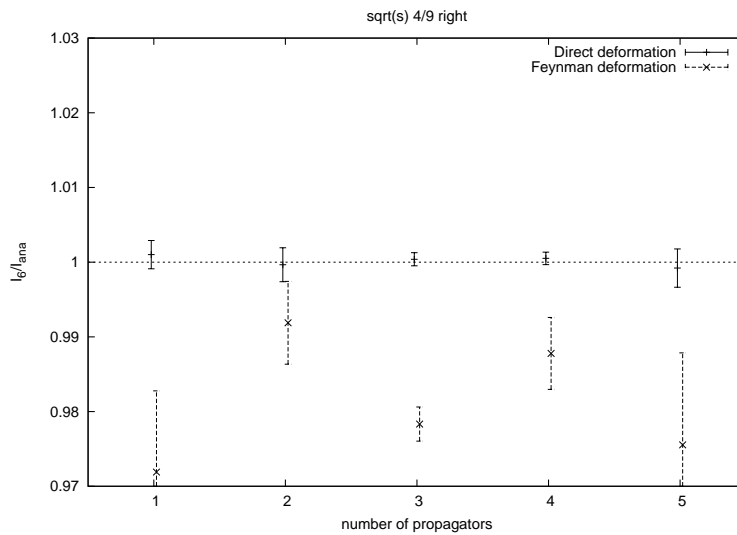
6 Direct integration of two- and three-loop diagrams

In this chapter we discuss the numerical calculation of multi-loop integrals with the contour deformation discussed in chapter 5.

6.1 Introduction

In chapter 2 we discuss in detail the numerical calculation of an infrared save observable at NLO. We give a short outlook to the NNLO calculation to motivate the contour deformation for multi-loop integrals. At the NNLO one has to calculate the following contributions

$$
\begin{aligned}
|\mathcal{A}_n|^2_{\mathrm{NNLO}} &= 2\,\mathrm{Re}\left(\mathcal{A}_n^{(0)*}\mathcal{A}_n^{(2)}\right) + \left|\mathcal{A}_n^{(1)}\right|^2 \\
|\mathcal{A}_{n+1}|^2_{\mathrm{NNLO}} &= 2\,\mathrm{Re}\left(\mathcal{A}_{n+1}^{(0)*}\mathcal{A}_{n+1}^{(1)}\right) \\
|\mathcal{A}_{n+2}|^2_{\mathrm{NNLO}} &= \left|\mathcal{A}_{n+2}^{(0)}\right|^2.
\end{aligned}
\tag{6.1}
$$

Here $\mathcal{A}_n^{(l)}$ denotes an amplitude with n final-state partons and l loops. One would naively expect that in the calculation of $\left|\mathcal{A}_n^{(1)}\right|^2$ one need to calculate the $\mathcal{O}(\epsilon)$- and $\mathcal{O}(\epsilon^2)$-terms of the one-loop amplitudes. A numerical calculation in $D = 4$ dimension is of course not sensitive to these terms. But in [69] it is shown that the $\mathcal{O}(\epsilon)$- and $\mathcal{O}(\epsilon^2)$-terms of a one-loop amplitudes are not needed. We quote here the important result of this publication:

Theorem: For an NNLO calculation it is sufficient to know the tree-level amplitudes $\mathcal{A}_n^{(0)}$, $\mathcal{A}_{n+1}^{(0)}$ and $\mathcal{A}_{n+2}^{(0)}$, the $\mathcal{O}(\epsilon^0)$-terms of the one-loop finite remainder function $\mathcal{F}_n^{(1)}$ and $\mathcal{F}_{n+1}^{(1)}$, as well as the $\mathcal{O}(\epsilon^0)$-terms of the two-loop finite remainder function $\mathcal{F}_n^{(2)}$. The $\mathcal{O}(\epsilon)$- and $\mathcal{O}(\epsilon^2)$-terms of the one-loop finite remainder function $\mathcal{F}_n^{(1)}$ drop out from the final result and are therefore not needed.

This theorem open the gate for a numerical NNLO calculation analogues to the NLO calculations presented in chapter 2. The finite remainder functions can be
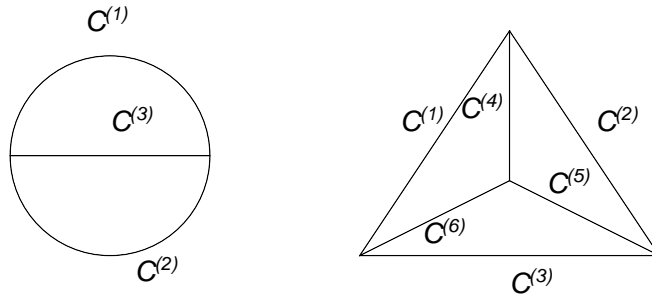
Figure 6.1: Simple chain diagrams for a two loop diagram (left) and a three loop diagram (right). In the two-loop case we can have up to three chains and in the three-loop case up to six chains.

written as

$$
\begin{aligned}
\mathcal{F}_n^{(1)} &= \mathcal{A}_n^{(1)} - \mathbf{I}^{(1)} \mathcal{A}_n^{(0)} \\
\mathcal{F}_n^{(2)} &= \mathcal{A}_n^{(2)} - \mathbf{I}^{(1)} \mathcal{A}_n^{(1)} - \mathbf{I}^{(2)} \mathcal{A}_n^{(0)}.
\end{aligned}
\tag{6.2}
$$

If a local integral representation of the insertion operators $\mathbf{I}^{(1)}$ and $\mathbf{I}^{(2)}$ are known one can perform the integrals on the right hand side numerical in $D = 4$ dimensions.

We conclude, a numerical NNLO calculation is possible but one need local subtraction terms for one- and two-loop amplitudes and a suitable contour deformation. The local subtraction terms at two-loop level are not known yet. Contour deformations at two-loop level are known [14–17] but only for methods based on Feynman parameters. In a single two-loop diagram with n external partons coupling directly to the loops, $n + 3$ different propagators appear. In a two-loop primitive amplitude in the leading colour approximation i.e. only planar diagrams contribute, the number of different propagators appearing in the calculation increase to $2n + 1$. Therefore, we have in the Feynman parameter approach a denominator function to the very high power $2n + 1$. As discussed in chapter 4 this could lead to numerical instabilities. For this reason we develop a contour deformation based on the Direct deformation which is suitable for two-loop integrals. As a proof of principles we apply the contour deformation also to three-loop integrals.

6.2 The chain diagram

In this section we discuss the representation of multi-loop diagrams in terms of so called "chain diagrams" [53]. We consider an arbitrary Feynman diagram

containing n internal lines. To each internal boson line i we have a propagator

$$D_i \;\; = \;\; \frac{1}{(k_i - q_i)^2 - m_i^2 + i\epsilon} \tag{6.3}$$

where k_i, q_i and m_i represent variable and fixed momenta and masses. We note that in general the fixed momenta q_i are not simply given by the sum of the momenta of the external particles like in the one loop case. We can always choose k_i and q_i, in such a way that conservation of four-momentum holds at each vertex for k and q separately. One writes a N-loop diagram with n internal lines as

$$\int \prod_{i=1}^{N} d^4 k_i F \prod_{j=1}^{n} D_j \tag{6.4}$$

where the numerator function F represents the contribution from vertices and numerators of fermion propagators. In a subtraction approach the function F also contains subtraction terms for the infrared and ultraviolet divergences such that the integral is finite. Assuming the integral is finite one needs a suitable contour deformation to be able to perform the integral numerically with Monte Carlo methods. For this purpose, let us introduce the notion of a chain. A chain α is defined as the largest set of internal lines having the same momentum variable k_α. Obviously, each internal line can only belong to a single chain. If a vertex is only connected via chains to the rest of the diagram we called it an internal vertex. Otherwise it will be called an external vertex. A new diagram is obtained from a Feynman diagram by omitting all external lines and corresponding vertices. This will be called chain diagram. An example of a two- and three-loop chain diagram is shown in fig.(6.1).

In the following let M the number of chains and n_α the number of internal lines of a chain α. We write the N-loop integral

$$\int \prod_{i}^{N} d^4 k^{(i)} F \prod_{\alpha=1}^{M} \prod_{j=1}^{n_\alpha} D_j^{(\alpha)}. \tag{6.5}$$

We emphasize that each chain can be parameterized by one variable momentum called a chain momentum, a set of fixed momenta and a set of masses.

$$C^{(\alpha)} \;\; := \;\; \left\{ k^{(\alpha)} | q_1^{(\alpha)}, \ldots, q_{n_\alpha}^{(\alpha)} | m_1^{(\alpha)}, \ldots, m_{n_\alpha}^{(\alpha)} \right\} \tag{6.6}$$

In chapter 5 we showed how to construct a suitable contour deformation for a diagram containing only a single chain. In the following section we discuss the construction of the contour deformation for multi-loop integrals by reducing the problem to the construction of a deformation for a single chain.
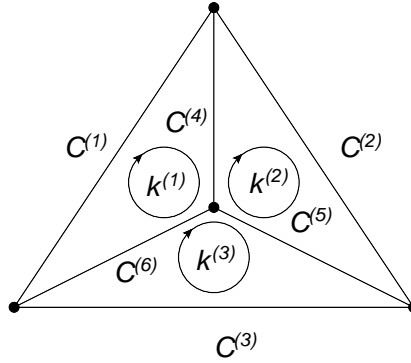
Figure 6.2: Definition of the three-loop chain diagram. $k^{(1)}$, $k^{(2)}$ and $k^{(3)}$ are the three independent loop momenta. The variable momenta of the other chains are given by the following linear combinations of the loop momenta: $k^{(4)} = k^{(1)} - k^{(2)}$, $k^{(5)} = k^{(2)} - k^{(3)}$ and $k^{(6)} = k^{(3)} - k^{(1)}$.

6.3 The deformation for a multi loop integral

Our starting point is a N-loop integral like in eq.(6.5) with chains defined like in eq.(6.6). First we note that in general $N < M$ and we are therefore not able to deform each single chain momentum into the complex plane separately. We choose a framework in which the first N chain momenta correspond exactly to the N loop momenta. The remaining $M - N$ chain momenta are linear combinations of the loop momenta. For up to three loops, we can ensure that for every topology the $M - N$ chain momenta are given by one loop momentum minus another loop momentum. This is shown in fig.(6.2).

The contour deformation of a N-loop diagram is defined by the deformation of the N independent loop momenta.

$$k^{(\alpha)} \quad \rightarrow \quad k^{(\alpha)} = \tilde{k}^{(\alpha)} + \imath \kappa^{(\alpha)}(\tilde{k}^{(1)}, \ldots, \tilde{k}^{(N)}), \qquad \alpha \in \{1, \ldots, N\}. \quad (6.7)$$

After applying this deformation to the multi-loop integral, it reads

$$\int \prod_i^N d^4 k^{(i)} F \left| \frac{\partial k^{(\beta)\mu}}{\partial \tilde{k}^{(\gamma)\nu}} \right| \prod_{\alpha=1}^M \prod_{j=1}^{n_\alpha} \tilde{D}_j^{(\alpha)} \quad (6.8)$$

with

$$\tilde{D}_j^{(\alpha)} = \frac{1}{\left(\tilde{k}^{(\alpha)} - q_j^{(\alpha)}\right)^2 + 2\imath \kappa^{(\alpha)} \cdot \left(\tilde{k}^{(\alpha)} - q_j^{(\alpha)}\right) - \left(\kappa^{(\alpha)}\right)^2}. \quad (6.9)$$

We note that for $\alpha > N$ the deformation vector $\kappa^{(\alpha)}$ is given by a linear combination of two deformation vectors and the chain momenta are given by linear

combinations of two loop momenta.

$$
\begin{aligned}
\tilde{k}^{(\alpha)}|_{\alpha>N} &= \tilde{k}^{(\beta)} - \tilde{k}^{(\gamma)}, & (\beta \neq \gamma) \in \{1,\ldots,N\}, & \qquad (6.10)\\
\Rightarrow \quad \kappa^{(\alpha)}|_{\alpha>N} &= \kappa^{(\beta)} - \kappa^{(\gamma)}, & (\beta \neq \gamma) \in \{1,\ldots,N\}. & \qquad (6.11)
\end{aligned}
$$

Because it is not possible to construct a deformation for each chain separately we have to find deformation vectors which deform in different chains correctly at the same time. Technically we merge two or more chains together by simply rewriting the propagators of a chain and then constructing a deformation vector for the merged chain with the algorithm presented in chapter 5. The final deformation vectors will be a linear combinations of the deformation vectors constructed from these merged chains.

We define a $N \times M$ matrix S whose entries S_{ij} are by default 1 and S_{ij} is (-1) if a chain momentum $k^{(j)}$ depends on the independent loop momentum $k^{(i)}$ with a relative sign. For the example given in fig.(6.2) this matrix reads

$$
S = \begin{pmatrix}
1 & 1 & 1 & 1 & 1 & -1\\
1 & 1 & 1 & -1 & 1 & 1\\
1 & 1 & 1 & 1 & -1 & 1
\end{pmatrix}. \qquad (6.12)
$$

The contribution of two chains to the integrand are now rewritten. To simplify the notation we set the masses to zero for a moment. We have for $\alpha \leq N$:

$$
\begin{aligned}
\prod_{i=1}^{n_\alpha} D_i^{(\alpha)} \prod_{j=1}^{n_\beta} D_j^{(\beta)} &= \prod_{i=1}^{n_\alpha}\prod_{j=1}^{n_\beta} \frac{1}{\left(k^{(\alpha)} - q_i^{(\alpha)}\right)^2 \left(k^{(\beta)} - q_j^{(\beta)}\right)^2}\\
&= \prod_{i=1}^{n_\alpha}\prod_{j=1}^{n_\beta} \frac{1}{\left(k^{(\alpha)} - q_i^{(\alpha)}\right)^2 \left(k^{(\alpha)} - \left(k^{(\alpha)} - S^{(\alpha\beta)}\left(k^{(\beta)} - q_j^{(\beta)}\right)\right)\right)^2}\\
&= \prod_{i=1}^{n_\alpha} \frac{1}{\left(k^{(\alpha)} - q_i^{(\alpha)}\right)^2} \prod_{j=1}^{n_\beta} \frac{1}{\left(k^{(\alpha)} - q_j^{(\alpha\beta)}\right)^2} \qquad (6.13)
\end{aligned}
$$

where we introduced a new "fixed momentum"

$$
q_i^{(\alpha\beta)} = k^{(\alpha)} - S^{(\alpha\beta)}\left(k^{(\beta)} - q_i^{(\beta)}\right) \qquad (6.14)
$$

which is in general not fixed at all. But for the contour deformation it plays for the moment no role that the $q^{(\alpha\beta)}$'s depend on variable momenta. We note that $S^{(\alpha\beta)}$ is a scalar and we do not summarize over β in eq.(6.13) and eq.(6.14). Because the propagators are squared the sign of $S^{(\alpha\beta)}$ drops out in eq.(6.13) and the introduction of $S^{(\alpha\beta)}$ in eq.(6.14) seems to be unnecessary or arbitrary. In the following we motivate the factor $S^{(\alpha\beta)}$ in eq.(6.14). Let us first remember of eq.(5.7) which defines the basic property of the deformation vector.

$$
k_i^2 - m_i^2 = 0 \qquad \Rightarrow \qquad \kappa \cdot k_i \geq 0 \qquad (6.15)
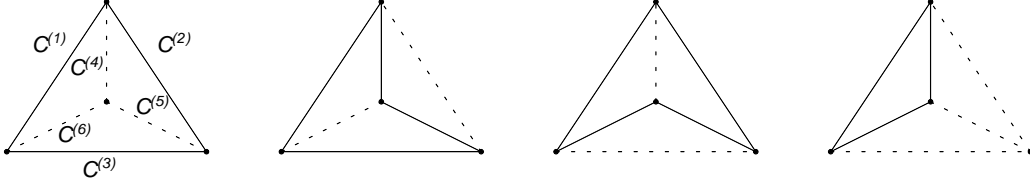$$

Figure 6.3: Example for the four different possibilities to reduce a three-loop chain diagram to a one-loop chain diagram, holding chain $C^{(1)}$ fixed. As a result we get four sets of chains. $C^{(123)} = \{C^{(1)}, C^{(2)}, C^{(3)}\}$, $C^{(1345)} = \{C^{(1)}, C^{(3)}, C^{(4)}, C^{(5)}\}$, $C^{(1256)} = \{C^{(1)}, C^{(2)}, C^{(5)}, C^{(6)}\}$ and $C^{(146)} = \{C^{(1)}, C^{(4)}, C^{(6)}\}$.

If we have a chain momentum $k^{(\gamma)} = S_{\alpha\gamma} k^{(\alpha)} + S_{\beta\gamma} k^{(\beta)}$, which is a linear combination of the two loop momenta $k^{(\alpha)}$ and $k^{(\beta)}$, we like to merge the chain γ with the chain α. Therefore we rewrite the propagator to

$$\left(k^{(\gamma)} - q^{(\gamma)}\right)^2 - \left(m^{(\gamma)}\right)^2 \;=\; \left(k^{(\alpha)} - q^{(\alpha\gamma)}\right)^2 - \left(m^{(\gamma)}\right)^2. \tag{6.16}$$

We apply the usual deformation to the loop momentum

$$k^{(\alpha)} \rightarrow k^{(\alpha)} + \imath \kappa^{(\alpha)} \tag{6.17}$$

where $\kappa^{(\alpha)}$ is constructed such that it fulfils eq.(6.15) for both chains α and γ simultaneously.

$$\left(k^{(\alpha)} - q^{(\alpha)}\right)^2 \;=\; \left(m^{(\alpha)}\right)^2 \quad\Rightarrow\quad \kappa^{(\alpha)} \cdot \left(k^{(\alpha)} - q^{(\alpha)}\right) \;\geq\; 0 \tag{6.18}$$

$$\left(k^{(\alpha)} - q^{(\alpha\gamma)}\right)^2 \;=\; \left(m^{(\gamma)}\right)^2 \quad\Rightarrow\quad \kappa^{(\alpha)} \cdot \left(k^{(\alpha)} - q^{(\alpha\gamma)}\right) \;\geq\; 0 \tag{6.19}$$

After applying the deformation the imaginary part of the propagator of chain γ which is proportional to $\kappa^{(\alpha)}$ is given by

$$\mathrm{Im}\left(\left(k^{(\gamma)} - q^{(\gamma)}\right)^2 - \left(m^{(\gamma)}\right)^2\right) \;=\; 2 S_{\alpha\gamma} \kappa^{(\alpha)} \cdot \left(k^{(\gamma)} - q^{(\gamma)}\right). \tag{6.20}$$

To fulfil eq.(6.15) we demand

$$S_{\alpha\gamma} \left(k^{(\gamma)} - q^{(\gamma)}\right) \;=\; k^{(\alpha)} - q^{(\alpha\gamma)}. \tag{6.21}$$

From the last equation the definition of eq.(6.14) follows directly.

Analogously to eq.(6.6) we define a merged chain by

$$C^{(i_1,\ldots,i_r)} \;=\; \left\{k^{(i_1)} \,\middle|\, q_1^{(i_1)},\ldots,q_{n_{i_1}}^{(i_1)}, q_1^{(i_1 i_2)},\ldots,q_{n_{i_r}}^{(i_1 i_r)} \,\middle|\, m_1^{(i_1)},\ldots,m_{n_{i_r}}^{(i_r)}\right\} \tag{6.22}$$

For each such a merged chain we can construct a corresponding deformation vector $\kappa^{(i_1,\ldots,i_r)}$ and we note that the deformation

$$k^{(i_1)} \rightarrow k^{(i_1)} + \imath \kappa^{(i_1,\ldots,i_r)} \tag{6.23}$$

provides the correct imaginary part for all propagators in the merged chain in the sense that eq.(6.15) is fulfilled.

Naively one would now expect to get the right deformation for a loop momentum by merging all chains whose chain momenta depend on this loop momentum and constructing the corresponding deformation vector from this single merged chain only. For the two-loop case, where we have $k^{(3)} = k^{(1)} - k^{(2)}$, one would expect

$$\kappa^{(1)} \;=\; \kappa^{(13)} \qquad \text{and} \qquad \kappa^{(2)} \;=\; \kappa^{(23)}. \tag{6.24}$$

But the situation is not so simple! The deformation vector for a loop momentum will be the sum of deformation vectors constructed from different merged chains. The different merged chains are defined by the different combinations of chains which are merged. The procedure to get all the necessary combinations of chains to construct the different merged chains is the following: We take the N-loop chain diagram, keep the line fixed which corresponds to the loop momentum for which we want construct the deformation vector. We note that by cutting out a chain from the chain diagram we reduce the N-loop chain diagram to a $N-1$ loop chain diagram. By taking into account all the possibilities to reduce a N-loop chain diagram to a one-loop chain diagram by cutting out successive single chains, we get all the necessary combinations of chains we need to merge. This procedure is exemplarily shown for a three-loop diagram in fig.(6.3).

In the two-loop case with $k^{(3)} = k^{(1)} - k^{(2)}$ we have the deformation vectors:

$$
\begin{aligned}
\kappa^{(\mathbf{1})} &\;=\; \kappa^{(\mathbf{12})} + \kappa^{(\mathbf{13})} \\
\kappa^{(\mathbf{2})} &\;=\; \kappa^{(\mathbf{12})} + \kappa^{(\mathbf{23})} \\
\kappa^{(\mathbf{3})} &\;=\; \kappa^{(\mathbf{13})} - \kappa^{(\mathbf{23})}
\end{aligned}
\tag{6.25}
$$

We note that $\kappa^{(12)} = \kappa^{(21)}$. In the three-loop case with the notation given in fig.(6.2) we have the deformation vectors:

$$
\begin{aligned}
\kappa^{(\mathbf{1})} &\;=\; \kappa^{(\mathbf{123})} + \kappa^{(\mathbf{146})} + \kappa^{(\mathbf{1256})} + \kappa^{(1345)} \\
\kappa^{(\mathbf{2})} &\;=\; \kappa^{(\mathbf{123})} + \kappa^{(\mathbf{245})} + \kappa^{(\mathbf{1256})} + \kappa^{(2346)} \\
\kappa^{(\mathbf{3})} &\;=\; \kappa^{(\mathbf{123})} + \kappa^{(\mathbf{356})} + \kappa^{(\mathbf{1345})} + \kappa^{(2346)} \\
\kappa^{(\mathbf{4})} &\;=\; \kappa^{(\mathbf{146})} - \kappa^{(\mathbf{245})} + \kappa^{(\mathbf{1345})} - \kappa^{(2346)} \\
\kappa^{(\mathbf{5})} &\;=\; \kappa^{(\mathbf{245})} - \kappa^{(\mathbf{356})} + \kappa^{(\mathbf{1256})} - \kappa^{(1345)} \\
\kappa^{(\mathbf{6})} &\;=\; \kappa^{(\mathbf{356})} - \kappa^{(\mathbf{146})} + \kappa^{(\mathbf{2346})} - \kappa^{(1256)}
\end{aligned}
\tag{6.26}
$$

The bold indices imply that each single summand on the right hand side of the definitions deforms correctly in the corresponding chain. One can ask why we need all these terms? We define a soft chain momentum by

$$k^{(\alpha)} \;=\; q_i^{(\alpha)} \qquad \text{and} \qquad m_i^{(\alpha)} \;=\; 0. \tag{6.27}$$

6 Direct integration of two- and three-loop diagrams

If the chain momentum $k^{(\alpha)}$ becomes soft the corresponding deformation vector $\kappa^{(\alpha)}$ has to vanish because of continuous arguments. If the loop momentum lies on the forward cone it points into the forward cone and if the momentum lies on the backward cone it points into the backward cone. Because the deformation has to be continuous it has to vanish at the origin of the cone. If $k^{(3)}$ becomes soft in the two-loop example then $\kappa^{(13)}$ and $\kappa^{(23)}$ vanish separately. Therefore $\kappa^{(3)}$ is zero as it should be. But we can still deform in the chains $C^{(1)}$ and $C^{(2)}$, that why we need the extra terms. As $\kappa^{(3)} = 0$ implies we have in this case $\kappa^{(1)} = \kappa^{(2)} = \kappa^{(12)}$.

Cutting a chain out of a chain diagram corresponds to setting the chain momentum soft in this chain. Therefore cutting chains out of a chain diagram until a single chain remains corresponds to making all these chain momenta soft but we can still deform correctly in the remaining chain. Because we have to deform if possible we have to consider every combination of soft chains which reduces the N-loop chain diagram to a one-loop chain diagram.

We take a closer look at the deformation vector

$$\kappa^{(i_1,\ldots,i_n)} \;\; = \;\; \lambda^{(i_1,\ldots,i_n)} \left(\kappa_{int}^{(i_1,\ldots,i_n)} + \kappa_{ext}^{(i_1,\ldots,i_n)} \right). \tag{6.28}$$

The scaling parameter $\lambda^{(i_1,\ldots,i_n)}$ is calculated by interpreting the merged chain defined by eq.(6.22) as an one-loop diagram and using the algorithm discussed in chapter 5.

The vector $\kappa^{(i_1,\ldots,i_n)}$ must be a smooth function of the variable momenta. The vector v_{ij} defined in eq.(5.45) is not a smooth function in the momenta q_i, q_j and therefore in the multi-loop case not a smooth function in the variable momenta. In the multi-loop case we rewrite

$$k - v_{ij} \;\; \rightarrow \;\; \theta(z_{ij}) \frac{z_{ij}}{z_{ij} + M_2^2} \left(k - (1 - X_{ij}) \frac{V_{ij} + V_{ji}}{2} - X_{ij} W_{ij} \right) \tag{6.29}$$

The expression on the right hand side is a smooth function in the variable momentum k and the fixed momenta q_i, q_j. We have

$$X_{ij} \;\; = \;\; \theta(x_{ij}) \frac{x_{ij}}{x_{ij} + M_2} \theta(x_{ji}) \frac{x_{ji}}{x_{ji} + M_2}, \qquad M_2 \;\; = \;\; \frac{\sqrt{s}}{90} \tag{6.30}$$

and

$$W_{ij} \;\; = \;\; \frac{q_i k_j^0 - q_j k_i^0}{q_i^0 - q_j^0} \tag{6.31}$$

The variables x_{ij}, z_{ij} and V_{ij} are defined in chapter 5 and s is the center of mass energy squared of the considered process

In the construction of κ_{ext}, more specifically in the definition of the vector P_+ and P_-, we make use of the fact that we have only up to two strains in the loop
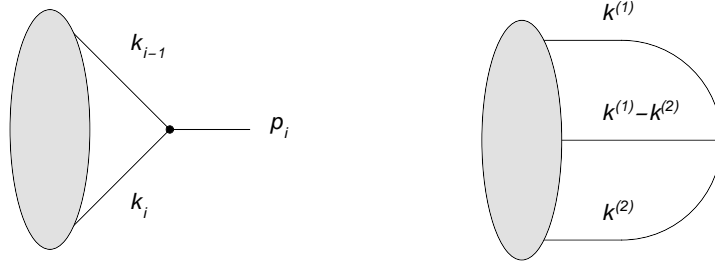
Figure 6.4: Examples for one-loop diagram with an external vertex (left) and an example for an two-loop diagram with an internal vertex (right).

momentum space for a one-loop amplitude fig.(5.2). For a generic merged chain this is no longer true but it is graphically clear that we can still find points in the loop momentum space whose light cones contain all the appearing strains. In the following we present a way to calculate the vectors $P_\pm$ in the multi-loop case. Consider a merged chain with n fixed momenta $q_1, \ldots, q_n$, we set

$$P_\pm = P_\pm^{(n)} \tag{6.32}$$

where $P_\pm^{(n)}$ is defined recursively by

$$P_\pm^{(i)} = \begin{cases} Z_\pm \left(P_\pm^{(i-1)} + q_i, P_\pm^{(i-1)} - q_i \right) & : & \left(P_\pm^{(i-1)} - q_i \right)^2 < 0 \\ P_\pm^{(i-1)} & : & \left(P_\pm^{(i-1)} - q_i \right)^2 > 0, \left(P_\pm^{(i-1)(0)} - q_i^{(0)} \right) \lessgtr 0 \\ q_i & : & \left(P_\pm^{(i-1)} - q_i \right)^2 > 0, \left(P_\pm^{(i-1)(0)} - q_i^{(0)} \right) \gtrless 0 \end{cases} . \tag{6.33}$$

The recursion start at $P_\pm^{(1)} = q_1$ and $Z_\pm(x, y)$ is defined by eq.(5.25).

6.4 Collinear configurations

At one-loop level the contour deformation is pinched if two collinear loop lines connected via an external vertex. This lead to an non integrable singularity. One could expect that at multi-loop level something similar happens if two collinear loop lines are connected via an internal vertex. We show exemplary at two-loops that this is not the case.

First we review the collinear configuration of an one-loop diagram fig.(6.4). We have a massless external on-shell particle $p_i^2 = 0$. If the two adjoint loop propagators get collinear to the external particle the contour deformation is pinched and a non integrable singularity appear. We note that at least one of the loop propagators must correspond to an gluon in order that the singularity is non

integrable. To show that the singularity is pinched we write down explicitly the imaginary part of the two loop propagators which are on-shell in the collinear limit.

$$k \quad \to \quad q_{i-1} + xp_i \quad \Rightarrow \begin{cases} \text{Im}(k_{i-1}^2) & \to & x\kappa \cdot p_i \\ \text{Im}(k_i^2) & \to & (x-1)\kappa \cdot p_i \end{cases} , \quad x \in (0,1) \quad (6.34)$$

Obviously it is impossible to find a deformation vector κ such both propagators get a positive imaginary part and therefore is in this collinear limit $\kappa \cdot p_i = 0$.

Now the two-loop case. The loop momentum $k^{(3)} = k^{(1)} - k^{(2)}$ is connected via an internal vertex to the loop momenta $k^{(1)}$ and $k^{(2)}$. The masses in the corresponding propagators are zero. We set $k^{(2)}$ on-shell and $k^{(1)}, k^{(3)}$ collinear to $k^{(2)}$.

$$k^{(2)} \quad \to \quad p \qquad p^2 = 0 \tag{6.35}$$
$$k^{(1)} \quad \to \quad xp \tag{6.36}$$
$$k^{(3)} \quad \to \quad (x-1)p \tag{6.37}$$

In this set up three loop propagators are on-shell. With the definition given in eq.(6.25), the corresponding imaginary parts are

$$\text{Im}\left((k^{(1)})^2\right) \quad \to \quad x\kappa^{(12)} \cdot p + x\kappa^{(13)} \cdot p \tag{6.38}$$
$$\text{Im}\left((k^{(2)})^2\right) \quad \to \quad \kappa^{(12)} \cdot p + \kappa^{(23)} \cdot p \tag{6.39}$$
$$\text{Im}\left((k^{(3)})^2\right) \quad \to \quad (x-1)\kappa^{(13)} \cdot p - (x-1)\kappa^{(23)} \cdot p. \tag{6.40}$$

For all values of x the singularity is never pinched. We construct our deformation vectors such that:

$$x < 0$$
$$\Rightarrow \quad \kappa^{(12)} \cdot p = 0, \qquad \kappa^{(13)} \cdot p < 0, \qquad \kappa^{(23)} \cdot p > 0. \tag{6.41}$$
$$x \in (0,1)$$
$$\Rightarrow \quad \kappa^{(12)} \cdot p > 0, \qquad \kappa^{(13)} \cdot p = 0, \qquad \kappa^{(23)} \cdot p > 0. \tag{6.42}$$
$$x > 1$$
$$\Rightarrow \quad \kappa^{(12)} \cdot p > 0, \qquad \kappa^{(13)} \cdot p > 0, \qquad \kappa^{(23)} \cdot p = 0. \tag{6.43}$$

For $x = 0$ or $x = 1$ the singularity is pinched but only for a single propagator and therefore don't lead to an non integrable singularity. We summarize, a necessary condition for an non integrable collinear singularity in a loop integration is a massless on-shell external particle which is connected directly to the loop.

6.5 Checks and examples

In this section we test the contour deformation for multi-loop diagrams by calculating some simple diagrams and compare the numerical results with the known

Figure 6.5: Definition of the L-loop two-point ladder diagram. The analytic expression for this diagram is given by $B^{(L)}(p^2)$.

Figure 6.6: Definition of the L-loop three-point ladder diagram. The analytic expression for this diagram is given by $C^{(L)}(p_1^2, p_2^2, p_3^2)$.

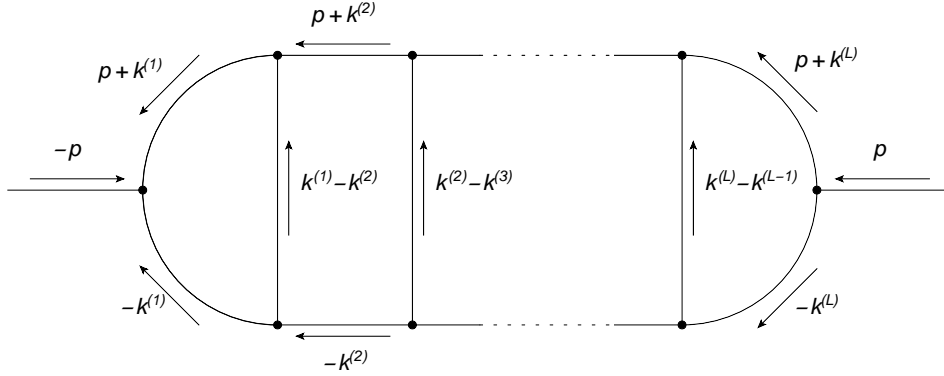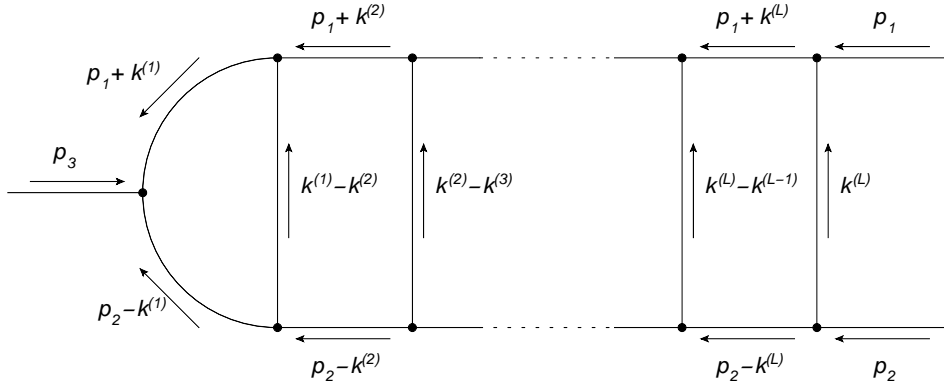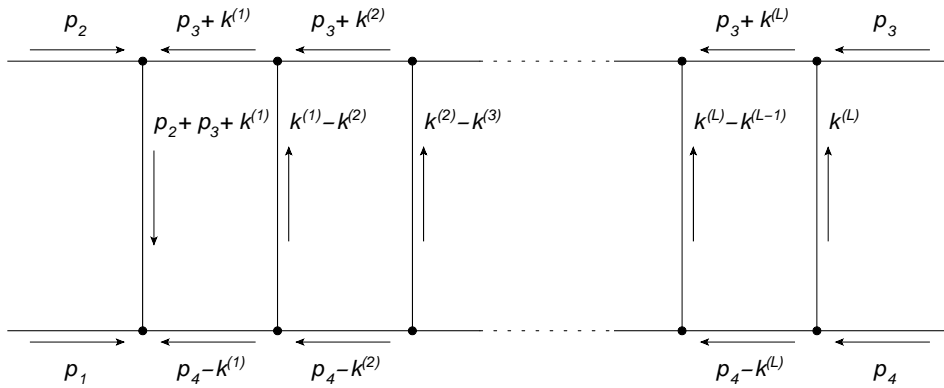**Figure 6.7:** Definition of the L-loop four-point ladder diagram. The analytic expression for this diagram is given by $D^{(L)}(p_1^2, p_2^2, p_3^2, p_4^2, s, t)$.

analytical results. Scalar multi-loop diagrams with all external particles off shell are infrared safe. With no one-loop self-energy type sub diagrams these diagrams are also ultraviolet finite. In the literature [61] we find simple analytical results for the two-, three- and four-point ladder diagrams shown in fig.(6.5, 6.6, 6.7). We repeat here the analytical results for these ladder diagrams.

$$B^{(L)}(p^2) = \left(\frac{\imath\pi^2}{p^2}\right)^L p^2 \frac{(2L)!}{(L!)^2}\zeta(2L-1) \tag{6.44}$$

$$C^{(L)}(p_1^2, p_2^2, p_3^2) = \left(\frac{\imath\pi^2}{p_3^2}\right)^L \Phi^{(L)}(x, y) \tag{6.45}$$

$$D^{(L)}(p_1^2, p_2^2, p_3^2, p_4^2, s, t) = \left(\frac{\imath\pi^2}{s}\right)^L \frac{1}{t}\Phi^{(L)}(X, Y) \tag{6.46}$$

The function Φ can be expressed in terms of polylogarithms

$$\Phi^{(L)}(x, y) = -\frac{1}{L!\lambda}\sum_{j=L}^{2L}\frac{(-1)^j j! \ln^{2L-j}(y/x)}{(j-L)!(2L-j)!}\left[\mathrm{Li}_j\left(-\frac{1}{\rho x}\right) - \mathrm{Li}_j(-\rho y)\right] \tag{6,47}$$

The definitions of the variables are

$$\begin{aligned}
x &= \frac{p_1^2}{p_3^2}, & y &= \frac{p_2^2}{p_3^2}, \\
X &= \frac{p_1^2 p_3^2}{st}, & Y &= \frac{p_2^2 p_4^2}{st} \\
s &= (p_1 + p_2)^2, & t &= (p_2 + p_3)^2
\end{aligned} \tag{6.48}$$

$$\lambda(x, y) = \sqrt{(1-x-y)^2 - 4xy} \qquad \rho(x, y) = \frac{2}{1-x-y-\lambda}$$

In [62] it is shown that the non-planar two-loop three-point function can also be expressed in terms of these functions:

$$C_{np}^{(2)}(p_1^2, p_2^2, p_3^2) = \left(C^{(1)}(p_1^2, p_2^2, p_3^2)\right)^2 \tag{6.49}$$

The chain diagram of the three-loop ladder diagram is degenerate and therefore simplifies the construction of the deformation vector a little bit. We get the degenerate chain diagram by removing the chain $C^{(6)}$ from fig.(6.2). The resulting chain diagram is shown in fig.(6.8). The deformation vectors for such chain diagram are defined by

$$\begin{aligned}
\kappa^{(1)} &= \kappa^{(14)} + \kappa^{(123)} + \kappa^{(125)} \\
\kappa^{(2)} &= \kappa^{(245)} + \kappa^{(123)} + \kappa^{(125)} + \kappa^{(234)} \\
\kappa^{(3)} &= \kappa^{(35)} + \kappa^{(123)} + \kappa^{(234)} \\
\kappa^{(4)} &= \kappa^{(14)} - \kappa^{(245)} - \kappa^{(234)} \\
\kappa^{(5)} &= \kappa^{(245)} + \kappa^{(125)} - \kappa^{(35)}
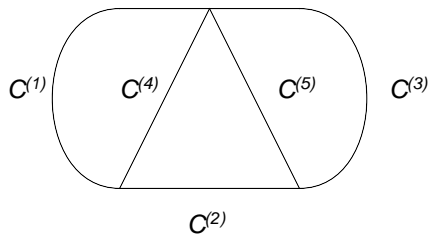\end{aligned} \tag{6.50}$$

Figure 6.8: The degenerate chain diagram of an three-loop ladder diagram.

In our test program we use the VEGAS algorithm from the CUBA library. After a warm-up phase of five VEGAS runs the program performs 20 VEGAS runs. Each VEGAS run is performed with 10^7 iterations. The final result is calculated via a weighted arithmetical average of the 20 VEGAS runs, see chapter 4 for more details. For the calculation of the three-loop ladder diagrams we increase the statistic by another factor of 10. The detailed set up i.e. the external momenta of the diagrams for the calculation is given in appendix D.

In tab.(6.1) we show the analytic results together with the numeric results calculated with our method for the two- and three-loop ladder diagrams defined in fig.(6.5, 6.6, 6.7) and the non planar two-loop triangle. In tab.(6.2) we show the numeric results for different two-loop six-point topologies. For such diagrams no analytic results are known but we can check if or how strongly the statistical error depends on the topology we calculate.

The numerical results shown in tab.(6.1) are in good agreement with the analytic results. At the two-loop level we reach a accuracy of about one percent. At three-loop level the accuracy decrease to about 10 percent but as a proof of principles these results are still good. The numerical results for the two-loop six-point functions shown in tab.(6.2) are at a accuracy of about five percent and shown no strong dependence of the given topology. In terms of the contour deformation we do not expect any difficulties from calculating non-planar diagrams.

In this chapter we successfully apply the Direct deformation approach to multi-loop integrals. So far we are limited in the calculation of two- and three-loop integrals. An extension to even higher-loops are thinkable but not practical for the moment. We tested the contour deformation only for massless diagrams, but because the Direct deformation is suitable for masses at one-loop level we expect it is also suitable for masses at multi-loop level.

	analytic result	numerical result
$B^{(2)}$	$-8.67343 * 10^{-2}$	$(-8.651 \pm 0.0509) * 10^{-2}$
$C^{(2)}$	$-4.44938 * 10^{-5}$	$(-4.4842 \pm 0.0569) * 10^{-5}$
$C_{np}^{(2)}$	$-7.05339 * 10^{-5}$	$(-7.0829 \pm 0.0905) * 10^{-5}$
$D^{(2)}$	$-1.43249 * 10^{-7}$	$(-1.4489 \pm 0.0172) * 10^{-7}$
$B^{(3)}$	$-\imath \, 3.03884 * 10^{-4}$	$-\imath \, (3.0403 \pm 0.3241) * 10^{-4}$
$C^{(3)}$	$-\imath \, 2.04016 * 10^{-7}$	$-\imath \, (2.0804 \pm 0.2432) * 10^{-7}$
$D^{(3)}$	$-\imath \, 2.55297 * 10^{-9}$	$-\imath \, (2.8133 \pm 0.2482) * 10^{-9}$

Table 6.1: Results for various two- and three-loop diagrams corresponding to two-, three- and four-point functions.
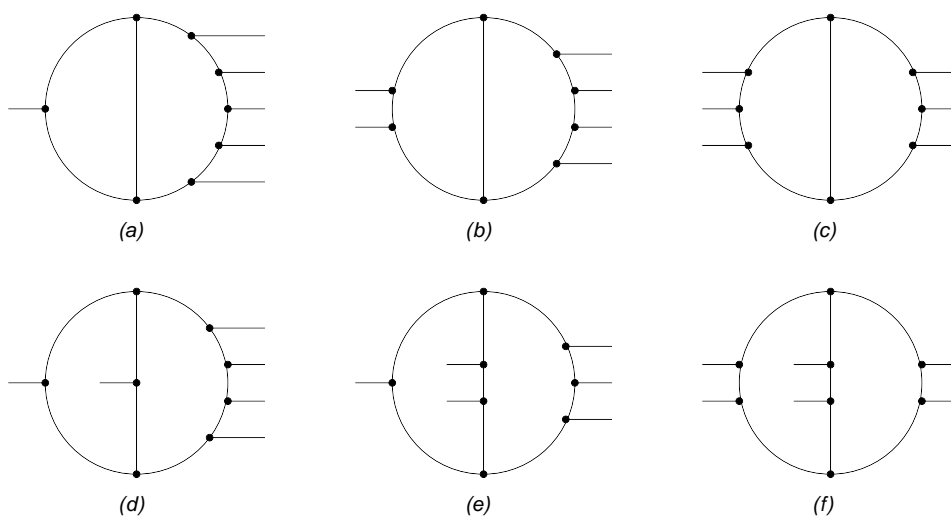
Figure 6.9: Definition of various two-loop six-point topologies.

	numerical result	relative error
(a)	$(-2.0191 \pm 0.0505) * 10^{-12}$	2.5%
(b)	$(-2.8192 \pm 0.1266) * 10^{-12}$	4.5%
(c)	$(-1.5706 \pm 0.1288) * 10^{-12}$	8.2%
(d)	$(-4.148 \pm 0.1817) * 10^{-13}$	4.4%
(e)	$(-9.7411 \pm 0.6512) * 10^{-13}$	6.7%
(f)	$(-2.4069 \pm 0.1543) * 10^{-12}$	6.4%

Table 6.2: Results for various two-loop six-point diagrams.

7 Summary and outlook

In this thesis we mainly discuss the numerical calculation of loop integrals with contour deformation. As a motivation we present in chapter 2 the subtraction method at NLO level. This method uses subtraction terms and contour deformation for a fully numerical calculation of NLO observables. The necessary ingredients, the tree-level partial amplitudes and the integrands of the primitive one-loop amplitudes are calculated via Berends-Giele type recurrence relations. In chapter 3 we discussed the recurrence relations for these ingredients in detail. Furthermore we extended the method to the integrands of planar primitive two-loop amplitudes for a future application at NNLO calculations. The recurrence relations at loop level are based on tree-level recurrence relations and cut techniques to cut open the loops.

In chapter 4 and chapter 5 we discussed two different approaches to contour deformation for one-loop integrals. In chapter 4 we presented a contour deformation based on Feynman parameters. The advantage of this method is the relative simple deformation but on the other we observed numerical instabilities at large particle multiplicity. We presented the infrared mass approach and a suitable splitting of the integration region to overcome these instabilities. In chapter 5 we presented a contour deformation which works directly in the loop momentum space. This deformation is more complicated but do not face the numerical instabilities of the Feynman deformation. In chapter 5 we focused on the calculation of one-loop integrals with massive propagators and compared the performance of the Feynman deformation with the performance of the Direct deformation.

With a NNLO application in mind we presented in chapter 6 the extension of the Direct deformation discussed in chapter 5 to multi-loop integrals. We introduce there the notation of a chain and showed how to reduce the problem of calculating a deformation vector from the multi-loop level to the one-loop level. We have tested the contour deformation for various simple two- and three-loop diagrams.

The subtraction method is a well established method for NLO calculations. The process e^+e^- to up to seven *jets* were calculated and it is planned to publish results for $Z + jets$ at hadron colliders in the near future. With the work presented in this thesis the subtraction method is also suitable for NLO calculations in $t\bar{t}$ production or massive QCD in general. The recursion relations and contour

deformation at two-loop level were two small steps toward a NNLO implementation of the subtraction method. For an automated calculation of the two-loop contribution in a NNLO calculation the local infrared and ultraviolet subtraction terms for the two-loop amplitude are missed and open for future work.

A Colour ordered Feynman rules

In this appendix we give a list of the colour ordered Feynman [5]. They are obtained from the standard Feynman rules by extracting from each formula the coupling constant and the colour part. The propagators for quark, gluon and ghost particles are given by

$$
\begin{aligned}
\text{———} \quad &= \quad \imath \frac{\not{k} + m}{k^2 - m^2}, \\
\text{〰〰〰} \quad &= \quad -\imath \frac{g^{\mu\nu}}{k^2} \\
\text{- - -◄- - -} \quad &= \quad \imath \frac{1}{k^2}.
\end{aligned}
\tag{A.1}
$$

The colour ordered Feynman rules for the vertices are

 $\quad = \quad -\imath\gamma^\mu,$

 $\quad = \quad -\imath \left[g^{\mu\nu} \left(k_1^\lambda - k_2^\lambda \right) + g^{\nu\lambda} \left(k_2^\mu - k_3^\mu \right) + g^{\lambda\mu} \left(k_3^\nu - k_1^\nu \right) \right],$

 $\quad = \quad -\imath \left[g^{\mu\nu} g^{\lambda\rho} - 2 g^{\mu\lambda} g^{\nu\rho} + g^{\mu\rho} g^{\nu\lambda} \right],$

 $\mu \quad = \quad -\imath k_\mu.$
$\tag{A.2}$

B Generating the random points

In this appendix we show how to map the random numbers provided by the VEGAS algorithm to the integration variables.

B.1 Generating Feynman parameters

We show that for functions which are homogeneous of order $(-n)$

$$\int_0^1 d^n x \, \delta\left(1 - \sum_{i=1}^n x_i\right) f(x_1, \ldots, x_n) = \sum_{i=1}^n \int_0^1 d^n x \, \delta\left(1 - x_i\right) f(x_1, \ldots, x_n) \quad \text{(B.1)}$$

Proof:

$$\int d^n x \, \delta\left(1 - \sum_{i=1}^n x_i\right) f(x_1, \ldots, x_n)$$

$$= \int_0^1 dx_1 \int_0^{1-x_1} dx_2 \cdots \int_0^{1-x_1-\ldots-x_{n-2}} dx_{n-1} f\left(x_1, \ldots, x_{n-1}, 1 - x_1 - \ldots - x_{n-1}\right)$$

$$\text{(B.2)}$$

We substitute

$$
\begin{aligned}
x_1 &= y_1 \\
x_2 &= (1 - y_1) y_2 \\
&\vdots \\
x_{n-1} &= (1 - y_1) \cdots (1 - y_{n-2}) y_{n-1}
\end{aligned}
\quad \text{(B.3)}
$$

This yields

$$= \int_0^1 dy_1 \cdots \int_0^1 dy_{n-1} \prod_{i=1}^{n-2} (1 - y_i)^{n-i-1} f\left(y_1, (1 - y_1) y_2, \ldots, (1 - y_1) \cdots (1 - y_{n-1})\right)$$

$$\text{(B.4)}$$

B Generating the random points

We split the integration into n regions

$$
= \left(\sum_{j=1}^{n-1} \int_0^{1/2} dy_1 \cdots \int_{1/2}^1 dy_j \int_0^1 dy_{j+1} \cdots \int_0^1 dy_{n-1} + \int_0^{1/2} dy_1 \cdots \int_0^{1/2} dy_{n-1} \right)
$$

$$
\prod_{i=1}^{n-2} (1-y_i)^{n-i-1} f\left(y_1, (1-y_1)y_2, \ldots, (1-y_1)\cdots(1-y_{n-1})\right). \quad \text{(B.5)}
$$

For the j-th channel we have

$$
\int_0^{1/2} \cdots \int_{1/2}^1 \cdots \int_0^1 d^{n-1}y \prod_{i=1}^{n-2} (1-y_i)^{n-i-1} \left((1-y_1)\cdots(1-y_{j-1})y_j\right)^{-n}
$$

$$
f\left(z_1, \ldots, z_{j-1}, 1, z_j, \ldots, z_{n-1}\right) \quad \text{(B.6)}
$$

with the definition

$$
z_1 = \frac{y_1}{(1-y_1)\cdots(1-y_{j-1})y_j}
$$

$$
\vdots
$$

$$
z_{j-1} = \frac{y_{j-1}}{(1-y_{i-1})y_j}
$$

$$
z_j = \frac{(1-y_j)y_{j+1}}{y_j}
$$

$$
\vdots
$$

$$
z_{n-1} = \frac{(1-y_j)\cdots(1-y_{n-1})}{y_j} \quad \text{(B.7)}
$$

The Jacobian matrix for this transformation is given by

$$
J^{-1} = \left| \frac{\partial z_i}{\partial y_j} \right| = \left(\prod_{i=1}^{j-1} \frac{\partial z_i}{\partial y_i} \right) * \left. \left| \frac{\partial z_s}{\partial y_t} \right| \right|_{s,t \geq j} \quad \text{(B.8)}
$$

$$
\frac{\partial z_i}{\partial y_i} = \frac{1}{(1-y_i)^2(1-y_{i+1})\cdots(1-y_{j-1})y_j} \quad i < j \quad \text{(B.9)}
$$

$$
\left. \left| \frac{\partial z_s}{\partial y_t} \right| \right|_{s,t \geq j} = (-1)^{n-j} \left(\prod_{i=j}^{n-2} (1-y_i)^{n-i-1} \right) y_j^{j-n-1}
$$

$$
* \begin{vmatrix} y_{j+1} & (1-y_{j+1})y_{j+2} & \cdots & (1-y_{j+1})\cdots(1-y_{n-1}) \\ -1 & y_{j+2} & & (1-y_{j+2})\cdots(1-y_{n-1}) \\ 0 & -1 & & (1-y_{j+3})\cdots(1-y_{n-1}) \\ \vdots & & \ddots & \vdots \\ 0 & 0 & -1 & 1 \end{vmatrix} \quad \text{(B.10)}
$$

It can be easily shown that the determinant of the matrix is 1. Combining all the results we obtain the Jacobian

$$J = (-1)^{n-j} \left(\prod_{i=1}^{n-2} (1 - y_i)^{n-i-1} \left((1 - y_1) \cdots (1 - y_{j-1}) y_j \right)^{-n} \right)^{-1} \quad \text{(B.11)}$$

The minus signs are eaten up by making the integration boundaries right. So the integral for the j-th channel is given by the simple expression

$$= \int_0^1 d^{n-1} z f \left(z_1, \ldots, z_{j-1}, 1, z_j, \ldots, z_{n-1} \right) \quad \text{(B.12)}$$

After renaming the integration variables and introducing a delta distribution we have

$$= \int_0^1 d^n x \delta \left(1 - x_j \right) f(x_1, \ldots, x_n) \quad \text{(B.13)}$$

A similar calculation holds for the n-th channel. With this we have shown that for a homogeneous function of degree $(-n)$ the integration over the $n-1$ dimensional simplex can be replaced by the integration over the n surfaces of the n dimensional hyper cube. We can now write our integral as

$$I = \sum_{i=1}^n \int_0^1 d^n x \delta(1 - x_i) f(x_1, \ldots, x_n)$$

$$= n \sum_{i=1}^n \int_0^1 d\lambda \lambda^{n-1} \int_0^1 d^{n-1} x f(x_1, \ldots, x_{i-1}, 1, x_{i+1}, \ldots, x_n). \quad \text{(B.14)}$$

substituting $y_j = \lambda x_j$ for all $j \neq i$ yields

$$= n \sum_{i=1}^n \int_0^1 d\lambda \int_0^\lambda d^{n-1} y f \left(\frac{y_1}{\lambda}, \ldots, \frac{y_{i-1}}{\lambda}, \frac{\lambda}{\lambda}, \frac{y_{i+1}}{\lambda}, \ldots, \frac{y_n}{\lambda} \right) \quad \text{(B.15)}$$

$$= n \int_0^1 d^n z f(u_1, \ldots, u_n), \qquad u_i = \frac{z_i}{\max\{z_1, \ldots, z_n\}}. \quad \text{(B.16)}$$

The definition of the integration variables is suitable for our Monte Carlo programme and can be used for any Feynman parameter integral.

B.2 Generating the loop momentum

In this section we discuss the construction of the loop momentum from four numbers randomly distributed in the unit hyper cube $[0,1]^4$. We define for $u_0, u_1, u_2, u_3 \in [0,1]$ a radius k_E and three angles ζ, θ, ϕ by the following equations:

$$
\begin{aligned}
k_E &= \mu_1 \sqrt{\tan \frac{\pi}{2} u_0} \\
\zeta &= \arccos(1 - 2u_1) \\
\theta &= \arccos(1 - 2u_2) \\
\phi &= 2\pi u_3
\end{aligned}
\tag{B.17}
$$

μ_1 is an arbitrary scale, which we take to be the order of the center-of-mass energy. The loop momentum is then given by

$$
k = k_E \begin{pmatrix} \cos \zeta \\ \sin \zeta \sin \theta \sin \phi \\ \sin \zeta \sin \theta \cos \phi \\ \sin \zeta \cos \theta \end{pmatrix}
\tag{B.18}
$$

The Jacobian of this transformation is

$$
\left| \frac{\partial k}{\partial u} \right| = 2\pi^2 \frac{k_E^2}{\mu_1^2} \left(k_E^4 - \mu_1^4 \right) \sin \zeta
\tag{B.19}
$$

We note that in the case of an multi-loop integral we construct all the loop momenta with this method.

C Proof of the direct deformation

In this appendix we give detailed proof for some statements made in chapter 5.

C.1 Proof for z_{ij}

We show that for all loop momenta k which lie on the intersection of a forward hyperboloid with a backward hyperboloid the constant z_{ij} is greater zero. Therefore the statement $z_{ij} > 0$ is equivalent to the statement that there exists an intersection of a forward hyperboloid with a backward hyperboloid. We define the forward hyperboloid by

$$k_i^2 - m_i^2 \;=\; 0 \qquad k_i^0 > 0 \tag{C.1}$$

and the backward hyperboloid by

$$k_j^2 - m_j^2 \;=\; 0 \qquad k_j^0 < 0. \tag{C.2}$$

We calculate the constant

$$
\begin{aligned}
z_{ij} \;&=\; (q_i - q_j)^2 - (m_i + m_j)^2 \\
&=\; (k_i - k_j)^2 - (m_i + m_j)^2 \\
&=\; 2(|k_i^0||k_j^0| - m_i m_j + |\vec{k}_i||\vec{k}_j| \cos\phi) \\
&\geq\; 2|\vec{k}_i||\vec{k}_j|(1 + \cos\phi),
\end{aligned}
\tag{C.3}
$$

in the last step we made use of

$$|k_i^0||k_j^0| - m_i m_j \;\geq\; |\vec{k}_i||\vec{k}_j|, \tag{C.4}$$

which can be easily shown. We note that in the massless case and with $(q_i - q_j)$ light-like the intersection of a forward hyperboloid with a backward hyperboloid is given by the region where a forward cone is tangential to a backward cone. This region corresponds to the collinear singularity and the deformation is pinched. Therefore if $z_{ij} \leq 0$ we set c_{ij} in eq.(5.29) to zero.

C.2 Proof for x_{ij}

We show that if $x_{ij} > 0$ and $x_{ji} > 0$ the minimum of the forward hyperboloid lies in the interior of the backward hyperboloid and the maximum of the backward hyperboloid lies in the interior of the forward hyperboloid. For points k which lie inside a forward hyperboloid with origin q_i we have

$$0 \quad < \quad k_i^0 - \sqrt{\vec{k}_i^2 + m_i^2}. \tag{C.5}$$

For points k which lies inside a backward hyperboloid with origin q_i we have

$$0 \quad < \quad -k_i^0 - \sqrt{\vec{k}_i^2 + m_i^2}. \tag{C.6}$$

For $q_i^0 < q_j^0$ the minimum of the forward hyperboloid is at $q_i + \hat{e}^0 m_i$ and the maximum of the backward hyperboloid is at $q_j - \hat{e}^0 m_j$. The conditions that the extremum lies in the correlated hyperboloid reads in this case

$$0 \quad < \quad q_j^0 - m_j - q_i^0 - \sqrt{(\vec{q}_i - \vec{q}_j)^2 + m_i^2} \tag{C.7}$$

$$0 \quad < \quad -(q_i^0 + m_i - q_j^0) - \sqrt{(\vec{q}_i - \vec{q}_j)^2 + m_j^2} \tag{C.8}$$

For $q_i^0 > q_j^0$ the minimum of the forward hyperboloid is at $q_j + \hat{e}^0 m_j$ and the maximum of the backward hyperboloid is at $q_i - \hat{e}^0 m_i$. The conditions that the extremum lies in the correlate hyperboloid reads in this case

$$0 \quad < \quad q_i^0 - m_i - q_j^0 - \sqrt{(\vec{q}_i - \vec{q}_j)^2 + m_j^2} \tag{C.9}$$

$$0 \quad < \quad -(q_j^0 + m_j - q_i^0) - \sqrt{(\vec{q}_i - \vec{q}_j)^2 + m_i^2} \tag{C.10}$$

We combine eq.(C.8) and eq.(C.9) to

$$0 \quad < \quad x_{ij} \;=\; |q_i^0 - q_j^0| - m_i - \sqrt{(\vec{q}_i - \vec{q}_j)^2 + m_j^2} \tag{C.11}$$

and we combine eq.(C.7) and eq.(C.10) to

$$0 \quad < \quad x_{ji} \;=\; |q_i^0 - q_j^0| - m_j - \sqrt{(\vec{q}_i - \vec{q}_j)^2 + m_i^2}. \tag{C.12}$$

C.3 Proof for κ_{ext}

We show that κ_{ext} always deforms correctly as long as the loop momentum lies either on a forward hyperboloid or on a backward hyperboloid. If the loop momentum k lies on a forward hyperboloid with origin q_i we have

$$k_i^2 - m_i^2 \;=\; 0 \qquad k_i^0 \;>\; 0 \quad \Rightarrow \quad k_i^0 \;\geq\; |\vec{k}_i|, \tag{C.13}$$

and it follows that k lies also inside the forward cone with origin P_+

$$k_+^0 \;\geq\; |\vec{k}_+|. \tag{C.14}$$

Because k lies on a forward hyperboloid we also have $h_{\delta+}(k_i, m_i^2) = 0$, therefore $c_- = 0$ and $c_+ \approx 1$. The imaginary part of the critical propagator reads

$$
\begin{aligned}
\kappa_{ext} \cdot k_i \;&\approx\; k_+ \circ k_i \\
&\geq\; |\vec{k}_+||\vec{k}_i|(1 + \cos\theta) \\
&\geq\; 0
\end{aligned}
\tag{C.15}
$$

If the loop momentum k lies on the backward hyperboloid with origin q_i we have

$$k_i^2 - m_i^2 \;=\; 0 \qquad k_i^0 \;<\; 0 \quad \Rightarrow \quad k_i^0 \;\leq\; -|\vec{k}_i|, \tag{C.16}$$

and it follows that k lies also inside the backward cone with origin P_-

$$k_-^0 \;\leq\; -|\vec{k}_-|. \tag{C.17}$$

Because k lies on a backward hyperboloid we also have $h_{\delta-}(k_i, m_i^2) = 0$, therefore $c_+ = 0$ and $c_- \approx 1$. The imaginary part of the critical propagator reads

$$
\begin{aligned}
\kappa_{ext} \cdot k_i \;&\approx\; k_- \circ k_i \\
&\geq\; |\vec{k}_-||\vec{k}_i|(1 + \cos\theta) \\
&\geq\; 0
\end{aligned}
\tag{C.18}
$$

The equal sign in eq.(C.15) and eq.(C.18) only appear in the soft limit $k = q_i$, because if

$$k_i^0 \;=\; \pm|\vec{k}_i| \qquad \text{and} \qquad k_\pm^0 \;=\; \pm|\vec{k}_\pm| \tag{C.19}$$

the two cones are tangential and therefore we have $\cos\phi = 1$ in this case.

C.4 Proof for $\kappa_{\mathbf{int}}$

We show that κ_{int} deforms correctly if the loop momentum k lies on the intersection of a forward hyperboloid with a backward hyperboloid. This intersection is defined by

$$
\begin{aligned}
k_i^2 - m_i^2 &= 0 \qquad k_i^0 > 0 \tag{C.20} \\
k_j^2 - m_j^2 &= 0 \qquad k_j^0 < 0 \tag{C.21}
\end{aligned}
$$

To show that κ_{int} deforms correctly we only need to show that $-(k - v_{ij})$ leads to a positive imaginary part in the two critical propagators. First we consider $x_{ij} > 0$ and $x_{ji} >$. Then

$$v_{ij} \;=\; \frac{q_i k_j^0 - q_j k_i^0}{q_i^0 - q_j^0} \tag{C.22}$$

and we rewrite the conditions to

$$x_{ij} > 0 \quad \Rightarrow \quad \vec{k}_i \cdot \vec{k}_j > m_i(k_i^0 - k_j^0) + k_i^0 k_j^0 - m_i^2 \tag{C.23}$$

$$x_{ji} > 0 \quad \Rightarrow \quad \vec{k}_i \cdot \vec{k}_j > m_j(k_i^0 - k_j^0) + k_i^0 k_j^0 - m_j^2. \tag{C.24}$$

The imaginary part for the i-th propagator is given by

$$
\begin{aligned}
\kappa_{int} \cdot k_i &\geq -(k - v_{ij}) \cdot k_i \\
&= \frac{k_i k_j^0 - k_j k_i^0}{k_i^0 - k_j^0} \cdot k_i \\
&= \frac{\vec{k}_j \cdot \vec{k}_i k_i^0 - \vec{k}_i^2 k_j^0}{k_i^0 - k_j^0} \\
&> \frac{k_i^0 \left(m_i(k_i^0 - k_j^0) + k_i^0 k_j^0 - m_i^2 \right) - \vec{k}_i^2 k_j^0}{k_i^0 - k_j^0} \\
&= m_i \left(k_i^0 - m_i \right) \geq 0.
\end{aligned}
\tag{C.25}
$$

The imaginary part for the j-th propagator is given by

$$
\begin{aligned}
\kappa_{int} \cdot k_j &\geq -(k - v_{ij}) \cdot k_j \\
&= \frac{k_i k_j^0 - k_j k_i^0}{k_i^0 - k_j^0} \cdot k_j \\
&= \frac{\vec{k}_j^2 k_i^0 - \vec{k}_i \cdot \vec{k}_j k_j^0}{k_i^0 - k_j^0} \\
&> \frac{\vec{k}_j^2 k_i^0 - k_j^0 \left(m_j(k_i^0 - k_j^0) + k_i^0 k_j^0 - m_j^2 \right)}{k_i^0 - k_j^0} \\
&= m_j \left(-k_j^0 - m_j \right) \geq 0.
\end{aligned}
\tag{C.26}
$$

The equal sign in eq.(C.25) and eq.(C.26) never appears in practise because in this case we have $x_{ij} = 0$ or $x_{ji} = 0$. Eq.(C.25) is zero if the loop momentum lies in the minimum of the forward hyperboloid with origin q_i and eq.(C.26) is zero if the loop momentum lies in the maximum of the backward hyperboloid with origin q_j but by construction ($x_{ij} > 0, x_{ji} > 0$) it is forbidden that an extremum of one hyperboloid lie on the other hyperboloid.

Next we consider the case that $x_{ij} \leq 0$ or $x_{ji} \leq 0$ and $z_{ij} > 0$. We note that

$$z_{ij} > 0 \quad \Rightarrow \quad \sqrt{(k_i - k_j)^2} > m_i + m_j \tag{C.27}$$

and therefore we also have

$$-k_i \cdot k_j > m_i m_j \geq 0. \tag{C.28}$$

The imaginary part for the i-th propagator is given by

$$
\begin{aligned}
\kappa_{int} \cdot k_i \quad \geq \quad & -(k - v_{ij}) \cdot k_i \\
= \quad & -\frac{k_i}{2}\left(k_i - m_i \frac{k_i - k_j}{\sqrt{(k_i - k_j)^2}} + k_j + m_j \frac{k_i - k_j}{\sqrt{(k_i - k_j)^2}} \right) \\
= \quad & -\frac{1}{4}\left(k_i - m_i \frac{k_i - k_j}{\sqrt{(k_i - k_j)^2}} \right)^2 - \frac{k_i}{2}\left(k_j + m_j \frac{k_i - k_j}{\sqrt{(k_i - k_j)^2}} \right) \\
\geq \quad & -\frac{1}{4}\left(k_i - m_i \frac{k_i - k_j}{\sqrt{(k_i - k_j)^2}} \right)^2 - \frac{k_i \cdot k_j}{2}\left(1 - \frac{m_i + m_j}{\sqrt{(k_i - k_j)^2}} \right) \\
\geq \quad & 0.
\end{aligned}
\tag{C.29}
$$

The imaginary part for the j-th propagator is given by

$$
\begin{aligned}
\kappa_{int} \cdot k_j \quad \geq \quad & -(k - v_{ij}) \cdot k_j \\
= \quad & -\frac{k_j}{2}\left(k_i - m_i \frac{k_i - k_j}{\sqrt{(k_i - k_j)^2}} + k_j + m_j \frac{k_i - k_j}{\sqrt{(k_i - k_j)^2}} \right) \\
= \quad & -\frac{k_j}{2}\left(k_i - m_i \frac{k_i - k_j}{\sqrt{(k_i - k_j)^2}} \right) - \frac{1}{4}\left(k_j - m_j \frac{k_j - k_i}{\sqrt{(k_i - k_j)^2}} \right)^2 \\
\geq \quad & -\frac{k_i \cdot k_j}{2}\left(1 - \frac{m_i + m_j}{\sqrt{(k_i - k_j)^2}} \right) - \frac{1}{4}\left(k_j - m_j \frac{k_j - k_i}{\sqrt{(k_i - k_j)^2}} \right)^2 \\
\geq \quad & 0
\end{aligned}
\tag{C.30}
$$

In the last step of eq.(C.29) and eq.(C.30) we make use of the fact that the distance of two points on the same mass hyperboloid is spacelike. We note that the equal sign in eq.(C.29) and eq.(C.30) only appears if $m_i = m_j = 0$ and $(q_i - q_j)^2 = 0$ but this configuration correspond to a pinch singularity called the collinear singularity.

C Proof of the direct deformation

D   Test program set-up's

In the case that someone like to verify our results calculated in this thesis we present in this appendix the explicit numbers for external momenta we use in our test program.

D.1   Massless six-point function

In chapter 4 and chapter 5 we make use of an six-point function with all external momenta on-shell and massless to test our contour deformation, Fig.(4.2) and 5.6. The momenta of the external massless on-shell particles are given in our test program by:

$$
\begin{aligned}
p_1 &= (29.91523, -18.184584, -8.692535, 22.106147) \\
p_2 &= (9.827193, 4.075286, 8.795244, -1.615378) \\
p_3 &= (22.170989, -9.264169, 14.187043, -14.298802) \\
p_4 &= (28.086588, 23.373467, -14.289752, -6.191967) \\
p_5 &= (-45, 0, 0, 45) \\
p_6 &= (-45, 0, 0, -45)
\end{aligned}
$$

We note that the center of mass energy is around the Z-Boson mass.

D.2   Massive six-point function

In chapter 5 we make use of an six-point function with two massive and four massless external on-shell momenta to test our contour deformation, Fig.(5.7) and 5.9. The external on-shell particles with $p_1^2 = p_4^2 = 100$ are given in our test

program by:

$$
\begin{aligned}
p_1 &= (30.447087, -17.481165, -8.356289, 21.251033) \\
p_2 &= (9.447056, 3.917645, 8.455025, -1.552891) \\
p_3 &= (21.313366, -8.905811, 13.638257, -13.745693) \\
p_4 &= (28.792489, 22.469331, -13.736994, -5.952449) \\
p_5 &= (-45, 0, 0, 45) \\
p_6 &= (-45, 0, 0, -45)
\end{aligned}
$$

and the external on-shell particles with $p_1^2 = p_4^2 = 1600$ are given by:

$$
\begin{aligned}
p_1 &= (40.785589, -4.842567, -2.314828, 5.886881) \\
p_2 &= (2.616988, 1.085251, 2.342179, -0.430176) \\
p_3 &= (5.904149, -2.467054, 3.778019, -3.80778) \\
p_4 &= (40.693274, 6.224369, -3.80537, -1.6489249) \\
p_5 &= (-45, 0, 0, 45) \\
p_6 &= (-45, 0, 0, -45)
\end{aligned}
$$

D.3 Ladder diagrams

In chapter 6 we make use of the two-, three- and four-point ladder diagrams with all external particles off shell to test our contour deformation for multi-loop integrals. For the two-point function the external off-shell momentum is given by:

$$
p = (90, 0, 0, 0).
$$

For the three-point function the external off-shell momenta are given by:

$$
\begin{aligned}
p_1 &= (39.7424, -14.1093, 0.102709, 20.4908) \\
p_2 &= (50.2576, 14.1093, -0.102709, -20.4908) \\
p_3 &= (-90, 0, 0, 0)
\end{aligned}
$$

For the four-point function the external off-shell momenta are given by:

$$
\begin{aligned}
p_1 &= (19.6586, -7.15252, -0.206016, 8.96383) \\
p_2 &= (26.874, 7.04203, -0.0501295, -12.9055) \\
p_3 &= (43.4674, 0.110491, 0.256146, 3.9417) \\
p_4 &= (-90, 0, 0, 0)
\end{aligned}
$$

D.4 Off-shell six-point function

In chapter 6 we make use of the two-loop six-point function with all external particles off shell Fig.(6.9) to test our contour deformation for multi-loop integrals. The external off-shell momenta are given by:

$$
\begin{aligned}
p_1 &= (9.64873, -1.60843, -7.38348, -0.535027) \\
p_2 &= (18.9132, -10.5194, 10.0603, 10.8508) \\
p_3 &= (11.8059, -3.17397, -6.77661, -3.43232) \\
p_4 &= (29.6765, 21.5419, 5.75578, -5.06762) \\
p_5 &= (19.9556, -6.24009, -1.65597, -1.81582) \\
p_6 &= (-90, 0, 0, 0)
\end{aligned}
$$

D Test program set-up's

Bibliography

[1] M. Assadsolimani, S. Becker and S. Weinzierl, Phys. Rev. D **81** (2010) 094002 [arXiv:0912.1680 [hep-ph]].

[2] M. Assadsolimani, S. Becker, C. .Reuschle and S. Weinzierl, Nucl. Phys. Proc. Suppl. **205-206** (2010) 224 [arXiv:1006.4609 [hep-ph]].

[3] Z. Nagy and D. E. Soper, JHEP **0309** (2003) 055 [hep-ph/0308127].

[4] S. Becker, D. Goetz, C. Reuschle, C. Schwan and S. Weinzierl, Phys. Rev. Lett. **108** (2012) 032005 [arXiv:1111.1733 [hep-ph]].

[5] S. Becker, C. Reuschle and S. Weinzierl, JHEP **1012** (2010) 013 [arXiv:1010.4187 [hep-ph]].

[6] S. Becker, C. Reuschle and S. Weinzierl, JHEP **1207** (2012) 090 [arXiv:1205.2096 [hep-ph]].

[7] D. E. Soper, Phys. Rev. D **62** (2000) 014009 [hep-ph/9910292].

[8] T. Binoth, G. Heinrich and N. Kauer, Nucl. Phys. B **654** (2003) 277 [hep-ph/0210023].

[9] Z. Nagy and D. E. Soper, Phys. Rev. D **74** (2006) 093006 [hep-ph/0610028].

[10] T. Binoth, J. P. .Guillet, G. Heinrich, E. Pilon and C. Schubert, JHEP **0510** (2005) 015 [hep-ph/0504267].

[11] W. Gong, Z. Nagy and D. E. Soper, Phys. Rev. D **79** (2009) 033005 [arXiv:0812.3686 [hep-ph]].

[12] A. Lazopoulos, K. Melnikov and F. Petriello, Phys. Rev. D **76** (2007) 014001 [hep-ph/0703273].

[13] A. Lazopoulos, K. Melnikov and F. J. Petriello, Phys. Rev. D **77** (2008) 034021 [arXiv:0709.4044 [hep-ph]].

[14] Y. Kurihara and T. Kaneko, Comput. Phys. Commun. **174** (2006) 530 [hep-ph/0503003].

[15] C. Anastasiou, S. Beerli and A. Daleo, JHEP **0705** (2007) 071 [hep-ph/0703282].

Bibliography

[16] C. Anastasiou, S. Beerli and A. Daleo, Phys. Rev. Lett. **100** (2008) 241806 [arXiv:0803.3065 [hep-ph]].

[17] S. Beerli,

[18] D. A. Kosower, Phys. Rev. D **67** (2003) 116003 [hep-ph/0212097].

[19] S. Weinzierl, JHEP **0303** (2003) 062 [hep-ph/0302180].

[20] W. B. Kilgore, Phys. Rev. D **70** (2004) 031501 [hep-ph/0403128].

[21] S. Frixione and M. Grazzini, JHEP **0506** (2005) 010 [hep-ph/0411399].

[22] P. Bolzoni, G. Somogyi and Z. Trocsanyi, JHEP **1101** (2011) 059 [arXiv:1011.1909 [hep-ph]].

[23] S. Catani and M. Grazzini, Phys. Rev. Lett. **98** (2007) 222002 [hep-ph/0703012].

[24] M. Czakon, Nucl. Phys. B **849** (2011) 250 [arXiv:1101.0642 [hep-ph]].

[25] C. Anastasiou, F. Herzog and A. Lazopoulos, JHEP **1103** (2011) 038 [arXiv:1011.4867 [hep-ph]].

[26] C. F. Berger, Z. Bern, L. J. Dixon, F. Febres Cordero, D. Forde, T. Gleisberg, H. Ita and D. A. Kosower *et al.*, Phys. Rev. Lett. **102** (2009) 222001 [arXiv:0902.2760 [hep-ph]].

[27] C. F. Berger, Z. Bern, L. J. Dixon, F. Febres Cordero, D. Forde, T. Gleisberg, H. Ita and D. A. Kosower *et al.*, Phys. Rev. D **80** (2009) 074036 [arXiv:0907.1984 [hep-ph]].

[28] C. F. Berger, Z. Bern, L. J. Dixon, F. Febres Cordero, D. Forde, T. Gleisberg, H. Ita and D. A. Kosower *et al.*, Phys. Rev. D **82** (2010) 074002 [arXiv:1004.1659 [hep-ph]].

[29] C. F. Berger, Z. Bern, L. J. Dixon, F. Febres Cordero, D. Forde, T. Gleisberg, H. Ita and D. A. Kosower *et al.*, Phys. Rev. Lett. **106** (2011) 092001 [arXiv:1009.2338 [hep-ph]].

[30] H. Ita, Z. Bern, L. J. Dixon, F. Febres Cordero, D. A. Kosower and D. Maitre, Phys. Rev. D **85** (2012) 031501 [arXiv:1108.2229 [hep-ph]].

[31] Z. Bern, G. Diana, L. J. Dixon, F. Febres Cordero, S. Hoeche, D. A. Kosower, H. Ita and D. Maitre *et al.*, arXiv:1112.3940 [hep-ph].

[32] R. K. Ellis, K. Melnikov and G. Zanderighi, JHEP **0904** (2009) 077 [arXiv:0901.4101 [hep-ph]].

[33] R. K. Ellis, K. Melnikov and G. Zanderighi, Phys. Rev. D **80** (2009) 094002 [arXiv:0906.1445 [hep-ph]].

[34] T. Melia, K. Melnikov, R. Rontsch and G. Zanderighi, JHEP **1012** (2010) 053 [arXiv:1007.5313 [hep-ph]].

[35] G. Bevilacqua, M. Czakon, C. G. Papadopoulos and M. Worek, Phys. Rev. Lett. **104** (2010) 162002 [arXiv:1002.4009 [hep-ph]].

[36] G. Bevilacqua, M. Czakon, C. G. Papadopoulos, R. Pittau and M. Worek, JHEP **0909** (2009) 109 [arXiv:0907.4723 [hep-ph]].

[37] R. Frederix, S. Frixione, K. Melnikov and G. Zanderighi, JHEP **1011** (2010) 050 [arXiv:1008.5313 [hep-ph]].

[38] A. Bredenstein, A. Denner, S. Dittmaier and S. Pozzorini, Phys. Rev. Lett. **103** (2009) 012002 [arXiv:0905.0110 [hep-ph]].

[39] V. Hirschi, R. Frederix, S. Frixione, M. V. Garzelli, F. Maltoni and R. Pittau, JHEP **1105** (2011) 044 [arXiv:1103.0621 [hep-ph]].

[40] G. Bevilacqua, M. Czakon, M. V. Garzelli, A. van Hameren, A. Kardos, C. G. Papadopoulos, R. Pittau and M. Worek, arXiv:1110.1499 [hep-ph].

[41] G. Cullen, J. P. .Guillet, G. Heinrich, T. Kleinschmidt, E. Pilon, T. Reiter and M. Rodgers, Comput. Phys. Commun. **182** (2011) 2276 [arXiv:1101.5595 [hep-ph]].

[42] G. Cullen, N. Greiner, G. Heinrich, G. Luisoni, P. Mastrolia, G. Ossola, T. Reiter and F. Tramontano, Eur. Phys. J. C **72** (2012) 1889 [arXiv:1111.2034 [hep-ph]].

[43] S. Badger, B. Biedermann and P. Uwer, Comput. Phys. Commun. **182** (2011) 1674 [arXiv:1011.2900 [hep-ph]].

[44] T. Binoth, J. -P. .Guillet, G. Heinrich, E. Pilon and T. Reiter, Comput. Phys. Commun. **180** (2009) 2317 [arXiv:0810.0992 [hep-ph]].

[45] A. van Hameren, Comput. Phys. Commun. **182** (2011) 2427 [arXiv:1007.4716 [hep-ph]].

[46] A. Denner and S. Dittmaier, Nucl. Phys. B **844** (2011) 199 [arXiv:1005.2076 [hep-ph]].

[47] G. Ossola, C. G. Papadopoulos and R. Pittau, JHEP **0803** (2008) 042 [arXiv:0711.3596 [hep-ph]].

[48] G. Aad *et al.* [ATLAS Collaboration], arXiv:1207.7214 [hep-ex].

Bibliography

[49] A. Freitas, JHEP **1207** (2012) 132 [arXiv:1205.3515 [hep-ph]].

[50] A. Gehrmann-De Ridder, T. Gehrmann, E. W. N. Glover and G. Heinrich, JHEP **0711** (2007) 058 [arXiv:0710.0346 [hep-ph]].

[51] P. Baernreuther, M. Czakon and A. Mitov, arXiv:1204.5201 [hep-ph].

[52] A. Gehrmann-De Ridder, E. W. N. Glover and J. Pires, JHEP **1202** (2012) 141 [arXiv:1112.3613 [hep-ph]].

[53] T. Kinoshita, J. Math. Phys. **3** (1962) 650.

[54] T. D. Lee and M. Nauenberg, Phys. Rev. **133** (1964) B1549.

[55] T. Binoth and G. Heinrich, Nucl. Phys. B **585** (2000) 741 [hep-ph/0004013].

[56] M. Roth and A. Denner, Nucl. Phys. B **479** (1996) 495 [hep-ph/9605420].

[57] K. Hepp, Commun. Math. Phys. **2** (1966) 301.

[58] S. Borowka, J. Carter and G. Heinrich, arXiv:1204.4152 [hep-ph].

[59] T. Hahn and M. Perez-Victoria, Comput. Phys. Commun. **118** (1999) 153 [hep-ph/9807565].

[60] L. D. Landau, Nucl. Phys. **13** (1959) 181.

[61] N. I. Usyukina and A. I. Davydychev, Phys. Lett. B **305** (1993) 136.

[62] N. I. Usyukina and A. I. Davydychev, Phys. Lett. B **332** (1994) 159 [hep-ph/9402223].

[63] F. A. Berends and W. T. Giele, Nucl. Phys. B **306** (1988) 759.

[64] A. van Hameren, JHEP **0907** (2009) 088 [arXiv:0905.1005 [hep-ph]].

[65] S. Catani and M. H. Seymour, Nucl. Phys. B **485** (1997) 291 [Erratum-ibid. B **510** (1998) 503] [hep-ph/9605323].

[66] S. Dittmaier, Nucl. Phys. B **565** (2000) 69 [hep-ph/9904440].

[67] L. Phaf and S. Weinzierl, JHEP **0104** (2001) 006 [hep-ph/0102207].

[68] S. Catani, S. Dittmaier, M. H. Seymour and Z. Trocsanyi, Nucl. Phys. B **627** (2002) 189 [hep-ph/0201036].

[69] S. Weinzierl, Phys. Rev. D **84** (2011) 074007 [arXiv:1107.5131 [hep-ph]].

[70] P. Cvitanovic, P. G. Lauwers and P. N. Scharbach, Nucl. Phys. B **186** (1981) 165.

[71] F. A. Berends and W. Giele, Nucl. Phys. B **294** (1987) 700.

[72] M. L. Mangano, S. J. Parke and Z. Xu, Nucl. Phys. B **298** (1988) 653.

[73] D. Kosower, B. -H. Lee and V. P. Nair, Phys. Lett. B **201** (1988) 85.

[74] Z. Bern and D. A. Kosower, Nucl. Phys. B **362** (1991) 389.

[75] Z. Bern, L. J. Dixon and D. A. Kosower, Nucl. Phys. B **437** (1995) 259 [hep-ph/9409393].

[76] N. I. Usyukina and A. I. Davydychev, Phys. Lett. B **298** (1993) 363.

[77] H. J. Lu and C. A. Perez, SLAC-PUB-5809.

[78] Z. Bern, L. J. Dixon, D. A. Kosower and S. Weinzierl, Nucl. Phys. B **489** (1997) 3 [hep-ph/9610370].

[79] G. P. Lepage, J. Comput. Phys. **27** (1978) 192.

[80] G. P. Lepage, CLNS-80/447.

[81] T. Hahn, Comput. Phys. Commun. **168** (2005) 78 [hep-ph/0404043].